Field Effect Transistor Biosensor Functionalized with Sensing Interface Based on Biomolecular Interaction

生体分子間相互作用に基づく分子認識界面により機能化した電界効果トランジスタバイオセンサ

February 2021

Hiroki HAYASHI

林　宏樹

Field Effect Transistor Biosensor Functionalized with Sensing Interface Based on Biomolecular Interaction

生体分子間相互作用に基づく分子認識界面により機能化した電界効果トランジスタバイオセンサ

February 2021

Waseda University
Graduate School of Advanced Science and Engineering
Department of Nanoscience and Nanoengineering
Research on Electrochemical Nano-systems

Hiroki HAYASHI

林　宏樹

Supervisor:	Prof. Dr. Toshiyuki Momma (Waseda University)
Referees:	Prof. Dr. Yoshiyuki Sugahara (Waseda University)
	Prof. Dr. Takayuki Homma (Waseda University)

I sincerely appreciate their reviewing the doctoral thesis

Contents

Chapter 1:

General Introduction

1.1 Increase in health consciousness in modern society

Since the World Health Organization (WHO) proposed a healthy life expectancy in 2000, there has been a growing interest in extending not only lifetime, but also the period of healthy living. In 2015, the average lifetime of males and females was 69.0 years and 74.8 years, respectively, of which about ten years were reported to be spent in an unhealthy state.[1] A century ago, many people lost their lives due to infectious diseases,[2] but in recent years, lifestyle-related diseases such as cancer, stroke, and heart disease have significantly influenced people's health. The number of deaths from heart disease and cancer in the United States was 647,457 and 599.108 in 2017, respectively (Data source: National Center for Health Statistics and Centers for Disease Control and Prevention).[3] Moreover, the mental disorder due to mental stress has become a major problem in recent years. In 2017, 25.8 million people worldwide suffered from depression, twice as many as in 1990.[4] The number of depression patients will be the highest in 2030. Additionally, the COVID-19 outbreak in 2020 tremendous impacted on people's lives around the world. As of December 2020, Covid-19 continues its spread across the world with 75 million patients and nearly two million deaths (Data source: Johns Hopkins University and National Public Health Agencies). Lifestyle change due to the spread of the COVID-19 is estimated to affect the mental state of many people and increase the number of patients with mental disorders.[5–7] Since people become even more health-conscious, simply understanding their own health status will be of great significance in future society with/after the Covid-19 pandemic. Hence, there is a need to maintain health status through not only advanced medical technology but also simple and noninvasive diagnosis.

1.2 Field effect transistor (FET) biosensor

In an entire society, as people become more and more health-conscious, diagnosis of health conditions and diseases are needed to improve the quality of life (QOL). Thus, people are required to check their health status not only during regular health checkups but also in their daily lives. To achieve the above requirements, quick and simple biosensors are needed to detect biomarkers in biological samples. A biosensor is composed of a bio-recognition element (receptor), transducer, and signal processing unit.[8] Various biomolecular interactions that occur on the bio-recognition element are converted into signals for the detection of target molecules. Among these components, the transducer and signal processing unit contribute to the simplicity and rapidity of the measurement operation.

So far, various types of biosensors have been developed. An enzyme-linked immunosorbent assay (ELISA)[9] and a polymerase chain reaction (PCR)[10,11] are used in specialized institutions for research and diagnosis. These biosensors, although they have high sensitivity, require various reagents for labeling, large equipment, and expertise, and thus they are inconvenient for measurement in daily lives; e.g., the long measurement time in PCR assay was noticed as a problem in COVID-19 diagnosis. Furthermore, an immunochromatography,[12,13] which is used for simple influenza diagnosis and pregnancy tests, has low sensitivity because the determination is done visually. As an alternative to these methods, a quartz crystal microbalance (QCM),[14–16] a surface plasmon resonance (SPR),[17,18] and an ion-sensitive field effect transistor (ISFET)[19] are candidates for the simple detection of biomarkers. These types of biosensors covert the adsorption of target molecules to bio-recognition elements to signals without any labeling.

FET biosensors are able to detect changes in the charge density on the gate surface caused by the formation of target-receptor complexes without any labeling process. Additionally, it can be easily miniaturized and integrated by standard complementary metal oxide semiconductor (CMOS) processes, and they are expected to be devices that enable simple measurements on a daily basis compared with SPR or QCM

sensors, which require the optical instrument or oscillator, respectively. The concept of an ISFET, which was derived from metal-oxide-semiconductor FET (MOSFET), was invented by P. Bergveld in 1970.[20] Furthermore, by immobilizing a bio-receptor on the gate surface of the ISFET, it can be made into an immuno-FET that detects biomolecules (Figure 1.1). Since then, various types of FET biosensors have been reported in the literature. However, the only practical application to date has been in DNA sequencing,[21] and further development research on FET biosensors is required. Therefore, researchs on FET biosensors is considered to be of interest and essential for improving people's QOL.

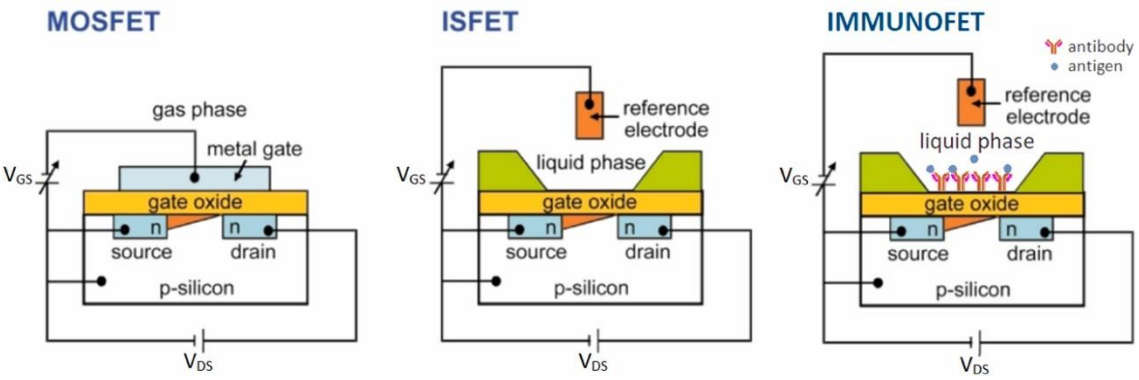

Figure 1.1 Schematic images of MOSFET, ISFET and immunoFET. V_{GS} and V_{DS} represent the gate voltage and the source-drain voltage, respectively. The ISFET was realized by replacing the metal gate of the MOSFET with a buffer solution and a reference electrode. The immunoFET was realized by immobilizing bioreceptor such as antibodies or DNA molecules, on the gate oxide of the ISFET.[19] Reprinted from *Biosensors and Bioelectronics*, 132, I. M. Bhattacharyya *et al.*, Specific and label-free immunosensing of protein-protein interactions with silicon-based immunoFETs, 143–161, Copyright (2019), with permission from Elsevier

1.2.1 Principle of FET biosensor

In general, FET biosensors detect surface potential change derived from the intrinsic charge of target molecules adsorbed on the FET gate surface. As shown in Figure 1.2, K. Schoorideh and C. O. Chui explained the sensing mechanism from a simplified potential diagram of a generalized FET biosensor.[22] Briefly, the FET responses were generated from the change in charge density ($\Delta\sigma_0$) on the FET gate surface. In the potential diagram, the charge depends on capacitances, which are presented as a parallel combination of the electric double-layer (C_{DL}) and FET (C_{FET}), on both of its sides. Then, the potential change on the FET gate surface is given by;[22,23]

$$\Delta V = \Delta\psi_0 = \frac{\Delta\sigma_0}{C_{DL} + C_{FET}} \qquad (1.1)$$

where C_{FET} comprises capacitances of the gate oxide (C_{OX}) and depletion (C_b). These capacitances are negligible in Eq 1.1, because the magnitudes of these capacitances are smaller than C_{DL}. Thus, the FET response, the threshold voltage shift (ΔV_g), is related to the charge density of the FET gate surface, resulting in the FET characteristics shift depending on the charges of the target molecules (Figure 1.3). When the negative charge on the interface increases, the V_g-I_d curve shifts in the positive direction because the electron density in the channel decreases.

Moreover, key parameter of FET biosensing is the charge detectable region on the gate insulator surface. The region represents a thickness of the electric double-layer, Debye length (λ_D), since counter ion species screens charges of target molecules. The Debye length in buffer solution is given by;[24]

$$\lambda_D = \sqrt{\frac{\varepsilon_W \varepsilon_0 kT}{2 \times 10^3 N_A e^2 I}} \qquad (1.2)$$

where ε_0 and ε_w are the permittivities of a vacuum and water at 25ºC, respectively, k is the Boltzmann constant, T is the absolute temperature in Kelvin, N_A is the Avogadro constant, e is the elementary charge, and I is the ionic strength of buffer solution. According to Eq. 1.2, the Debye length is determined by the ionic strength of solution, and the length is approximately 1 nm under biological environment. It means that a FET

biosensor detects only the change in charge due to target molecules adsorbed near the gate interface. So far, several strategies have been proposed to overcome the problem of the Debye length in FET biosensors, as described below.

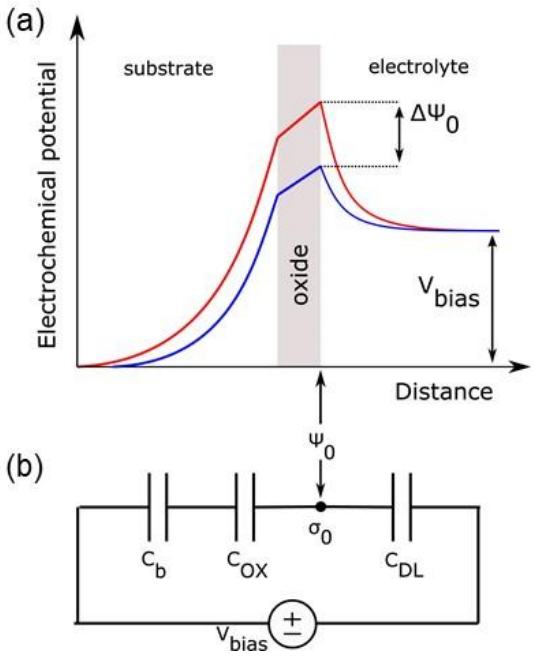

Figure 1.2 (a) Simplified model of potential diagram of ISFET with an oxide as the interfacial material. (b) Equivalent circuit model of the ISFET sensor. C_b, C_{OX}, C_{DL} and σ_0 represent the depletion capacitances, gate oxide, double-layer, and interfacial charge respectively. [23] Open Access Creative Commons Attribution-NonCommercial-No Derivatives License (CC BY NC ND) @ 2017 Elsevier B. V

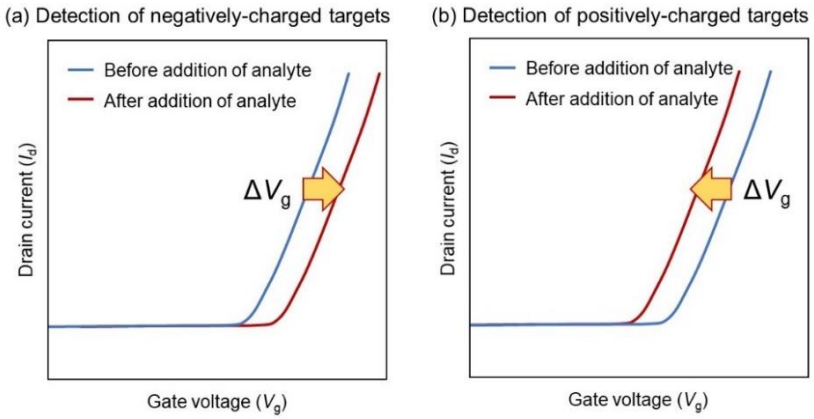

Figure 1.3 The threshold voltage shift (ΔV_g) of n-channel FET biosensors caused by the addition of (a) negatively and (b) positively charged targets, respectively.

First, the influence on the Debye length was reduced by the dilution of buffer solution. E. Stern *et al.* showed FET responses derived from biomolecules were depended on the ionic strength of buffer solution.[25] Under a low ionic strength, the FET responses were increased due to the expansion of the Debye length. Additionally, S. Hideshima *et al.* demonstrated the optimization of the ionic strength based on the charge distribution in a higher-order structure of biomolecule.[26] Second, small size receptors were used for the effective use of the Debye length.[27] When the buffering capacity of the measurement buffer solution is taken into account, there is an upper limit to the extension of the Debye length due to a reduction of the ionic strength. Small size receptors, such as antigen-binding fragment (Fab), single-chain variable fragment (scFv), glycan, and aptamer, etc., are useful for the improvement of the sensitivity of FET biosensors because of an increase in the number of captured target molecules within the Debye length.[27–31] Finally, N. Gao *et al.* proposed the application of a porous and biomolecule permeable polymer layer on the FET sensor.[32] A polyethylene glycol (PEG) layer enabled the detection of biomolecules under high ionic strength due to an increase in the effective Debye length in the region immediately adjacent to the FET gate surface (Figure 1.4). Recently, . Guti rrez-Sanz *et al.* demonstrated a combination of antibody fragments and PEG layer, resulting in the enhancement of FET responses to thyroid-stimulating hormone (TSH) in whole serum.[33]

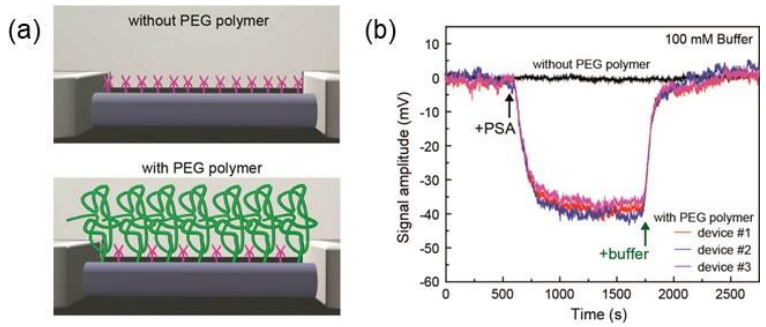

Figure 1.4 (a) Schematic illustration of a nanowire (NW) FET device (top) without and (bottom) with a PEG polymer modification. (b) Real-time PSA detection using NW FET devices with and without a PEG layer.[32] Reprinted with permission from Gao, N. *et al.* General strategy for biodetection in high ionic strength solutions using transistor-based nanoelectronic sensors. *Nano Lett.* 15, 2143–2148 (2015). Copyright (2015) American Chemical Society.

1.2.2 Classification of receptors for FET biosensors

FET biosensors are promising devices for the label-free detection of biomolecules, and thus much literature in terms of a design of biorecognition element of FET biosensor was reported. Generally, to design the biorecognition element of FET biosensors, each bioreceptor was immobilized to the FET gate surface via a self-assembled monolayer (SAM), such as silane coupling agents and alkanethiols.[34,35] FET biosensors are broadly classified into those that detect surface potential changes caused by products of catalytic reactions between enzymes and substrates and those that detect a change in charge density caused by receptor-ligand interactions; e.g., antigen-antibody interaction, glycan-lectin interaction, DNA hybridization, aptamer-target interaction. As shown in Figure 1.5, since the beginning of research on FET biosensors, it has been common to use enzymes and antibodies as receptors. In contrast, the number of publications on the FET biosensors functionalized by using DNA technology have been gradually increased since 2003. In addition, FET biosensors using glycans and lectins have been studied little by little in recent years. The details of each receptor were described as bellow.

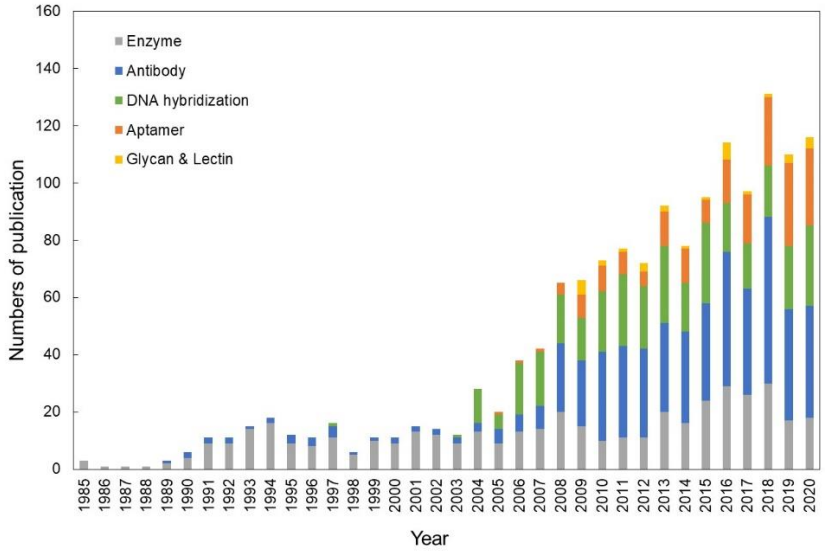

Figure 1.5 Number of publications related with field effect transistor biosensors from 1985 to 2020. Classification of receptors for FET biosensors is represented by (gray) enzyme, (blue) antibody, (green) DNA hybridization, (orange) aptamer, and (yellow) glycan and lectin. The data source was Clarivate Analytics Web of Science©.

(1) Enzyme

After the invention of the ISFET, J. Jarata *et al.* focused on pH responsiveness of ISFET and proposed the enzyme FET in 1975.[36] The enzyme FET consists of an enzyme or a membrane containing an enzyme immobilized on the FET gate surface. The concept of enzyme FET is to detect the pH change derived from the H^+ generated by the reaction between the enzyme and the substrate. After the proposition of the enzyme FET, S. Cars *et al.* demonstrated the detection of penicillin by a penicillinase-albumin membrane coated ISFET in 1980 (Figure 1.6).[37] Then, a lot of enzyme FETs have been reported to detect various substrates; e.g., urea, glucose, lactic acid, and acetylcholine.[38–43] Recently, immobilizing multiple enzymes to different elements on a single FET, which has several FET elements, for the simultaneous detection of substrates and employing the enzymatic cascade using multiple enzymes were examined.[44,45]

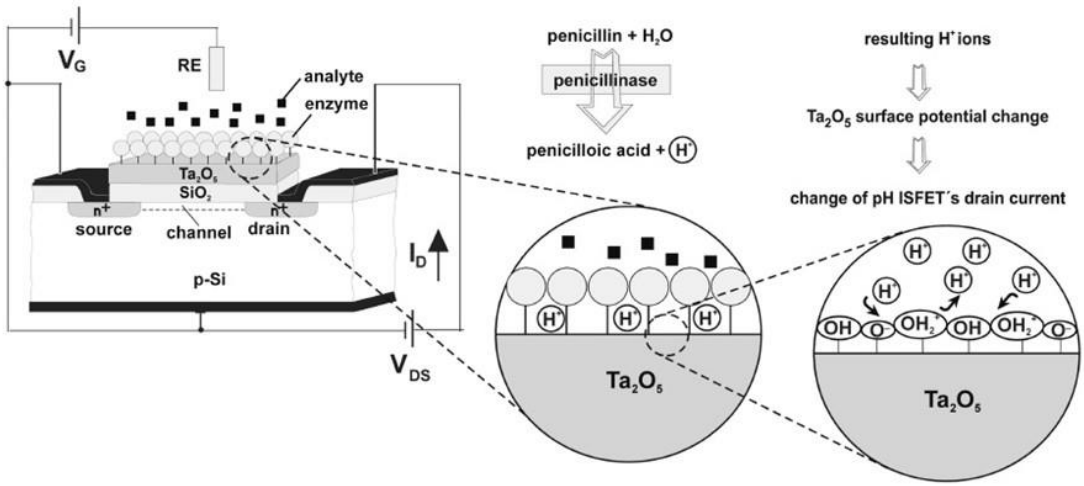

Figure 1.6 Schematic illustration of the enzyme FET and measurement principle. The penicillinase is immobilized on the Ta_2O_s gate oxide of a pH-sensitive ISFET.[46] Reprinted with permission from Schöning, M. J. & Poghossian, A. Recent advances in biologically sensitive field-effect transistors (BioFETs). *Analyst* 127, 1137–1151 (2002). Copyright (2002) Royal Society of Chemistry.

(2) Antibody

An antigen-antibody interaction has been applied to the biorecognition element of FET biosensors to detect various biomarkers. An antibody, immunoglobulins (Ig), produced by the immune system, have a high affinity and specificity for their target molecules. Thus, due to the broad affinity of antibodies, FET biosensors are able to detect various targets and are expected to be deployed in medical applications. The Immuno FETs were introduced by J. F. Schenck in 1978,[47] and a lot of many types of antibody-immobilized FET biosensors have been demonstrated (Figure 1.1). The sensing mechanism is that the charged antigens form a complex with the antibodies on the FET gate surface, and then the drain current is changed due to the change in the carrier concentration in a channel by electrostatic interaction.[48] Additionally, antibody fragments (F(ab')2, Fab, and scFv) could be generated by antibody cleavage or recombination techniques.[49] These fragments were applied to the FET receptor for the effective use of the Debye length, as mentioned above.[27,31]

Several immobilization methods have been investigated to induce antigen-antibody reactions on the FET gate surface efficiently. Classically, an antibody was immobilized via non-covalent bonding, such as electrostatic interaction, hydrophobic interactions, and van der Waals forces. In contrast, immobilization of antibodies by covalent bonding with SAM is commonly for the formation of a stable recognition interface.[50,51] However, the affinity of an antibody to an antigen is decreased due to random orientation on the surface. An intermediate protein with a natural affinity toward antibody was used for orientation of antibody.[50] Practically, an increase in the sensitivity of FET biosensors was demonstrated by immobilization of antibodies using protein G and protein A, which specifically recognizes the Fc region.[52]

(3) Glycan

Glycans, which are compounds of a large number of monosaccharides, contribute many biological reactions, such as cell adhesion, transmission, viral infection, and cancerization.[53] Hence, glycan has a potential of binding to various glycoproteins, viruses, and cells. So far, several examples have been applied as receptors for FET biosensors.[29,54–57] L. N. Cella *et al.* demonstrated the immobilization of polysaccharides on single-wall carbon nanotube (SWCNT) for the detection of glycan using displacement of plant lectin (concanavalin A) in 2010.[54] T. Osaka and his group reported the detection of charged lectin under high ionic strength using FET biosensor modified with small sialylglycan.[29] Additionally, they demonstrated the attomolar detection of hemagglutinin, an influenza viral protein, using the sialyllactose-immobilized FET biosensor.[56] Since glycans are expected to be candidates for receptors to detect various glycoproteins, which are biomarkers for many diseases and infections, and for glycan arrays, further research on the development of FET biosensors using glycans is required.

(4) DNA

With the advancement of nucleic acid technology, the applications of deoxyribonucleic acid (DNA) and ribonucleic acid (RNA) as receptors for biorecognition elements have attracted much attention. Hybridization, in which single-stranded DNA (ssDNA) and paired DNA are complementarily bound via high affinity, is first used as a recognition element in 1997. E. Souteyrand *et al.* reported DNA-FET using the DNA hybridization process.[58] As shown in Figure 1.7, double-stranded DNA (dsDNA) is formed by binding between ssDNA and complementary strands as a target DNA on the FET gate surface. As a result, the negative charges originated from the phosphate groups of the DNA backbone affect the FET characteristics.[46, 59]

Polymerase chain reaction (PCR), one of the DNA technologies, has also been applied to FET biosensors. After the hybridization between probe DNA and target DNA, DNA polymerase and deoxynucleotide (dCTP, dATP, dGTP, or dTTP) are added to the FET gate surface. As a result, DNA polymerase extends base sequence of the immobilized probe DNA, which results in increasing the number of negative charges on the FET gate surface (Figure 1.8).[60] Additionally, this PCR technique was applied to improve the sensitivity of DNA-FET to detect the hybridization phenomena.[61] Furthermore, ISFET detected the pH change caused by H^+ generated by PCR like a Enzyme FET.[21] This concept was then developed into a next-generation DNA sequencer by Ion torrent Systems, Inc. In recent years, FET biosensors using isothermal DNA amplification, such as rolling circle amplification (RCA) and loop-mediated isothermal amplification (LAMP), have been reported.[62,63] Therefore, the combination of DNA amplification technology and ISFETs will continue to attract attention.

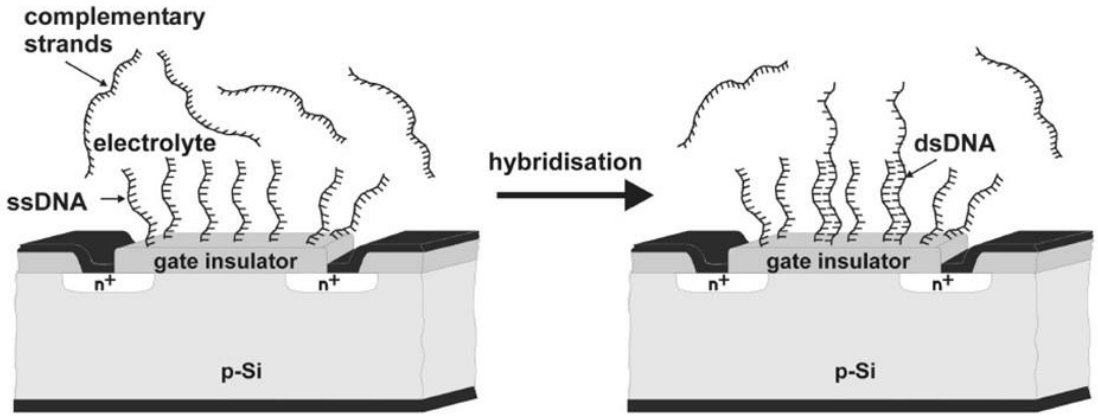

Figure 1.7 Schematic illustration of a DNA-FET and the principle of DNA-hybridisation detection.[46] Reprinted with permission from Schöning, M. J. & Poghossian, A. Recent advances in biologically sensitive field-effect transistors (BioFETs). *Analyst* 127, 1137–1151 (2002). Copyright (2002) Royal Society of Chemistry.

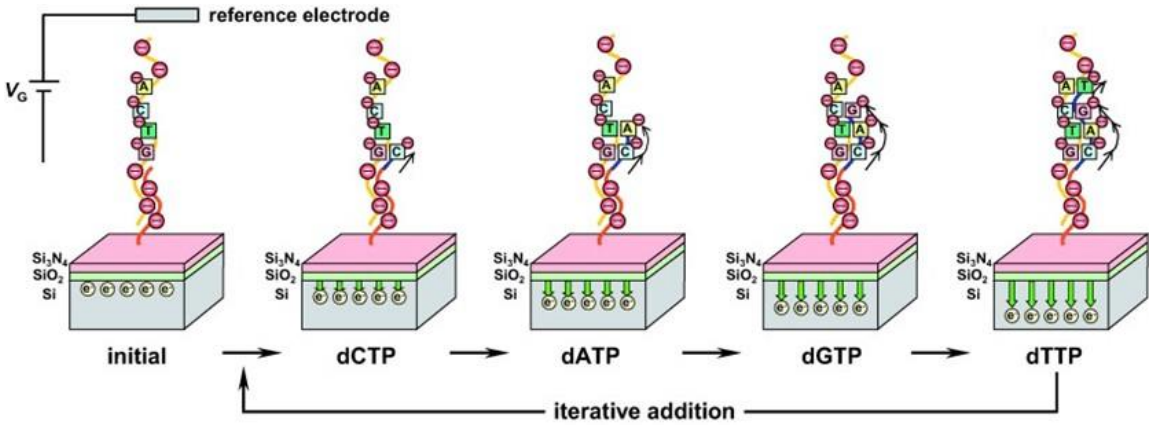

Figure 1.8 Schematic illustration of DNA sequencing using combination of FET sensing and an extension reaction. Deoxynucleotides, dCTP, dATP, dGTP, and dTTP, are added sequentially to the probe–target duplex on the FET.[60] Reprinted with permission from Sakata, T. & Miyahara, Y. DNA sequencing based on intrinsic molecular charges. *Angew. Chem. Ed.* 45, 2225–2228 (2006). Copyright (2006) John Wiley & Sons, Inc.

(5) Aptamer

Aptamers, which are short single-stranded DNA or RNA, are synthesized by selection from a large oligonucleotide library. The technology was developed in 1980 and named the systematic evolution of ligands by exponential enrichment (SELEX) or *in vitro* selection.[64,65] As aptamers have excellent properties such as affinity for various molecules, chemical stability, and low cost, they are expected to be bio-receptors as an alternative to antibodies.[66,67] Aptamers show a wide range of affinity to various molecules; metal ions, organic compounds, proteins, viral particles, and many more.[68–72] From these advantages, aptamers have been applied to FET biosensors. H.-M. So *et al.* firstly reported that aptamers were immobilized on single-walled carbon nanotube (SWCNT) FET to detect thrombin in 2005.[73] Moreover, K. Maehashi *et al.* showed the advantages of small aptamer as a FET receptor compared with monoclonal antibody due to overcoming the limitation of the Debye screening effect (Figure 1.9).[28]

A specific feature of aptamers is that the ease of structural design allows linking aptamers with multiple functions. Thus, aptamers are able to be designed to introduce the target-binding region and structure-switching region. N. Nakatsuka *et al.* demonstrated the detection of uncharged molecules, dopamine, serotonin, glucose, and sphingosine-1-phosphate (S1P), by FET biosensors using a conformational change of aptamers (Figure 1.10).[74] This concept enables the detection of uncharged molecules, which have been difficult to measure with FET biosensors, resulting in the expansion of variation of target molecules. Additionally, different strategies of FET biosensor detection using aptamers have also been proposed; e.g., desorption of aptamers by binding of target molecules, co-immobilization of multiple aptamers, and introduction of extra charges by aptamers.[75–77] From these backgrounds, a lot of investigation of aptamer FETs is expected to continue for the development of the FET biosensors.

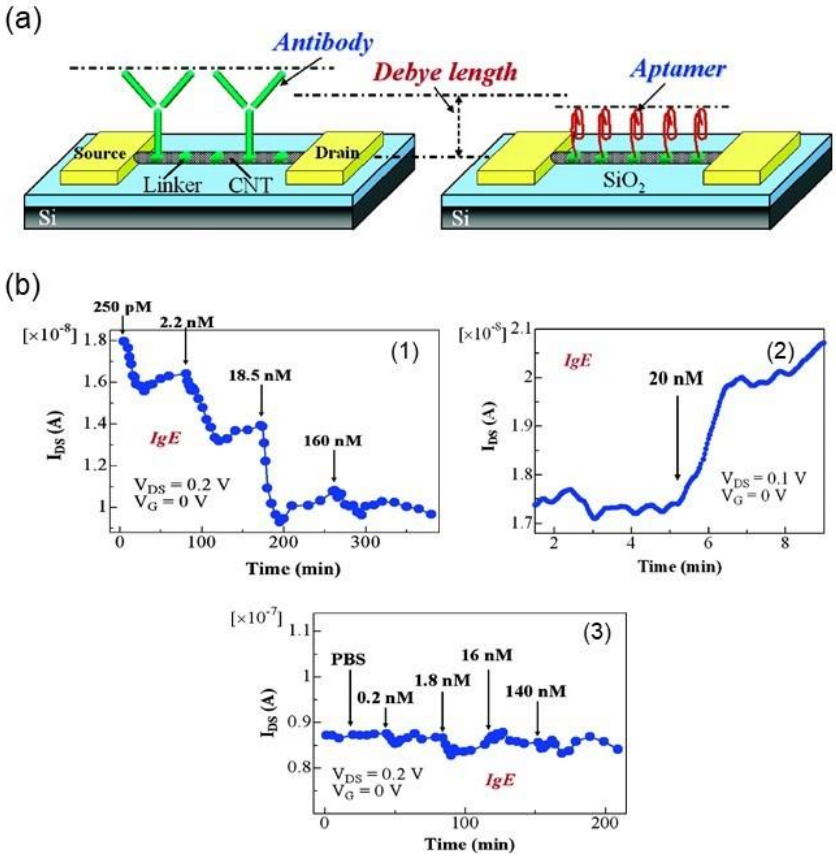

Figure 1.9 (a) Schematic images of antibody-modified CNT-FET and aptamer-modified CNT-FET for label-free detection. (b) Real-time measurement of the CNT-FET after the introduction of target IgE at various concentrations onto (1) the aptamer-modified CNT-FET, (2) the bare CNT-FET, and (3) the antibody-modified CNT-FET. [28] Reprinted with permission from Maehashi, K. *et al.* Label-free protein biosensor based on aptamer-modified carbon nanotube field-effect transistors. *Anal. Chem.* 79, 782–787 (2007). Copyright (2007) American Chemical Society.

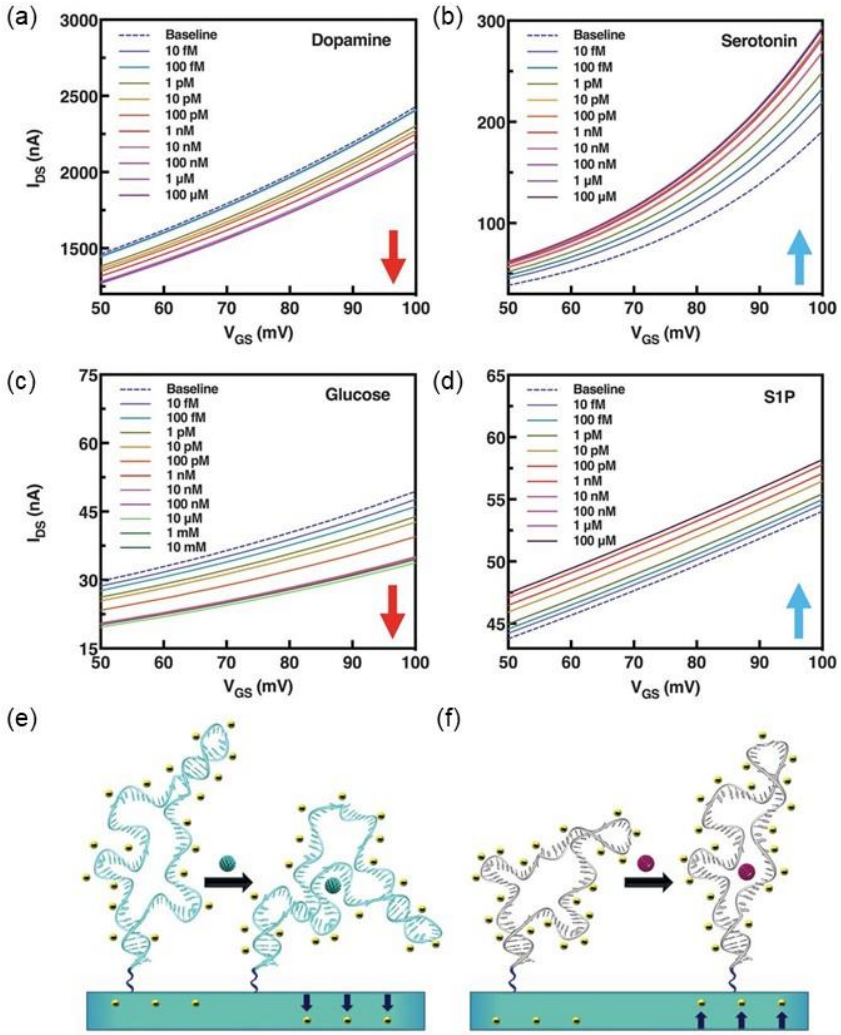

Figure 1.10 Sensing mechanism of the aptamer-immobilized FET biosensor. Dependence of source-drain currents caused by the addition of analytes with different concentrations (a) dopamine, (b) serotonin, (c) glucose and (d) S1P. (e and f) Sensing mechanism of stem-loop aptamer-immobilized FET biosensor. Target-induced reorientations of aptamer change the charge density within the Debye length from the FET gate surface. Aptamer molecules reorient (e) closer or (f) away from FET gate surface. Schematics are idealized and do not reflect individual aptamer secondary structural motifs.[74] From Nakatsuka, N. *et al.* Aptamer-field-effect transistors overcome Debye length limitations for small-molecule sensing. *Science* 362, 319–324 (2018). Reprinted with permission from AAAS.

1.2.3 Nanomaterials for the FET biosensor

Among the components of a biosensor, the transducer converts the phenomenon in the recognition element into a signal. Therefore, improving the performance of the transducer leads to an increase in sensitivity. To date, various nanomaterials, such as one-dimensional materials (carbon nanotube: CNT, and silicon nanowire: SiNW) and two-dimensional materials (graphene, transition metal dichalcogenide, black phosphorus, and MXene), have been applied to FET biosensors as channel materials because of their unique structure and properties.

In one-dimensional materials, single-wall carbon nanotube (SWCNT) and multi-wall carbon nanotube (MWCNT) FETs were introduced by S. J. Tans and R. Martel in 1998.[78,79] Since the CNT showed excellent mechanical, thermal, and electrical properties, CNT could complement silicon materials in FET biosensors. Then, CNT-based FETs were demonstrated as biosensors.[78,79] Recently, a horizontally aligned CNT-based FET sensing platform was proposed to improve the sensitivity for the detection of interleukin-6 (IL-6). This platform showed high selectivity and sensitivity compared with comparable ELISA and other assays.[80] Moreover, SiNW, developed in 2001,[81] was used as a channel material in FET, improving sensor sensitivity over planar silicon-based FET due to an increase in surface area to volume.[82–84] Recently, the honeycomb structure SiNW-FET demonstrated more sensitive detection of cardiac troponin I than the linear SiNW-FET.[85]

Nowadays, two-dimensional materials have attracted great attention due to their unique chemical and physical properties.[86] In particular, graphene shows a zero-band gap semiconductor and higher electron mobility, and thus it has been applied to various devices. After the first report about the graphene FET,[87] the formation of biorecognition elements on graphene FETs to sensitively detect various biomolecules has been demonstrated.[88] Furthermore, MoS_2,[89,90] phosphorene,[91,92] and MXene[93] FET biosensors are recently developed as new-nanomaterials FET biosensors. For the practical application of FET biosensors exploiting these new materials, it will be necessary to solve issues such as simplification of manufacturing and cost reduction.

1.3 Outline of this Thesis

This thesis describes the guidelines of the design on FET biosensing interface suitable for binding to target molecules based on the characteristics of receptors and their biomolecular interaction. So far, antigen-antibody reaction has been widely used to form the molecular recognition interface of FET biosensors (Figure 1.5). However, to improve the sensitivity of antibody-immobilized FET biosensors for practical use, the fragmentation process of antibodies, the control of their orientation, and their short stability due to denaturation are issues to be addressed. In order to overcome the issue for the practical application and promote the development of FET biosensors, it is necessary to expand the method of functionalizing the sensor interface using other receptors. In this research, interfacial design of FET biosensor was attempted using glycan, lectin, and aptamers. Additionally, the detection of target molecules in biological samples using FET biosensors was demonstrated toward practical application.

In Chapter 2, a glycan-lectin interaction, which is involved in various biological reactions, was applied to the molecular recognition interface of FET biosensors. Basically, the sensitivity of biosensors depends on the number of adsorption sites and their affinity to the target molecule. The interaction between glycans and lectins is strengthened by the occurrence of the cluster glycoside effect due to multivalent bonds. In addition, lectin molecules are multimerized to lead to the expression of the effect.[94,95] Thus, features of multimeric lectin and the cluster glycoside effect on the detection sensitivity of FET biosensors were clarified.

Chapter 2.1 describes the evaluation of the usefulness of multimeric lectin as a receptor of FET biosensors. As described in chapter 1.2.2 (2), since the random orientation of a receptor reduces its affinity, increasing the number of effective binding sites improves sensor sensitivity. Here, to assess multimeric and symmetric lectin for the suppression of the influence of the random orientation, electrical responses of lectin-immobilized FET biosensor were compared with FET biosensor functionalized with antigen-binding fragment (Fab), which has one binding site. In this chapter, a tetrameric

jacalin, which has symmetrically four glycan-binding sites to secretory immunoglobulin A (s-IgA), was selected as a receptor of the FET biosensor. Additionally, the detection of s-IgA in human sweat using the jacalin-immobilized FET biosensor was demonstrated.

Chapter 2.2 describes the detection of an influenza virus (IFV) under high ionic strength using the glycan-immobilized FET biosensor. The dense and highly oriented glycan-immobilized surface was expected to show the cluster glycoside effect with infectious viruses, which have a large number of lectin molecules on the viral membrane. Hence, the charge distribution of an IFV detected by the glycan-immobilized FET biosensor was considered to evaluate the cluster glycoside effect. Furthermore, I attempted to detect IFV particles in human nasal mucus by exploiting the viscosity reduction treatment using L-cysteine ethyl ester (LCEE).

Chapter 3 describes the control of the immobilization density of aptamers based on their characteristics from detection of the stress markers, chromogranin A (CgA), s-IgA, and cortisol. As described in chapter 1.2.2 (5), aptamers are attracting attention as alternative receptors to antibodies. Design of the aptamer-immobilized surface to cause efficient capture of the target molecule will lead to the development of aptamer immobilization FETs. Generally, aptamer immobilization conditions are determined by optimizing the concentration and incubation time during immobilization. Thus, controlling the immobilization state of aptamers is an important topic for the development of FET biosensors. Here, I examined a method to control the immobilization density of aptamer on the FET biosensing surface to increase the number of available binding sites. Briefly, controlling immobilization density was demonstrated based on characteristics of aptamers; (1) changes in the electrostatic interaction between aptamer molecules by varying the ionic strength of buffer solution during immobilization and (2) inducing the conformational change of aptamer to suppress the steric hindrance between immobilized aptamers for the detection of uncharged molecules.

References

1. Kassebaum, N. J. *et al.* Global, regional, and national disability-adjusted life-years (DALYs) for 315 diseases and injuries and healthy life expectancy (HALE), 1990–2015: a systematic analysis for the Global Burden of Disease Study 2015. *Lancet* **388**, 1603–1658 (2016).
2. Cohen, M. L. Changing patterns of infectious disease. *Nature* **406**, 762–767 (2000).
3. Siegel, R. L., Miller, K. D. & Jemal, A. Cancer statistics, 2020. *CA. Cancer J. Clin.* **70**, 7–30 (2020).
4. Liu, Q. *et al.* Changes in the global burden of depression from 1990 to 2017: Findings from the Global Burden of Disease study. *J. Psychiatr. Res.* **126**, 134–140 (2019).
5. Moreno, C. *et al.* How mental health care should change as a consequence of the COVID-19 pandemic. *The Lancet Psychiatry* **7**, 813–824 (2020).
6. Ettman, C. K. *et al.* Prevalence of Depression Symptoms in US Adults Before and During the COVID-19 Pandemic. *JAMA Netw. open* **3**, e2019686 (2020).
7. Pfefferbaum, B. & North, C. S. Mental Health and the Covid-19 Pandemic. *N. Engl. J. Med.* **383**, 510–512 (2020).
8. Grieshaber, D., Mackenzie, R., Vörös, J. & Reimhult, E. Electrochemical Biosensors-Sensor Principles and Architectures. *Sensors* **8**, 1400–1458 (2008).
9. Kato, K., Haguchi, Y., Fukui, H. & Ishikawa, E. Enzyme-Linked Immunoassay: Conjugation of Rabbit Anti-(Human Immunoglobulin G) Antibody with β-d-Galactosidase from Escherichia coli and Its Use for Human Immunoglobulin G Assay. *Eur. J. Biochem.* **62**, 285–292 (1976).
10. RK Saiki, S Scharf, F Faloona, KB Mullis, GT Horn, HA Erlich, N. A. Enzymatic amplification of beta-globin genomic sequences and restriction site analysis for diagnosis of sickle cell anemia. 1985. *Science* **230**, 1350–1354 (1985).
11. S.A. Deepak *et al.* Real-Time PCR: Revolutionizing Detection and Expression Analysis of Genes. *Curr. Genomics* **8**, 234–251 (2007).
12. Khamrin, P. *et al.* Evaluation of immunochromatography and commercial enzyme-linked immunosorbent assay for rapid detection of norovirus antigen in stool samples. *J. Virol. Methods* **147**, 360–363 (2008).
13. Posthuma-Trumpie, G. A., Korf, J. & Van Amerongen, A. Lateral flow (immuno)assay: Its strengths, weaknesses, opportunities and threats. A literature survey. *Anal. Bioanal. Chem.* **393**, 569–582 (2009).
14. Caruso, F., Rodda, E. & Furlong, D. N. Quartz crystal microbalance study of DNA

immobilization and hybridization for nucleic acid sensor development. *Anal. Chem.* **69**, 2043–2049 (1997).

15. Vashist, S. K. & Vashist, P. Recent advances in quartz crystal microbalance-based sensors. *J. Sensors* **2011**, 571405 (2011).
16. Cheng, C. I., Chang, Y. P. & Chu, Y. H. Biomolecular interactions and tools for their recognition: Focus on the quartz crystal microbalance and its diverse surface chemistries and applications. *Chem. Soc. Rev.* **41**, 1947–1971 (2012).
17. Homola, J. Surface plasmon resonance sensors for detection of chemical and biological species. *Chem. Rev.* **108**, 462–493 (2008).
18. Nguyen, H. H., Park, J., Kang, S. & Kim, M. Surface plasmon resonance: A versatile technique for biosensor applications. *Sensors* **15**, 10481–10510 (2015).
19. Bhattacharyya, I. M. *et al.* Specific and label-free immunosensing of protein-protein interactions with silicon-based immunoFETs. *Biosens. Bioelectron.* **132**, 143–161 (2019).
20. Bergveld, P. Development of an Ion-Sensitive Solid-State Device for Neurophysiological Measurements. *IEEE Trans. Biomed. Eng.* **BME-17**, 70–71 (1970).
21. Rothberg, J. M. *et al.* An integrated semiconductor device enabling non-optical genome sequencing. *Nature* **475**, 348–352 (2011).
22. Shoorideh, K. & Chui, C. O. On the origin of enhanced sensitivity in nanoscale FET-based biosensors. *Proc. Natl. Acad. Sci. U. S. A.* **111**, 5111–5116 (2014).
23. Kaisti, M. Detection principles of biological and chemical FET sensors. *Biosens. Bioelectron.* **98**, 437–448 (2017).
24. Huang, W., Diallo, A. K., Dailey, J. L., Besar, K. & Katz, H. E. Electrochemical processes and mechanistic aspects of field-effect sensors for biomolecules. *J. Mater. Chem. C* **3**, 6445–6470 (2015).
25. Stern, E. *et al.* Importance of the debye screening length on nanowire field effect transistor sensors. *Nano Lett.* **7**, 3405–3409 (2007).
26. Hideshima, S. *et al.* Theoretical Optimization Method of Buffer Ionic Concentration for Protein Detection Using Field Effect Transistors. *J. Electrochem. Soc.* **157**, J410 (2010).
27. Kim, J. P., Lee, B. Y., Hong, S. & Sim, S. J. Ultrasensitive carbon nanotube-based biosensors using antibody-binding fragments. *Anal. Biochem.* **381**, 193–198 (2008).
28. Maehashi, K. *et al.* Label-free protein biosensor based on aptamer-modified carbon nanotube field-effect transistors. *Anal. Chem.* **79**, 782–787 (2007).

29. Nakamura, T., Sakurai, Y., Hideshima, S., Kuroiwa, S. & Osaka, T. Sialylglycan-modified field effect transistor for detection of charged lectin under physiological conditions. *Chem. Lett.* **39**, 1245–1247 (2010).
30. Hideshima, S. *et al.* A label-free electrical assay of fibrous amyloid β based on semiconductor biosensing. *Chem. Commun.* **50**, 3476–3479 (2014).
31. Gao, Z. *et al.* Graphene transistor arrays functionalized with genetically engineered antibody fragments for Lyme disease diagnosis. *2D Mater.* **7**, 024001 (2020).
32. Gao, N. *et al.* General strategy for biodetection in high ionic strength solutions using transistor-based nanoelectronic sensors. *Nano Lett.* **15**, 2143–2148 (2015).
33. Gutiérrez-Sanz, Ó., Andoy, N. M., Filipiak, M. S., Haustein, N. & Tarasov, A. Direct, Label-Free, and Rapid Transistor-Based Immunodetection in Whole Serum. *ACS Sensors* **2**, 1278–1286 (2017).
34. Chaki, N. K. & Vijayamohanan, K. Self-assembled monolayers as a tunable platform for biosensor applications. *Biosens. Bioelectron.* **17**, 1–12 (2002).
35. Vashist, S. K., Lam, E., Hrapovic, S., Male, K. B. & Luong, J. H. T. Immobilization of Antibodies and Enzymes on Platforms for Biosensors and Diagnostics. *Chem. Rev.* **114**, 11083–11130 (2014).
36. Johnson, C. C., Moss, D. S. & Janata, J. A. Selective chemical sensitive FET transducers. U.S. Patent US-4020830-A (1975).
37. Caras, S. & Janata, J. Field effect transistor sensitive to penicillin. *Anal. Chem.* **52**, 1935–1937 (1980).
38. Caras, S. D., Petelenz, D. & Janata, J. pH-Based Enzyme Potentiometric Sensors. Part 2. Glucose-Sensitive Field Effect Transistor. *Anal. Chem.* **57**, 1920–1923 (1985).
39. Miyahara, Y., Moriizumi, T. & Ichimura, K. Integrated enzyme fets for simultaneous detections of urea and glucose. *Sensors and Actuators* **7**, 1–10 (1985).
40. Gotoh, M., Tamiya, E., Seki, A., Shimizu, I. & Karube, I. Glucose Sensor Based on an Amorphous Silicon Isfet. *Anal. Lett.* **22**, 309–322 (1989).
41. Miyahara, Y., Tsukada, K., Miyagi, H. & Simon, W. Urea sensor based on an ammonium-ion-sensitive field-effect transistor. *Sensors Actuators B. Chem.* **3**, 287–293 (1991).
42. Zayats, M., Kharitonov, A. B., Katz, E., Buückmann, A. F. & Willner, I. An integrated NAD+-dependent enzyme-functionalized field-effect transistor (ENFET) system: Development of a lactate biosensor. *Biosens. Bioelectron.* **15**, 671–680 (2000).
43. Kharitonov, A. B., Zayats, M., Lichtenstein, A., Katz, E. & Willner, I. Enzyme

monolayer-functionalized field-effect transistors for biosensor applications. *Sensors Actuators, B Chem.* **70**, 222–231 (2000).

44. Berninger, T., Bliem, C., Piccinini, E., Azzaroni, O. & Knoll, W. Cascading reaction of arginase and urease on a graphene-based FET for ultrasensitive, real-time detection of arginine. *Biosens. Bioelectron.* **115**, 104–110 (2018).
45. Bay, H. H. *et al.* Hydrogel Gate Graphene Field-Effect Transistors as Multiplexed Biosensors. *Nano Lett.* **19**, 2620–2626 (2019).
46. Schöning, M. J. & Poghossian, A. Recent advances in biologically sensitive field-effect transistors (BioFETs). *Analyst* **127**, 1137–1151 (2002).
47. Cheung, P. W. *Theory, design, and biomedical applications of solid state chemical sensors*. (CRC Press, 1978).
48. Schasfoort, R. B. M., Bergveld, P., Kooyman, R. P. H. & Greve, J. Possibilities and limitations of direct detection of protein charges by means of an immunological field-effect transistor. *Anal. Chim. Acta* **238**, 323–329 (1990).
49. Conroy, P. J., Hearty, S., Leonard, P. & O'Kennedy, R. J. Antibody production, design and use for biosensor-based applications. *Semin. Cell Dev. Biol.* **20**, 10–26 (2009).
50. Trilling, A. K., Beekwilder, J. & Zuilhof, H. Antibody orientation on biosensor surfaces: A minireview. *Analyst* **138**, 1619–1627 (2013).
51. Hideshima, S., Sato, R., Kuroiwa, S. & Osaka, T. Fabrication of stable antibody-modified field effect transistors using electrical activation of Schiff base cross-linkages for tumor marker detection. *Biosens. Bioelectron.* **26**, 2419–2425 (2011).
52. Oh, J. *et al.* A carbon nanotube metal semiconductor field effect transistor-based biosensor for detection of amyloid-beta in human serum. *Biosens. Bioelectron.* **50**, 345–350 (2013).
53. Varki, A. Biological roles of glycans. *Glycobiology* **27**, 3–49 (2017).
54. Cella, L. N., Chen, W., Myung, N. V. & Mulchandani, A. Single-walled carbon nanotube-based chemiresistive affinity biosensors for small molecules: Ultrasensitive glucose detection. *J. Am. Chem. Soc.* **132**, 5024–5026 (2010).
55. Vedala, H. *et al.* Nanoelectronic detection of lectin-carbohydrate interactions using carbon nanotubes. *Nano Lett.* **11**, 170–175 (2011).
56. Hideshima, S. *et al.* Attomolar detection of influenza A virus hemagglutinin human H1 and avian H5 using glycan-blotted field effect transistor biosensor. *Anal. Chem.* **85**, 5641–5644 (2013).
57. Zhang, G. J., Huang, M. J., Ang, J. J., Yao, Q. & Ning, Y. Label-free detection of carbohydrate-protein interactions using nanoscale field-effect transistor biosensors.

Anal. Chem. **85**, 4392–4397 (2013).

58. Souteyrand, E. *et al.* Direct detection of the hybridization of synthetic homo-oligomer DNA sequences by field effect. *J. Phys. Chem. B* **101**, 2980–2985 (1997).
59. Ohtake, T., Hamai, C., Uno, T., Tabata, H. & Kawai, T. Immobilization of probe DNA on Ta2O2 thin film and detection of hybridized helix DNA using IS-FET. *Japanese J. Appl. Physics, Part 2 Lett.* **43**, L1137 (2004).
60. Sakata, T. & Miyahara, Y. DNA sequencing based on intrinsic molecular charges. *Angew. Chem. Ed.* **45**, 2225–2228 (2006).
61. Gao, A. *et al.* Signal-to-noise ratio enhancement of silicon nanowires biosensor with rolling circle amplification. *Nano Lett.* **13**, 4123–4130 (2013).
62. Duarte-Guevara, C. *et al.* On-chip electrical detection of parallel loop-mediated isothermal amplification with DG-BioFETs for the detection of foodborne bacterial pathogens. *RSC Adv.* **6**, 103872–103887 (2016).
63. Veigas, B. *et al.* Quantitative real-time monitoring of RCA amplification of cancer biomarkers mediated by a flexible ion sensitive platform. *Biosens. Bioelectron.* **91**, 788–795 (2017).
64. Tuerk, C. & Gold, L. Systematic evolution of ligands by exponential enrichment: RNA ligands to bacteriophage T4 DNA polymerase. *Science* **249**, 505–510 (1990).
65. Ellington, A. D. & Szostak, J. W. In vitro selection of RNA molecules that bind specific ligands. *Nature* **346**, 818–822 (1990).
66. Crivianu-Gaita, V. & Thompson, M. Aptamers, antibody scFv, and antibody Fab' fragments: An overview and comparison of three of the most versatile biosensor biorecognition elements. *Biosens. Bioelectron.* **85**, 32–45 (2016).
67. Toh, S. Y., Citartan, M., Gopinath, S. C. B. & Tang, T. H. Aptamers as a replacement for antibodies in enzyme-linked immunosorbent assay. *Biosens. Bioelectron.* **64**, 392–403 (2015).
68. Pan, W. *et al.* Isolation of virus-neutralizing RNAs from a large pool of random sequences. *Proc. Natl. Acad. Sci. U. S. A.* **92**, 11509–11513 (1995).
69. Ciesiolka, J. & Yarus, M. Small RNA-divalent domains. *RNA* **2**, 785–793 (1996).
70. Minagawa, H. *et al.* Selection, Characterization and Application of Artificial DNA Aptamer Containing Appended Bases with Sub-nanomolar Affinity for a Salivary Biomarker. *Sci. Rep.* **7**, 42716 (2017).
71. Kaneko, N. *et al.* An aptamer-based biosensor for direct, label-free detection of melamine in raw milk. *Sensors* **18**, 3227 (2018).
72. Minagawa, H. *et al.* Fluorescence Polarization-Based Rapid Detection System for Salivary Biomarkers Using Modified DNA Aptamers Containing Base-Appended

Bases. *Anal. Chem.* **92**, 1780–1787 (2020).

73. So, H. M. *et al.* Single-walled carbon nanotube biosensors using aptamers as molecular recognition elements. *J. Am. Chem. Soc.* **127**, 11906–11907 (2005).
74. Nakatsuka, N. *et al.* Aptamer-field-effect transistors overcome Debye length limitations for small-molecule sensing. *Science* **362**, 319–324 (2018).
75. Das, B. K. *et al.* Single-walled carbon nanotubes chemiresistor aptasensors for small molecules: Picomolar level detection of adenosine triphosphate. *Chem. Commun.* **47**, 3793–3795 (2011).
76. Goda, T. *et al.* Dual aptamer-immobilized surfaces for improved affinity through multiple target binding in potentiometric thrombin biosensing. *Biosens. Bioelectron.* **73**, 174–180 (2015).
77. Vu, C. A., Hu, W. P., Yang, Y. S., Chan, H. W. H. & Chen, W. Y. Signal Enhancement of Silicon Nanowire Field-Effect Transistor Immunosensors by RNA Aptamer. *ACS Omega* **4**, 14765–14771 (2019).
78. You, A., Be, M. A. Y. & In, I. Single- and multi-wall carbon nanotube field- effect transistors. *Appl. Phys. Lett.* **73**, 2447–2449 (1998).
79. Tans, S. J., Verschueren, A. R. M. & Dekker, C. Room-temperature transistor based on a single carbon nanotube. *Nature* **393**, 49–52 (1998).
80. Chen, H. *et al.* Label-free electronic detection of interleukin-6 using horizontally aligned carbon nanotubes. *Mater. Des.* **90**, 852–857 (2016).
81. Cui, Y., Wei, Q., Park, H. & Lieber, C. M. Nanowire nanosensors for highly sensitive and selective detection of biological and chemical species. *Science* **293**, 1289–1292 (2001).
82. Patolsky, F. *et al.* Electrical detection of single viruses. *Proc. Natl. Acad. Sci. U. S. A.* **101**, 14017–14022 (2004).
83. Chen, K. I., Li, B. R. & Chen, Y. T. Silicon nanowire field-effect transistor-based biosensors for biomedical diagnosis and cellular recording investigation. *Nano Today* **6**, 131–154 (2011).
84. Noor, M. O. & Krull, U. J. Silicon nanowires as field-effect transducers for biosensor development: A review. *Anal. Chim. Acta* **825**, 1–25 (2014).
85. Kim, K. *et al.* Silicon nanowire biosensors for detection of cardiac troponin I (cTnI) with high sensitivity. *Biosens. Bioelectron.* **77**, 695–701 (2016).
86. Bolotsky, A. *et al.* Two-Dimensional Materials in Biosensing and Healthcare: From in Vitro Diagnostics to Optogenetics and beyond. *ACS Nano* **13**, 9781–9810 (2019).
87. Novoselov, K. S. *et al.* Electric Field Effect in Atomically Thin Carbon Films.

Science **306**, 666–669 (2004).

88. Fu, W., Jiang, L., van Geest, E. P., Lima, L. M. C. & Schneider, G. F. Sensing at the Surface of Graphene Field-Effect Transistors. *Adv. Mater.* **29**, 1603610 (2017).
89. Lee, J. *et al.* Two-dimensional layered MoS2 biosensors enable highly sensitive detection of biomolecules. *Sci. Rep.* **4**, 7352 (2014).
90. Sarkar, D. *et al.* MoS2 field-effect transistor for next-generation label-free biosensors. *ACS Nano* **8**, 3992–4003 (2014).
91. Chen, Y. *et al.* Field-effect transistor biosensors with two-dimensional black phosphorus nanosheets. *Biosens. Bioelectron.* **89**, 505–510 (2017).
92. Sang, D. K., Wang, H., Guo, Z., Xie, N. & Zhang, H. Recent Developments in Stability and Passivation Techniques of Phosphorene toward Next-Generation Device Applications. *Adv. Funct. Mater.* **29**, 1903419 (2019).
93. Xu, B. *et al.* Ultrathin MXene-Micropattern-Based Field-Effect Transistor for Probing Neural Activity. *Adv. Mater.* **28**, 3333–3339 (2016).
94. Lis, H. & Sharon, N. Lectins: Carbohydrate-specific proteins that mediate cellular recognition. *Chem. Rev.* **98**, 637–674 (1998).
95. Lundquist, J. J. & Toone, E. J. The cluster glycoside effect. *Chem. Rev.* **102**, 555–578 (2002).

Chapter 2:

Development of FET biosensor based on glycan-lectin interaction for the detection of biomolecules

2.1 Evaluation of tetrameric jacalin as a receptor of FET biosensor for detection of secretory immunoglobulin A (s-IgA) in human sweat

2.1.1 Introduction

FET biosensors are devices that detect changes in the charge density (σ_0) on the biofunctionalized FET gate surface. As the changes in the charge density is originated from the intrinsic charges of the target molecule, increasing the number of target molecules captured by immobilized receptors leads to the improvement of the sensitivity of the FET biosensors. The binding isotherm between receptors and target molecules is the following relationship:

$$[\mathrm{R}] + [\mathrm{L}] \underset{k_{\mathrm{off}}}{\overset{k_{\mathrm{on}}}{\rightleftarrows}} [\mathrm{RL}] \tag{2.1.1}$$

where [R] is the receptor concentration, [L] is the ligand concentration, [RL] is the complex concentration, k_{on} is the association rate constant, and k_{off} is the dissociation rate constant, respectively. Then, when adsorption and desorption are in equilibrium, the standard saturation isotherm is given by:

$$[\mathrm{RL}] = \frac{[\mathrm{L}][\mathrm{R_{tot}}]}{[\mathrm{L}] + K_d} \tag{2.1.2}$$

where K_d is dissociation constant (= k_{off}/k_{on}). Moreover, it should be noted that receptor concentration is defined as $[R] = [R_{tot}] - [RL]$ ($[R_{tot}]$ is a toral concentration of receptor), since it depends on the concentration of the complex of receptors and target molecules. From Eq. 2.1.2, increasing the number of effective receptors on the sensing surface contributes to improving the sensitivity of FET biosensors.

However, covalent immobilization of receptors raises disordered receptor orientation, and the binding capability of the receptor was decreased due to steric hindrance with an interface or adjacent receptors.[1] For this reason, it has been reported that the use of linkers such as protein A and G is effective for a method of orienting antibody.[1–3] Considering the Debye length, which is the charge detectable range on FET biosensors, the linker makes it difficult to capture the target molecule within the region.

Lectins, glycan-binding proteins are widely expressed in nature, are often multimeric in order to bind several glycans.[4] Moreover, each monomer of a lectin molecule has a glycan-binding site, which is located at various positions in its structure. Among them, I focused on lectins with point-symmetric glycan-binding sites in the structure, because they could provide effective binding sites on the sensor surface even in the case of random orientation. In this chapter, jacalin, which has four glycan binding sites symmetrically, was selected as the receptor for the FET biosensor. Jacalin, which is a small plant-derived lectin that is inexpensively extracted from jackfruit (*Artocarpus heterophyllus*) seeds, specifically recognizes *O*-glycans, galactose-β1-3-*N*-acetyl-galactosamine (Galβ1-3GalNAc) and *N*-acetylgalactosamine (GalNAc).[5,6] It is known that the jacalin interacts with secretory immunoglobulin A (s-IgA), which is a dimer of IgA, by binding with glycans at the hinge site. s-IgA is a stress marker present in non-invasive biological fluids such as saliva and sweat.[7–10] Thus, non-invasive s-IgA detection is expected to be enabled by FET biosensors functionalized with jacalin molecules. In this chapter, to evaluate the reduction of the effect of random orientation by multimeric and symmetric lectins, the detection of s-IgA using the jacalin-immobilized FET biosensor was demonstrated (Figure 2.1.1).

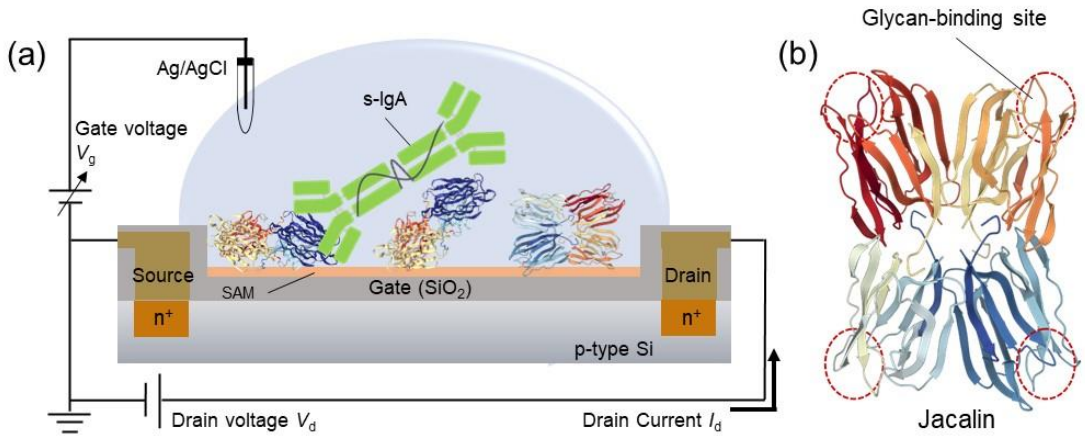

Figure 2.1.1 (a) Schematic images of the jacalin-immobilized FET biosensor for the detection of s-IgA. (b) The crystal structure of jacalin from the protein data bank (1JAC).[11]

2.1.2 Experimental

2.1.2.1 Fabrication procedure of jacalin-immobilized FET biosensor

The n-type FET device with a SiO_2 gate insulator (10 μm in length × 1000 μm in length), which was produced by Toppan Printing Co., Ltd., was sonicated in acetone, a mixture of toluene and methanol (1:1) for 10 min, in that order. To introduce silanol groups on the SiO_2 surface, the cleaned FET chips were exposed to O_2 plasma ashing (200 W, 1 min) using a gas plasma reactor (PR301, Yamato Scientific Co., Ltd.). Following that, a self-assembled monolayer, aminopropylsilane (APS), was formed on the SiO_2 insulator surface by immersing in 1%(v/w) 3-aminopropyltriethoxysilane (APTES, Sigma-Aldrich Inc.) diluted in toluene (60°C, 7 min) under Ar atmosphere. The FET chip was then rinsed with ethanol and sonicated in a mixture solution of methanol and toluene (1:1) for 10 min and rinsed again by ethanol. After that, 2.5% glutaraldehyde (GA, Kanto Chemical Co., Inc.) was reacted with amino bonds of APS for 30 min. Next, Schiff bases were reduced by gate voltage (V_g) scan from -3.0 V to +0.5 V using a System SourceMeter (2612A, Keithley Instruments Inc., USA). Jacalin (Extra Cellular Matrix Laboratories) diluted in PBS was incubated on the GA-modified FET gate surface (60 min). Finally, non-reacted aldehyde groups of GA, which is a concern for non-specific adsorption of contaminating molecules, were treated by ethanolamine (Kanto Chemical Co., Inc.). Figure 2.1.2 shows a schematic diagram of the above procedure.

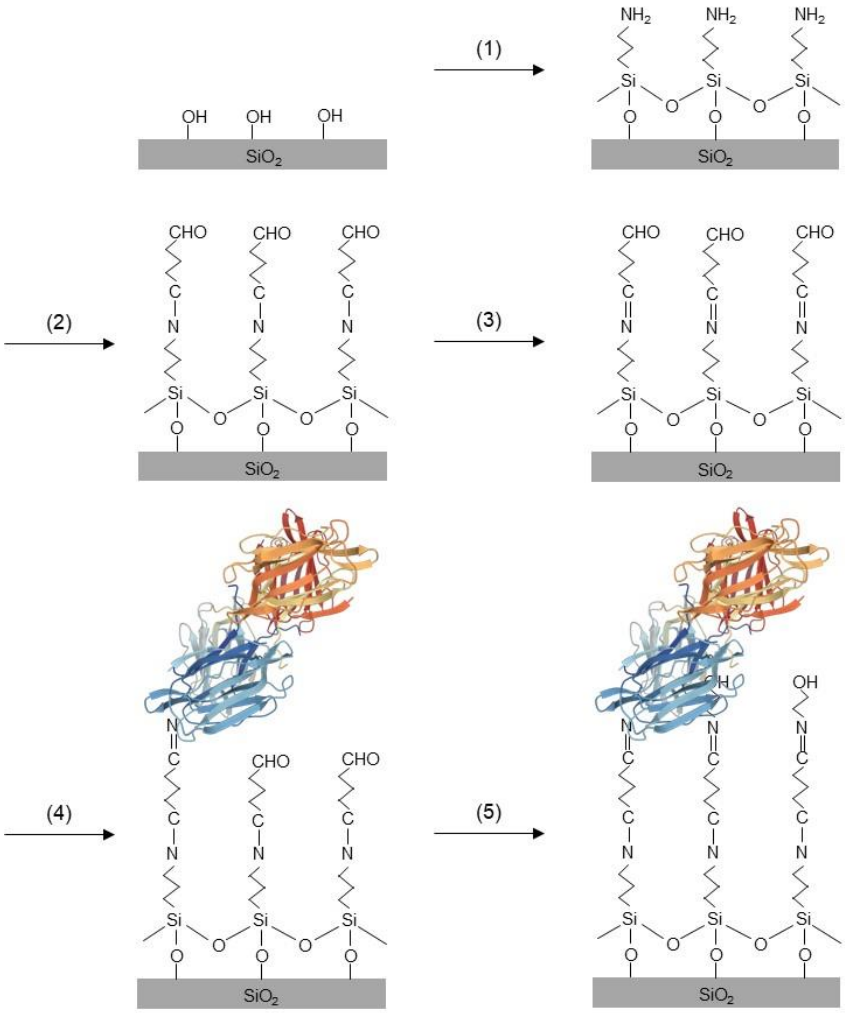

Figure 2.1.2 Fabrication of jacalin-immobilized FET biosensor. The procedure was (1) modification of aminopropylsilane layer, (2) modification of glutaraldehyde, (3) reduction of Schiff base, (4) immobilization of jacalin, and (5) ethanolamine capping.

2.1.2.2 Electrical measurement

The gate voltage (V_g) – drain current (I_d) curves before and after the addition of analytes were obtained by scanning V_g from -2.0 V to +0.5 V with drain voltage (V_d) of +0.1 V using a System SourceMeter (2612A, Keithley Instruments Inc., USA). The incubation time was 60 min. The reference electrode was Ag/AgCl (ALS Co., Ltd.). The measurement solution was 0.01 × PBS (pH 7.4). The gate voltage shift (ΔV_g) was calculated by comparing these curves.

2.1.2.3 Surface analysis

Surface morphologies of jacalin-immobilized FET gate surface before and addition of analytes were observed using atomic force microscopy (AFM, SPM-9600, Shimadzu Co., Japan). In the measurement, a silicon cantilever, whose spring constant and resonance frequency were 2 N/m and 70 kHz, respectively (OMCL-AC240TSC2, Olympus Co., Japan), was used. The image size was 1 μm × 1 μm with 512 × 512 pixels. Roughness parameters were obtained from AFM images. The density of fluorescence-modified s-IgA adsorbed to the jacalin-immobilized surface was obtained from using a variable mode imager (Typhoon 9410; Cytiva)

2.1.2.4 Preparation of sweat samples

Human sweat was collected from healthy adults using disposable droppers after light exercise. These two human sweat samples were treated with a filter (Steradisc, KURABO INDUSTRIES LTD.) to remove contaminating sweat components. The s-IgA concentration in human sweat samples was then measured using antibody-based ELISA by Nippon Flour Mills Co., Ltd.

2.1.3 Results and discussion

2.1.3.1 Optimization of condition for immobilization of jacalin to FET gate surface

To optimize the immobilization condition of jacalin to FET gate surface, jacalin-immobilized FET biosensors were prepared by varying the concentration of jacalin from 5 to 100 μg/mL and compared the FET responses caused by the addition of 100 μg/mL s-IgA as a positive control and 500 μg/mL human serum albumin (HSA, Sigma-Aldrich Inc.) as a negative control, respectively. FET biosensors prepared with 50 μg/mL jacalin solution yielded the maximum responses (+47 mV) caused by the addition of s-IgA (pI = 5.4-6.2[12]). On the other hand, suppression of the non-specific adsorption of HSA (pI = 4.7[13]) was indicated from small responses at negative control (Figure 2.1.3). In the case of 5 μg/mL, FET responses not only derived from s-IgA but also non-specific adsorption of HSA were confirmed. Due to the low immobilization density of jacalin, the amount of adsorbed s-IgA was decreased, and HSA might adsorb nonspecifically on unreacted aldehyde groups of GA-modified surfaces. Moreover, FET responses related to adsorption of s-IgA at 100 μg/mL jacalin immobilization conditions were decreased. It was considered by the steric hindrance between adjacent jacalin molecules to binding with s-IgA due to high immobilization density. Furthermore, to evaluate the specificity of the jacalin-immobilized FET biosensor prepared with 50 μg/mL jacalin, the surface morphologies were observed using AFM. Figure 2.1.4 shows that the morphology of the surface functionalized with 50 μg/mL jacalin changes due to the addition of s-IgA. The height profile and the root mean square roughness (R_q) of a cross-sectional view were increased after the addition of s-IgA. In contrast, the surface morphology did not change after the addition of HSA as a negative control. These results indicated that 50 μg/mL jacalin was the optimal immobilization condition, and jacalin-immobilized FET biosensors specifically detected s-IgA molecules.

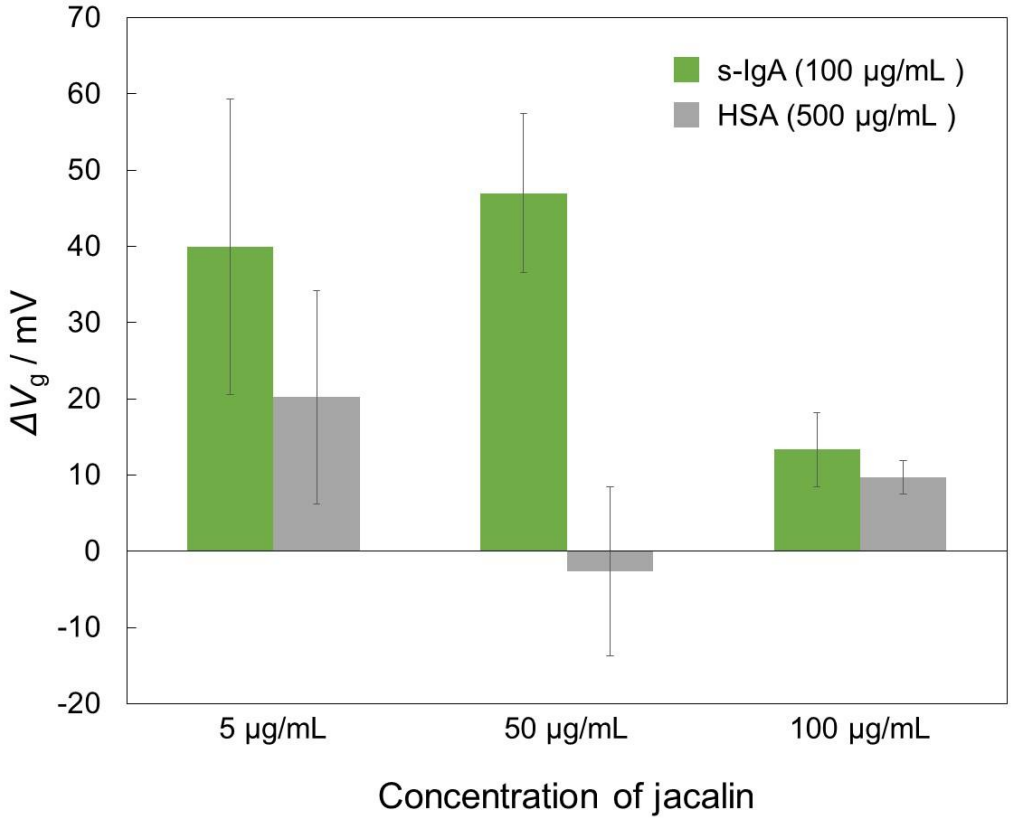

Figure 2.1.3 Relationship between the concentration of jacalin and FET responses caused by the addition of 100 μg/mL s-IgA or 500 μg/mL HSA (n = 6–12). Error bars indicate the 95% confidence interval.

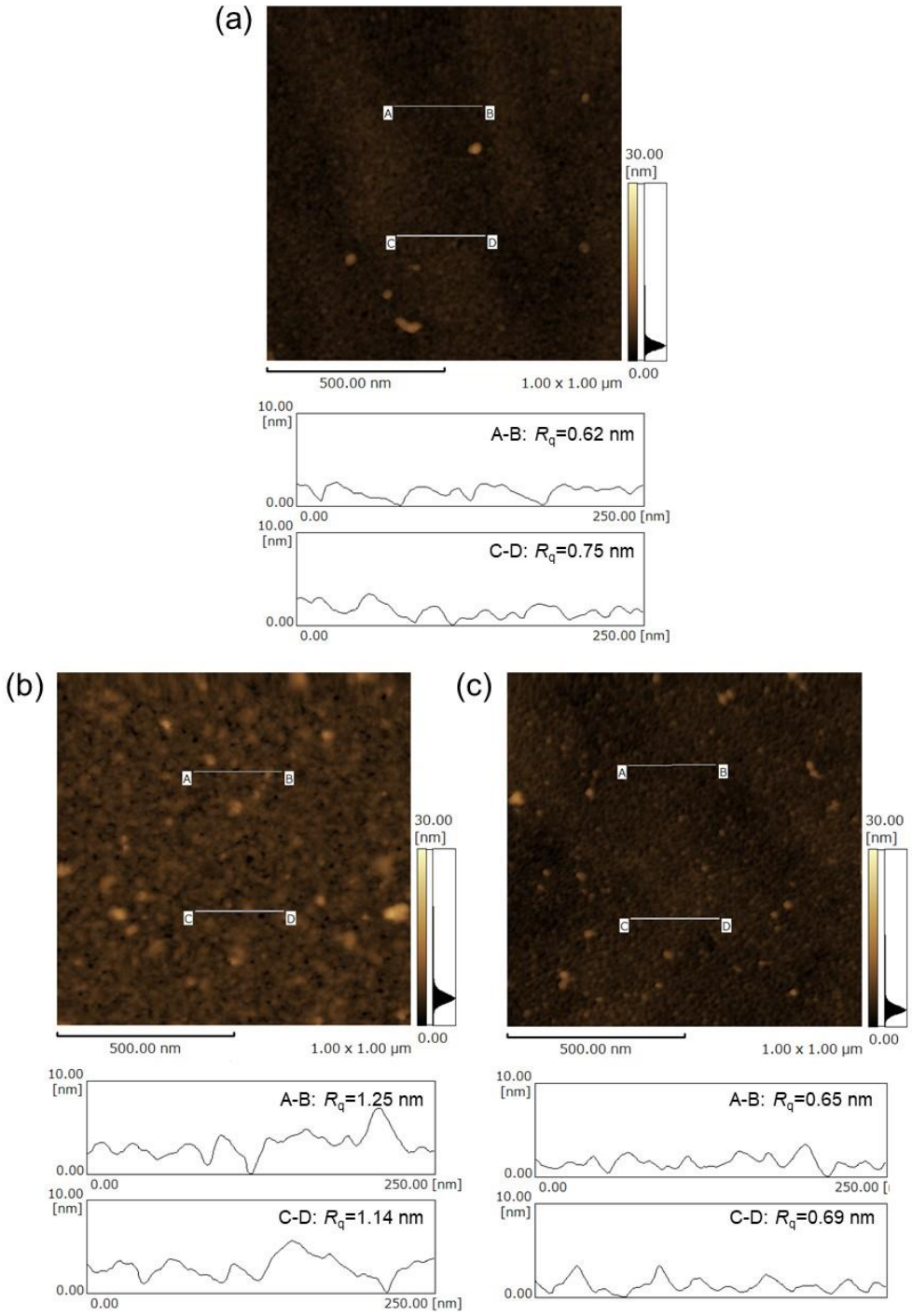

Figure 2.1.4 Atomic force microscopic images of (a) the FET gate surface functionalized with jacalin molecules, after (b) the addition of 100 µg/mL s-IgA, or (c) the addition of 500 µg/mL HSA.

2.1.3.2 Evaluation of multiple binding sites of jacalin to FET biosensing

To evaluate the advantage of multiple binding sites of jacalin, the magnitude of the FET responses of jacalin-immobilized FET was compared with that of antigen-binding fragment (Fab)-immobilized FET. The Fab molecule is a monovalent structure without the Fc region of the antibody, and its size is $7 \times 5 \times 4$ nm^3 (Protein data bank, 1AE6). It means that jacalin, whose size is $5.8 \times 6.3 \times 8.2$ nm^3 (Protein data bank, 1JAC), and Fab are similar in size and have different numbers of binding sites. Hence, a comparison of jacalin and Fab-immobilized FETs allows us to evaluate the influence of differences in the number of binding sites on the sensitivity of FET biosensors. As a result, the ΔV_g of Fab-immobilized FET biosensor caused by the addition of s-IgA and HSA were +17 mV and +5.9 mV, respectively, and a 95% significant difference was confirmed (Figure 2.1.5). The jacalin-immobilized FET biosensors showed larger responses related to adsorbed s-IgA than Fab-immobilized FET biosensors. These results indicated that jacalin as a FET receptor increased the sensitivity of FET biosensors to detect s-IgA molecules.

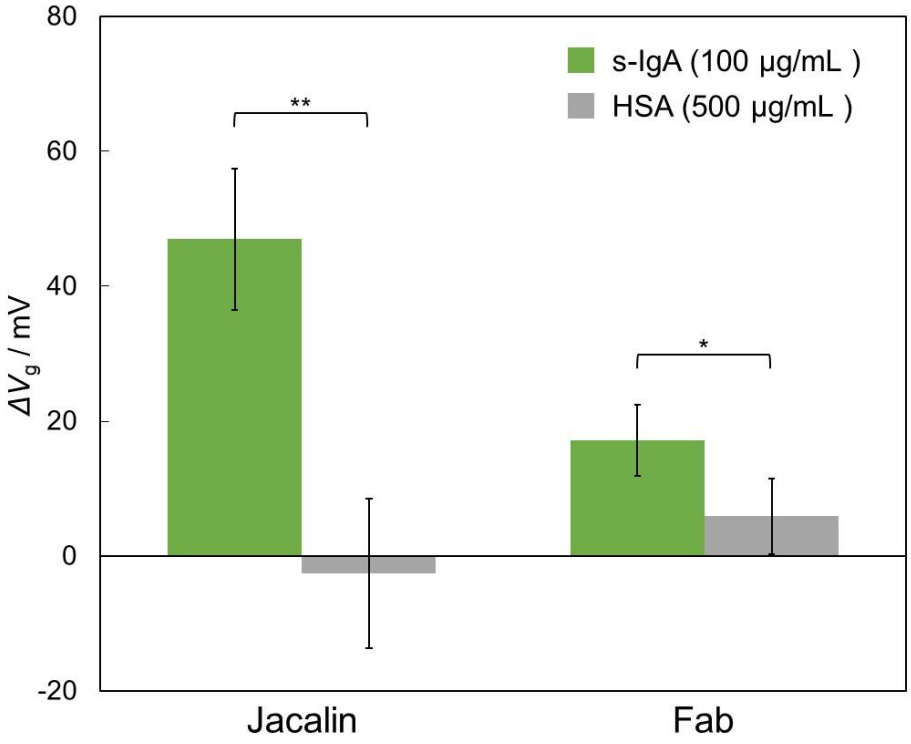

Figure 2.1.5 Comparison of the FET responses between jacalin- and Fab-immobilized FET biosensors caused by the addition of 100 μg/mL s-IgA or 500 μg/mL HSA (n = 6–12). Error bars represent the 95% confidence interval. The asterisks (* and **) are $p < 0.05$ and $p < 0.01$.

The aforementioned results confirmed that the jacalin-immobilized FETs showed a greater response to s-IgA than the Fab-immobilized FETs. In order to investigate the reason for these results, the charge density (σ_0) of s-IgA molecules detected by each FET biosensor was calculated using the Graham equation (2.1.3).[14]

$$\sigma_0 = \sqrt{8000 I \mathrm{N_A} \varepsilon_o \varepsilon_w \mathrm{k} T} \sinh \frac{\mathrm{e} \Delta V_g}{2kT} \qquad (2.1.3)$$

where I is the ionic strength of the buffer solution, N_A is the Avogadro constant, ε_0 is the permittivity of a vacuum, ε_w is the permittivity of water at 25°C, k is the Boltzmann constant, T is the absolute temperature in Kelvin, and e is the elementary charge. As a result, charge densities of s-IgA detected by the jacalin-immobilized and Fab-immobilized FET biosensors were 5.0×10^{-7} C·cm^{-2} and 1.6×10^{-7} C·cm^{-2}, respectively. From the calculation, the jacalin-immobilized FET biosensor detected three times more charges of s-IgA compared with the Fab-immobilized FET biosensor. Moreover, fluorescence analysis was conducted to measure the amount of fluorescence-modified s-IgA adsorbed on each receptor-immobilized surface. Here, each receptor was immobilized on a Si wafer for fluorescence analysis. The SiO_2 insulator of the FETs and the Si wafers used in this study were prepared by thermal oxidation, and the roughness value (R_q) of both films was approximately 0.2 nm. Also, each sensing interface was functionalized with the same receptor concentration. Thus, the immobilized states of each receptor were assumed to be nearly equal. Fluorescence analysis showed that 2.0×10^4 μm^{-2} and 1.4×10^4 μm^{-2} of s-IgA were adsorbed on the jacalin-immobilized and Fab-immobilized surfaces, respectively. These results suggested that the jacalin-immobilized surface captured more s-IgA molecules within the Debye length than the Fab-immobilized surface. Generally, protein receptors are immobilized in random orientations, regardless of physical adsorption and covalent bonding.[1] In this chapter, the amino groups of the lysine, which is an amino acid existing abundantly within proteins, bind to the aldehyde groups of glutaraldehyde, and thus each receptor is immobilized in various orientations. By random orientation, some binding sites of Fab molecules on the FET gate surface were inactive to capture s-IgA (Figure 2.1.6a). In contrast, jacalin, which has multiple binding sites symmetrically, appears to be capable of binding to s-IgA when immobilized in any orientation (Figure 2.1.6b). Furthermore, to consider the adsorption model of jacalin, the positions of lysine, which is an amino acid with an amino group on

its side chain, in the crystal structure of jacalin were calculated based on the amino acid sequence. As a result, the number of lysine inducing immobilization in Flat-on, Side-on, and End-on were 14, 8, and 2, respectively. Hence, jacalin molecule was likely to be immobilized in Flat-on. The height of jacalin immobilized in Flat-on is about 3 nm, which is smaller than the height of Fab molecules, suggesting that jacalin molecules could have captured a large number of s-IgA molecules within the Debye length. From the above mentions, the tetrameric jacalin molecules suppressed the influence of random orientation, allowing (1) capture of more s-IgA and (2) effective use of the Debye length. Therefore, the multimeric lectin could be useful as a receptor to improve the sensitivity of FET biosensors.

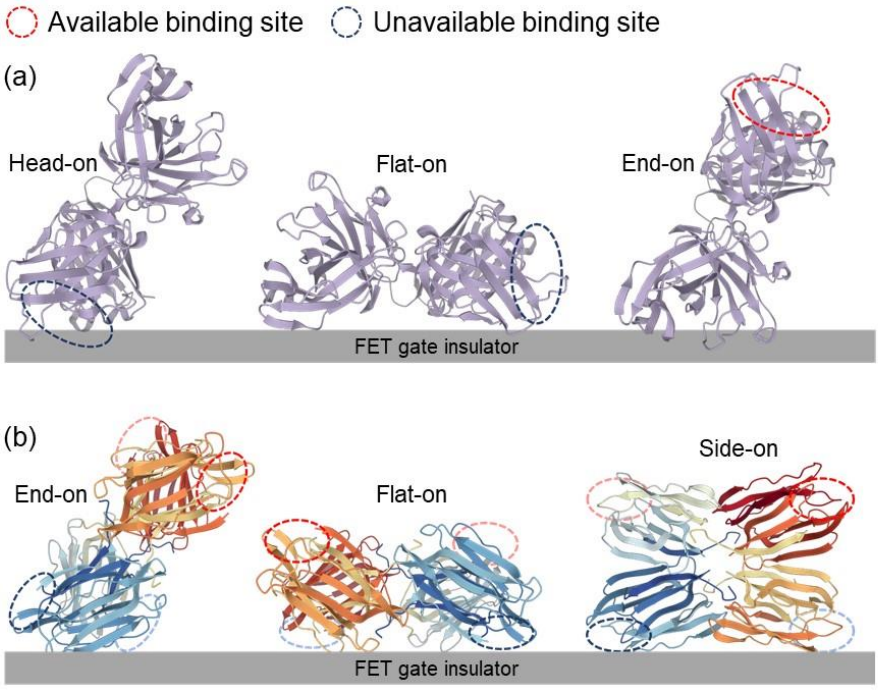

Figure 2.1.6 Schematic illustration of random-oriented (a) Fab and (b) jacalin on the FET gate insulator surface. The red circle and blue circles represent available and unavailable binding sites, respectively.

2.1.3.3 Quantitative detection of secretory immunoglobulin A (s-IgA) using jacalin-immobilized FET biosensor

To evaluate the quantitative capability of the jacalin-immobilized FET biosensor, the relationship between ΔV_g and different concentrations of s-IgA was determined. Figure 2.1.7 shows a linear correlation of FET responses to s-IgA concentrations ranging from 0.1 to 100 μg/mL. The concentrations of s-IgA in the sweat of healthy men and women are 13.0 μg/mL and 1.6 μg/mL, respectively.[9] Additionally, the 95% significant difference between the FET responses to s-IgA and HSA indicated that the limit of detection (LOD) of jacalin-immobilized FET was 1 μg/mL. Hence, these results suggested that jacalin-immobilized FET biosensors could detect s-IgA with high sensitivity.

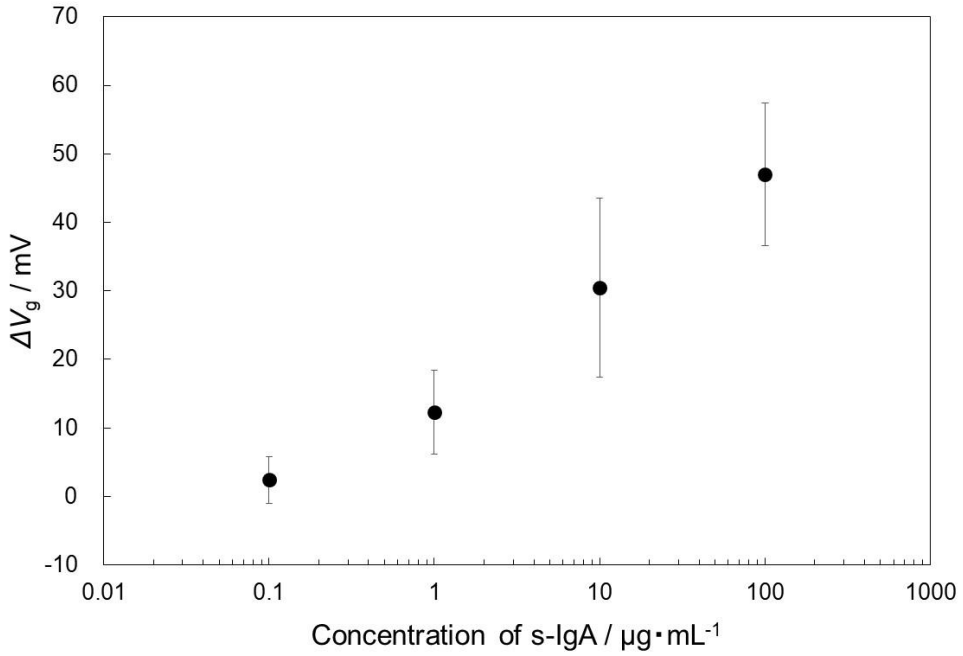

Figure 2.1.7 The relationship between ΔV_g and different concentrations of s-IgA from 0.1 to 100 μg/mL (n = 4–12). Error bars represent the 95% confidence interval.

2.1.3.4 Detection of secretory immunoglobulin A (s-IgA) in human sweat using jacalin-immobilized FET biosensor

The practical application of jacalin-immobilized FETs for stress monitoring requires to detect s-IgA in actual human sweat. The feasibility of detecting s-IgA in sweat using jacalin-immobilized FET biosensors was evaluated. When a 20 μL sweat sample collected from a healthy adult was dropped directly onto the jacalin-immobilized FET biosensor, the huge error bar of FET responses was confirmed (Figure 2.1.8). Besides, the jacalin-immobilized surface after the addition of an untreated sweat sample was analyzed using AFM. As shown in Figure 2.1.9, the film-like substances derived from sweat components were observed. Sweat contains various components, such as sebum, bacteria, and mucin.[15–19] Hence, these results suggested that non-specific adsorption of agglutinated sweat components reduced the specificity of the jacalin-immobilized FET biosensor. To suppress the non-specific adsorption of these components, the sweat sample was treated by filtration using a filter with a pore size of 450 nm. By filtering the sweat sample, the error bar of FET responses was decreased compared with the untreated sweat sample (Figure 2.1.8). Additionally, in the AFM image, film-like substances, which were thought to be aggregates of sweat components, were not observed on the jacalin-immobilized gate surface after dropping the filtered sweat sample (Figure 2.1.9).

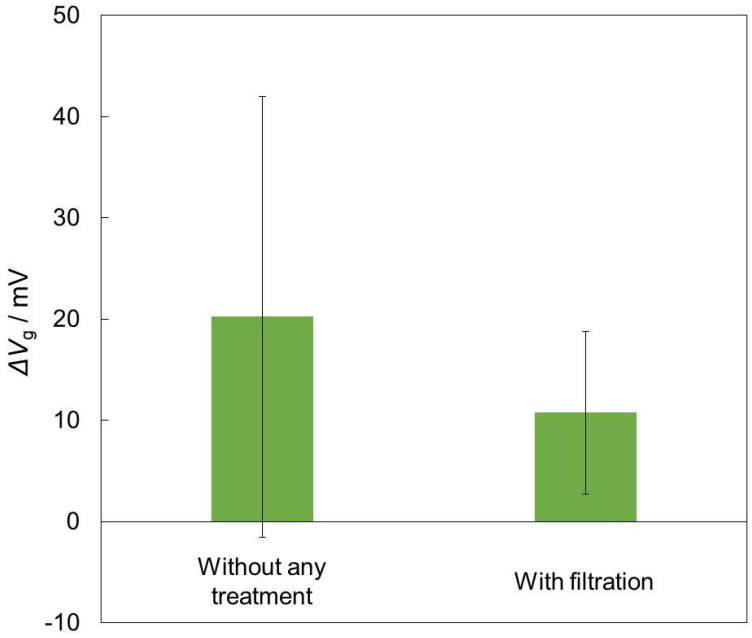

Figure 2.1.8 Comparison of the FET responses caused by the addition of human sweat samples with and without filtration treatment (n = 5–6). Error bars represent the 95% confidence interval.

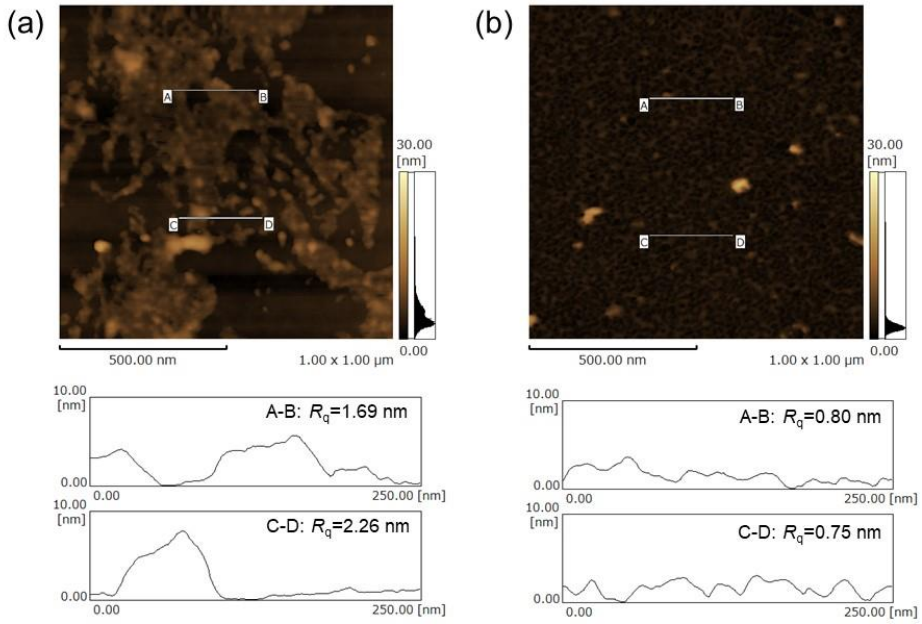

Figure 2.1.9 Atomic force microscopic images of the jacalin-immobilized FET gate surface after the addition of (a) untreated sweat sample, (b) filtered sweat sample.

Finally, to ensure the quantitative capability of the jacalin-immobilized FET biosensor to detect s-IgA in human sweat samples, the electrical responses were obtained from the addition of filtered samples. When two sweat samples, which were collected from different persons, were added to jacalin-immobilized FET biosensors, the magnitude of ΔV_g was +11 ± 8.0 mV and +28 ± 11 mV, respectively. Based on the relationship between these FET responses and the calibration curve of the detection of s-IgA in buffer solution, the s-IgA concentrations in each sweat sample were 0.5 μg/mL and 6.9 μg/mL. These sweat samples contained 0.5 μg/mL and 4.7 μg/mL s-IgA using sandwich-based ELISA, showing that the s-IgA concentration measured by the jacalin-immobilized FET biosensor agreed with the conventional method. These results were summarized in Table 2.2. Therefore, FET biosensors, which can measure s-IgA concentrations through only filtration processing, could be a non-invasive and simple detection method compared to ELISA, which requires multi-step operations using various reagents. In the result of sweat sample 2, the difference in concentration of s-IgA might be due to the non-specific adsorption of residues of sweat components, which vary in concentration between individuals.[20] Toward the increase in s-IgA detection accuracy, additional treatments, such as rinsing with surfactants, Tween 20[20], are expected to be useful for removing the residues of sweat components from the FET gate surface.

Table 2.1.1 Comparison of s-IgA detection in human sweat by the jacalin-immobilized FET biosensor and conventional ELISA

	s-IgA concentration from ELISA / μg mL^{-1}	Average of ΔV_g / mV	Caluclated s-IgA concentraiton / μg·mL^{-1}
Sweat sample (1)	0.49	11 ± 8.0	0.49
Sweat sample (2)	4.7	28 ± 11	6.9

2.1.4 Conclusion

In chapter 2.1, a tetrameric lectin, jacalin, was indicated to be useful for quantitative detection of s-IgA using FET biosensors. From these results, it was found that receptors with multiple recognition sites symmetrically suppressed the effect of random orientation and exhibit high capture capability for target molecules. Therefore, point-multimeric lectin molecules are expected to be used as receptors for FET biosensors instead of antibodies. The use of symmetric lectins, jacalin, concanavalin A, PA-IL, PA-IIL, and so on, will enable the development of FET platforms for the detection of various glycans and glycoproteins.

References

1. Trilling, A. K., Beekwilder, J. & Zuilhof, H. Antibody orientation on biosensor surfaces: A minireview. *Analyst* **138**, 1619–1627 (2013).
2. Tajima, N., Takai, M. & Ishihara, K. Significance of antibody orientation unraveled: Well-oriented antibodies recorded high binding affinity. *Anal. Chem.* **83**, 1969–1976 (2011).
3. Kausaite-Minkstimiene, A., Ramanaviciene, A., Kirlyte, J. & Ramanavicius, A. Comparative study of random and oriented antibody immobilization techniques on the binding capacity of immunosensor. *Anal. Chem.* **82**, 6401–6408 (2010).
4. Lis, H. & Sharon, N. Lectins: Carbohydrate-specific proteins that mediate cellular recognition. *Chem. Rev.* **98**, 637–674 (1998).
5. Kabir, S. Jacalin: A jackfruit (Artocarpus heterophyllus) seed-derived lectin of versatile applications in immunobiological research. *J. Immunol. Methods* **212**, 193–211 (1998).
6. Sharma, A., Sekar, K. & Vijayan, M. Structure, dynamics, and interactions of jacalin. Insights from molecular dynamics simulations examined in conjunction with results of X-ray studies. *Proteins Struct. Funct. Bioinforma.* **77**, 760–777 (2009).
7. Allen, A. C., Bailey, E. M., Barratt, J., Buck, K. S. & Feehally, J. Analysis of IgA1 O-glycans in IgA nephropathy by fluorophore-assisted carbohydrate electrophoresis. *J. Am. Soc. Nephrol.* **10**, 1763–1771 (1999).
8. Lee, K. M. *et al.* A pilot study on the association between job stress and repeated measures of immunological biomarkers in female nurses. *Int. Arch. Occup. Environ. Health* **83**, 779–789 (2010).
9. Okada, T., Konishi, H., Ito, M., Nagura, H. & Asai, J. Identification of Secretory Immunoglobulin A in Human Sweat and Sweat Glands. *J. Invest. Dermatol.* **90**, 648–651 (1988).
10. Morey, J. N., Boggero, I. A., Scott, A. B. & Segerstrom, S. C. Current directions in stress and human immune function. *Curr. Opin. Psychol.* **5**, 13–17 (2015).
11. Bourne, Y. *et al.* Structural basis for the unusual carbohydrate-binding specificity of jacalin towards galactose and mannose. *Biochem. J.* **364**, 173–180 (2002).
12. Elkon, K. B. Isoelectric focusing of human IgA and secretory proteins using thin layer agarose gels and nitrocellulose capillary blotting. *J. Immunol. Methods* **66**, 313–321 (1984).
13. Vlasova, I. M. & Saletsky, A. M. Study of the Denaturation of Human Serum

Albumin. *J. Appl. Spectrosc.* **76**, 536–541 (2009).

14. Allen J. Bard, L. R. F. *Electrochemical methods, fundamentals and applications*. (JOHN WILEY & SONS INC., 2000).
15. Patterson, M. J., Galloway, S. D. R. & Nimmo, M. A. Variations in regional sweat composition in normal human males. *Exp. Physiol.* **85**, 869–875 (2000).
16. Taylor, D. *et al.* Characterization of the microflora of the human axilla. *Int. J. Cosmet. Sci.* **25**, 137–145 (2003).
17. Cizza, G. *et al.* Elevated Neuroimmune Biomarkers in Sweat Patches and Plasma of Premenopausal Women with Major Depressive Disorder in Remission: The POWER Study. *Biol. Psychiatry* **64**, 907–911 (2008).
18. Park, J. H. *et al.* An antimicrobial protein, lactoferrin exists in the sweat: Proteomic analysis of sweat. *Exp. Dermatol.* **20**, 369–371 (2011).
19. Kumar, P., Ji, J., Thirkill, T. L. & Douglas, G. C. MUC1 Is Expressed by Human Skin Fibroblasts and Plays a Role in Cell Adhesion and Migration. *Biores. Open Access* **3**, 45–52 (2014).
20. Baker, L. B. Physiology of sweat gland function: The roles of sweating and sweat composition in human health. *Temperature* **6**, 211–259 (2019).

2.2 Evaluation of glycan-immobilized surface on FET biosensor for the detection of influenza virus (IFV) particles in human nasal mucus

2.2.1 Introduction

Improvement of the sensitivity of FET biosensors could be achieved by decreasing the dissociation constant (K_d) of the sensing surface based on Eq. 2.1.2. Among biomolecular interactions, the glycan-lectin interactions show the cluster glycoside effect due to the formation of multivalent bonds, resulting in the enhancement of binding affinity.[1] Generally, the dissociation constant reflecting the effect of multivalent bonds is given by;[2]

$$K_{d,multi} = \left(K_{d,mono}\right)^{m} \quad (2.2.1)$$

where m is multiplicity, $K_{d,mono,}$ and $K_{d,multi}$ were dissociation constant of monovalent and multivalent bond, respectively. The interaction between a single glycan and lectin is weak with the K_d value of the order of μM or more, while it is significantly reduced when a multivalent bond is formed.[3] Thus, the formation of glycan-immobilized surfaces, which show the cluster glycoside effect, leads to an increase in the sensitivity of FET biosensors.

Glycan-lectin interactions are involved in many biological reactions, such as cell adhesion and viral infection.[4] Various viruses, which initiate infection by binding to glycans on the cell surface, have a large number of lectin molecules on the viral membrane surface. Hence, the viral particles strongly adsorb to the glycan-immobilized surface by expressing the cluster glycoside effect.[5] Furthermore, the small glycan receptors enables detecting viral molecules by FET biosensors under high ionic strength.[6] Thus, it was expected that the glycan-immobilized FET biosensor detected viral particles under high ionic strength. In this chapter, influenza virus (IFV) was selected as a target molecule, because IFV specifically recognizes sialic acid-terminated glycans. Human and avian IFVs have affinities to trisaccharides terminating in sialic acid-α2,6-galactose (6'-sialyllactose: Siaα2,6'Lac) and in sialic acid-α2,3-galactose (3'-sialyllactose: Siaα2,3'Lac), respectively.[7] Previously, T. Osaka and his group demonstrated the detection of human or avian hemagglutinins (HA), which were envelope glycoprotein of IFVs, using FET

biosensors with immobilized Siaα2,6'Lac or Siaα2,3'Lac in high density and efficient orientation.[8] In this chapter, I evaluated the usefulness of glycan-immobilized surfaces in FET biosensors to the detection of IFV particles under high ionic strength (Figure 2.2.1). Additionally, a pandemic IFV accrues by a switch in receptor specificity of highly pathogenic avian IFV from α-2,3-linkage to α-2,6-linkage receptors by mutation.[9,10] The detection of human or avian IFV in nasal mucus using glycan-immobilized FET biosensors were attempted to identify the infectivity of IFV.

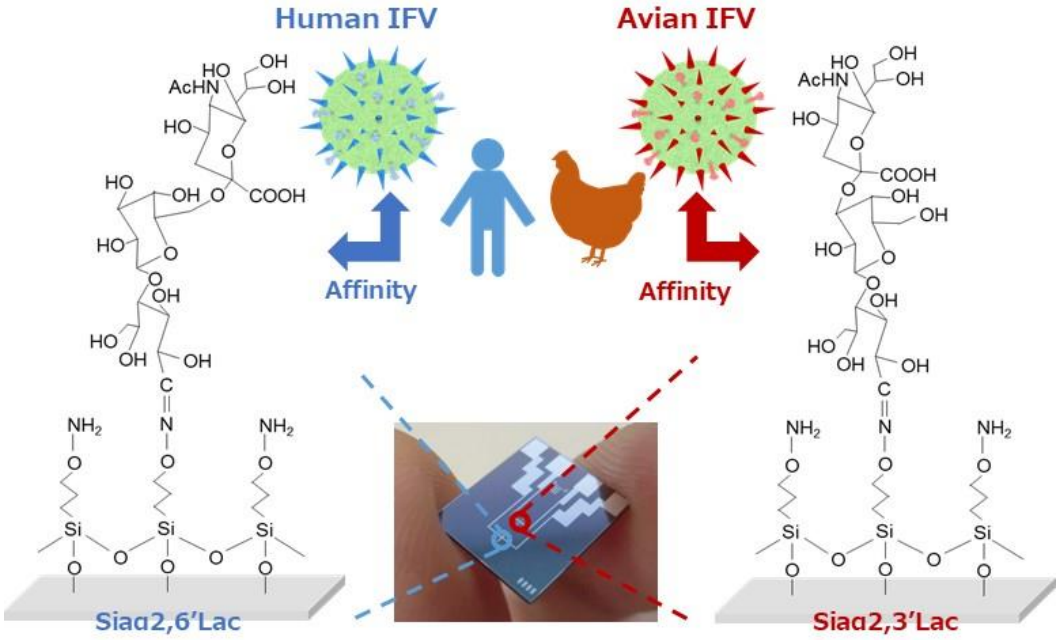

Figure 2.2.1 Schematic image of detection of human or avian IFVs using the glycan-immobilized FET biosensors.

2.2.2 Experimental

2.2.2.1 Fabrication of glycan-immobilized FET biosensor

The SiO_2 insulator (10 μm in length × 1000 μm in length) of n-type FET, which was produced by Toppan Printing Co., Ltd. (Japan), was sonicated in acetone, a mixture of toluene and methanol (1:1) for 10 min, in that order. To introduce silanol groups on the SiO_2 surface, the cleaned FET chips were exposed to O_2 plasma ashing (200 W, 1 min) using a gas plasma reactor (PR301, Yamato Scientific Co., Ltd., Japan). Then, the FET chips were immersed in toluene with 0.1%(v/v) (3-aminooxypropyl) triethoxysilane (AOPTES, Medicinal Chemistry Pharmaceuticals, LLC, Japan) at 60°C for 15 min under Ar atmosphere. After modification by aminooxypropylsilane (AOPS), 100 μM Siaα2,6'Lac or Siaα2,3'Lac (Biosynth Carbosynth, UK) in acetonic acid solution (pH 5.3) was dropped, and FET chips were incubated (60°C, 90 min). After washing with 1 × PBS and 0.01 × PBS, they were dried with N_2 gas. Figure 2.2.2 is a schematic diagram of the above procedure.

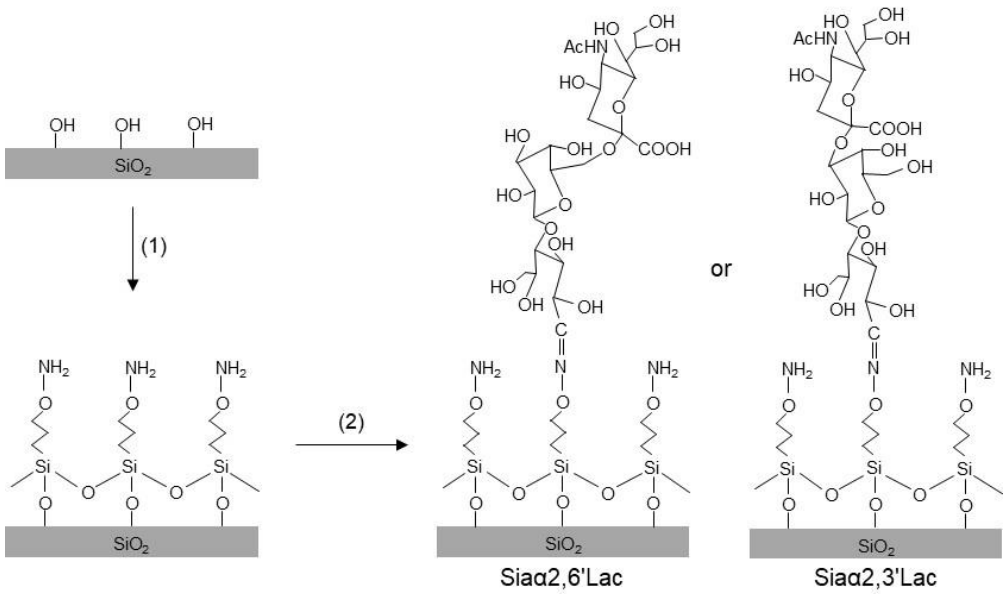

Figure 2.2.2 Fabrication of glycan-immobilized FET biosensor. The procedure was (1) modification of aminooxypropylsilane layer, (2) immobilization of glycans.

2.2.2.2 Electrical measurement

The gate voltage (V_g) – drain current (I_d) curves of glycan-immobilized FET biosensor was obtained by scanning V_g from -3.0 V to +0.5 V with drain voltage (V_d) of +0.1 V by using a System SourceMeter (2612A, Keithley Instruments Inc., USA). The FET measurements were performed using 1 × PBS as measurement buffer solution and Ag/AgCl reference electrode (ALS Co., Ltd.). The gate voltage shift (ΔV_g) was acquired from the V_g – I_d curves before and after the addition of analytes. IFV strains were A/Hyogo/YS/2011 (H1N1) 2009pdm and A/duck/Hokkaido/Vac-3/2007 (H5N1). These viruses were prepared were inactivated by treatment with β-propiolactone at Hokkaido University.

2.2.2.3 Surface observation using atomic force microscopy (AFM)

Glycan-immobilized FET gate surfaces were analyzed using atomic force microscopy (AFM, SPM-9600, Shimadzu Co., Japan). A silicon cantilever (OMCL-AC240TSC2, Olympus Co., Japan, spring constant 2 N/m, resonance frequency 70 kHz) was used in the measurement. The scanning definition was 512 × 512 pixels. The root-mean-square roughness (R_q) values were obtained from AFM images.

2.2.2.4 Preparation of IFV-suspended nasal mucus samples

Nasal mucus samples were collected from five healthy persons in the unstimulated state. It was briefly collected by blowing the nose that humans' physiological phenomenon and stored in a freezer. $10^{8.5}$ $TCID_{50}$/mL IFV solution (2 μL) was added to nasal mucus (18 μL). Subsequently, 10 mg/mL L-Cysteine Ethyl Ester (LCEE; Tokyo Chemical Industry Co., Ltd., Japan)/PBS (180 μL) was added to IFV-suspended nasal mucus for reduction of viscosity. The final concentration of IFV in nasal mucus was $10^{6.5}$ $TCID_{50}$/mL.

2.2.3 Results and discussion

2.2.3.1 Specificity and sensitivity of glycan-immobilized FET biosensor to detect influenza virus

First, the specificity of glycan-immobilized FET biosensors to IFV particles under a high ionic environment was examined. The V_g-I_d curves before and after adding H1N1 human IFV and H5N1 avian IFV to the Siaα2,6'Lac-immobilized FET biosensors were measured. When $10^{8.5}$ $TCID_{50}$/mL H1N1 human IFVs were added to the Siaα2,6'Lac-immobilized FET biosensor, a positive gate voltage shift in the V_g-I_d curve was confirmed (Figure 2.2.3a). It should be noted that the $TCID_{50}$/mL represents viral titers (50% tissue culture infectious dose). The gate voltage shift was caused by the specific adsorption of IFV particles (pI = 4.0-4.5[11]), which have negative charges in 1 × PBS (pH 7.4).[12] In contrast, the gate voltage was not shifted by adding H5N1 avian IFVs (Figure 2.2.3b). A high-density glycan-immobilized surface prevented the nonspecific adsorption of negative-control IFV strains because its hydrophilicity suppressed the hydrophobic interaction. Thus, the glycan-immobilized FET biosensor could detect the IFV whole particles under a high ionic strength, i.e., the ionic strength was nearly physiological conditions. Moreover, the Siaα2,3'Lac-immobilized FET biosensor showed responses to H5N1 avian IFVs, while no significant responses to H1N1 human IFVs were observed (Figure 2.2.3c and d). Subsequently, to confirm whether the above results are due to the specific adsorption of IFV particles, the glycan-immobilized surfaces after the addition of IFVs were analyzed using AFM. As shown in Figure 2.2.4, granular matters were observed when H1N1 human IFVs and H5N1 avian IFVs were added to Siaα2,6'Lac- and Siaα2,3'Lac-immobilized surfaces, respectively. In contrast, the surface morphologies of each glycan-immobilized surface were not changed after the addition of negative control subtypes. These results indicated that each glycan-immobilized FET biosensor possessed specificity to IFV subtypes.

Additionally, to investigate the influence of the ionic strength to the detection of IFV particles using FET biosensors, electrical responses due to the addition of each subtype of IFV to the Siaα2,6'Lac-immobilized FET were measured using 1 × PBS (I = 165 mM) or 0.01 × PBS (I = 1.65 mM) as a measurement buffer solution. When H1N1 human IFVs were added to the Siaα2,6'Lac-immobilized FET biosensor, a similar magnitude of a positive shift in the V_g-I_d curve was confirmed regardless of the ionic strength (Figure 2.2.5). In previous study, the magnitude of the FET responses caused by the addition of HA was decreased with increasing the ionic strength.[8] This result suggested that the charge of IFVs adsorbed on the glycan-immobilized surface was not affected by the Debye shielding.

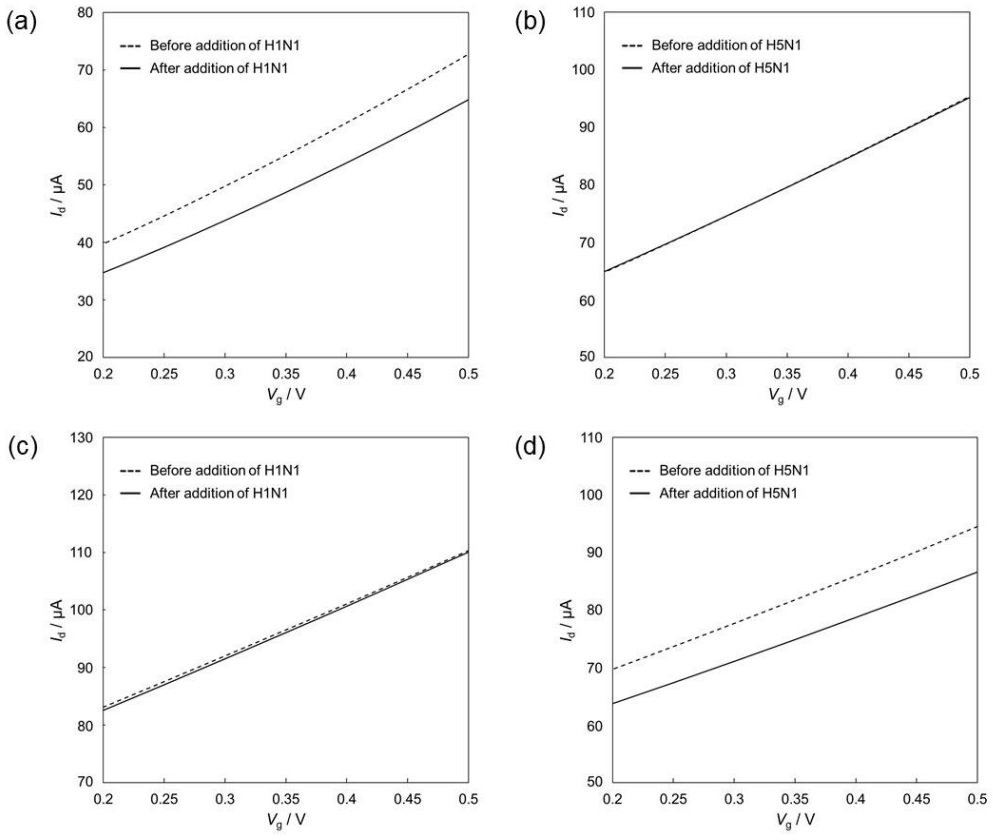

Figure 2.2.3 Gate voltage shifts (ΔV_g) of glycan-immobilized FET biosensor to IFV particles. The V_g-I_d curves of (a) (b) Siaα2,6'Lac- and (c) (d) Siaα2,3'Lac-immobilized FET biosensor by the addition of (left) H1N1 human IFV and (right) H5N1 avian IFV.

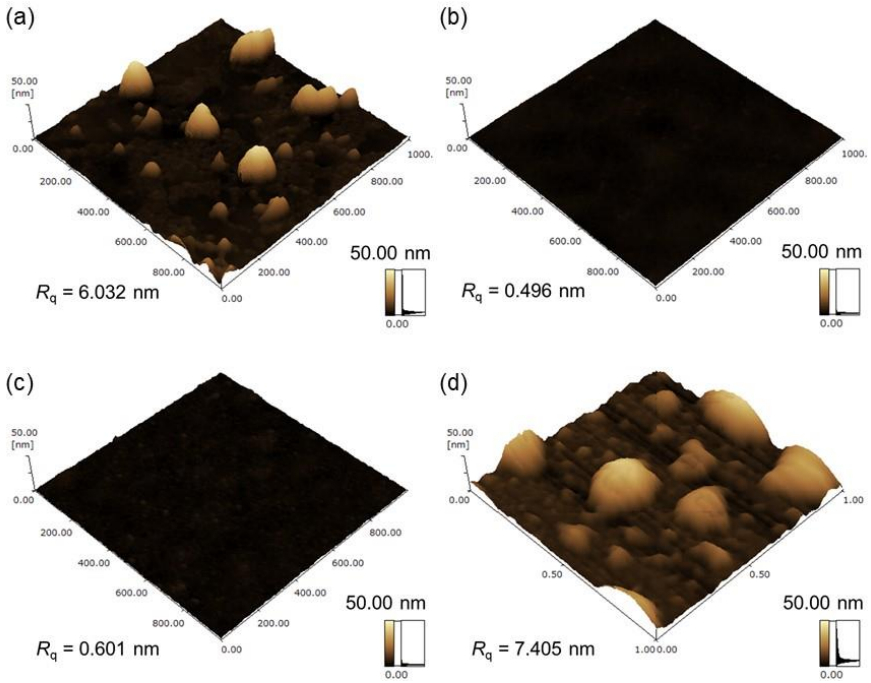

Figure 2.2.4 Atomic force microscopic images of glycan-immobilized surfaces after the addition of IFV. The surface of (a) (b) Siaα2,6'Lac- and (c) (d) Siaα2,3'Lac-immobilized FET biosensor by the addition of (left) H1N1 human IFV and (right) H5N1 avian IFV.

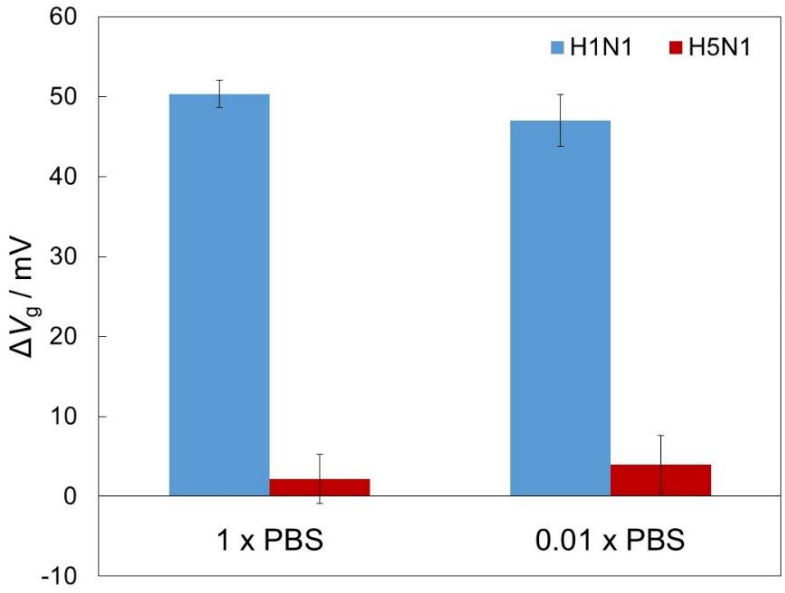

Figure 2.2.5 Comparison of the FET responses caused by the addition of IFVs in 1 × PBS or 0.01 × PBS as a measurement solution. Error bars indicate the standard deviation (n = 3).

Next, the sensitivity of each glycan-immobilized FET biosensor was investigated. The electrical responses were measured by adding different IFV concentrations. As a result, a plot of FET responses (ΔV_g) versus concentration of IFVs was obtained over a wide range ranging from $10^{0.5}$ to $10^{8.5}$ $TCID_{50}$/mL (Figure 2.2.6). In contrast, each glycan-immobilized FET biosensor showed no change in response dependent on the concentration of negative control IFV strains. Moreover, the FET responses of Siaα2,6'Lac- and Siaα2,3'Lac-immobilized FET to a blank solution (1 × PBS) were +0.4 ± 0.6 mV and -0.66 ± 1.9 mV, respectively. Thus, the limit of detection (LOD) of both glycan-immobilized FET biosensors was $10^{0.5}$ $TCID_{50}$/mL by the 3σ method. The LOD of the conventional method, immunochromatography, is approximately 10^3 $TCID_{50}$/mL,[13] indicating that the glycan-immobilized FET was more sensitive to detect IFV particles. These results suggested that glycan-immobilized FET biosensors have the quantitative capability to discriminate between H1N1 human IFV and H5N1 avian IFV.

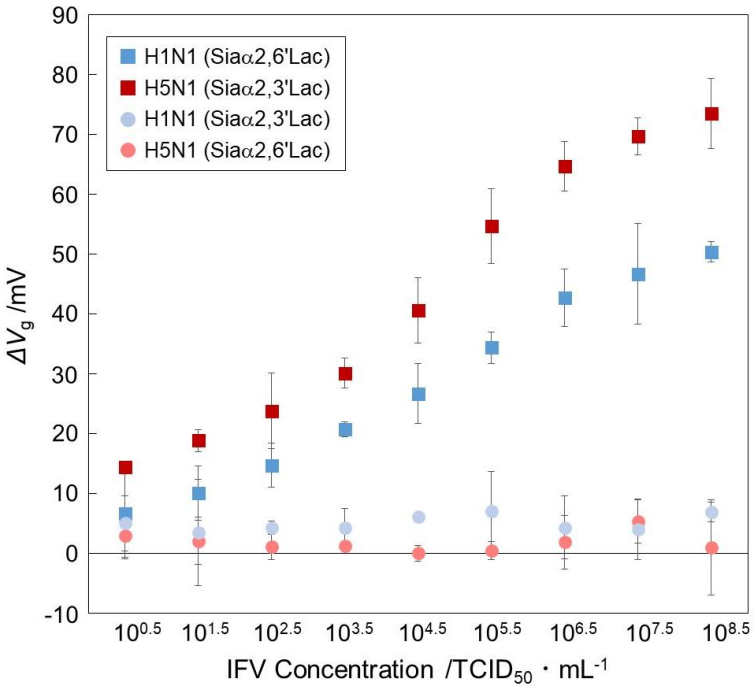

Figure 2.2.6 The relationship between ΔV_g and different concentrations of IFVs from $10^{0.5}$ to $10^{8.5}$ $TCID_{50}$/mL. Error bars represent the standard deviation (n = 3–4).

2.2.3.2 Evaluation of cluster glycoside effect

As shown above, the glycan-immobilized FET biosensor showed high sensitive detection of IFV particles, whose size is approximately 100 nm,[12] under 1 × PBS, i.e., the Debye length was 0.75 nm. To consider the mechanism underlying the detection of viral particles under a high ionic environment, the charge distribution of an IFV detected by the FET biosensor was calculated. In brief, the number of charges that contributed to the FET response was compared to the theoretical charge numbers of a single viral particle.

First, the number of charges detected by the FET biosensor was calculated from the magnitude of ΔV_g. In Figure 2.2.6, the ΔV_g caused by the addition of $10^{8.5}$ $TCID_{50}$/mL H5N1 avian IFVs to Siaα2,3'Lac-immobilized FET biosensors was +73.5 mV. Thus, the charge density (σ_0) detected by the FET was 9.4×10^{-7} C·cm^{-2} using the Graham equation (Eq. 2.1.3). Then, an electron density (ρ_e) was 5.9×10^{12} cm^{-2} by dividing σ_0 by the elementary charge (e = 1.60×10^{-19} C). Moreover, the density of H5N1 IFV particles (ρ_{IFV}) captured by the glycan-immobilized surface was estimated to be 6.9×10^8 cm^{-2} by counting the IFV particles in AFM images (Figure 2.2.7). From electron density and adsorbed-virus density, the negative charge numbers detected by the FET biosensor per virus particle (Z_d) was -8.5×10^3.

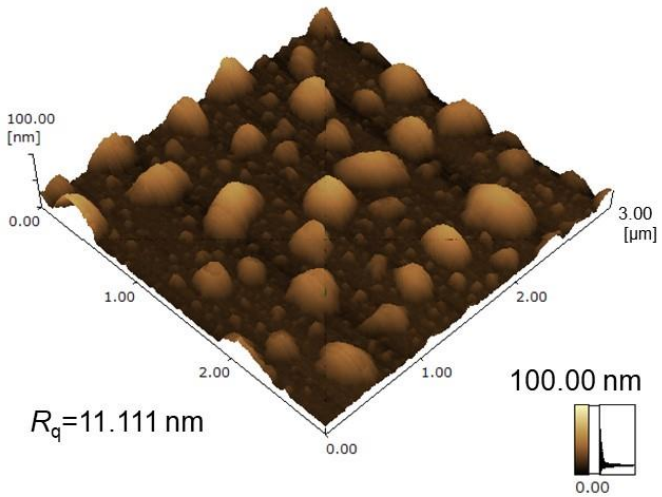

Figure 2.2.7 Atomic force microscopic image of the Siaα2,3'Lac-immobilized surface after the addition of $10^{8.5}$ $TCID_{50}$/mL H5N1 avian IFV.

Next, the theoretical charge numbers on the IFV envelope was calculated based on the intrinsic charges of the viral membrane molecules. On the IFV membrane, there are hemagglutinin (HA), neuraminidase (NA), matrix protein 2 (M2), and a part of phosphatide (Figure 2.2.8). The number of each viral protein per IFV particle is shown in Table 2.2.1.[14,15] Additionally, the number of phosphatide molecules was estimated to be 8.4×10^4 by considering the numbers of all viral proteins (HA, NA, and M2). The number of intrinsic charges of each viral membrane molecule at pH 7.4 was obtained based on their amino acid sequences. As a result, the monomer of HA, NA, M2, and phosphatide have -13.0, -6.25, -2.71, and -0.08 charges (Table 2.2.1). Thus, the number of charges on the viral membrane per virus particle was assumed to be -2.9×10^4.

Based on the results of the above calculations, the range of viral particle surfaces detected by the glycan-immobilized FET biosensor was estimated by comparing the experimentally-detected charge number and the theoretical charge number. As a result, 29% of viral membrane proteins and phosphatide were detected by the glycan-immobilized FET biosensor. This estimation meant that the flexible viral membrane[16] allows multiple hemagglutinins to bind to the glycan-immobilized surface. Thus, the interaction between the viral particles and the glycan-immobilized surface increased by the cluster glycoside effect, and they could firmly adhere to each other.[5] Hence, as the buffer solution between the interface and the viral membrane was eliminated by adhesion, the glycan-immobilized FET biosensor could detect IFVs without the influence of the Debye shielding effect in a high ionic strength environment. This consideration could be supported by the similar FET responses caused by the adsorption of H1N1 human IFV under 1 × PBS and 0.01 × PBS in Figure 2.2.5. Furthermore, the K_d value was increased with the number of binding between glycan-immobilized surface and viral particles, leading improvement of the sensitivity. Therefore, these results showed that the cluster glycoside effect enabled the detection of IFV under high ionic strength using glycan-immobilized FET biosensors.

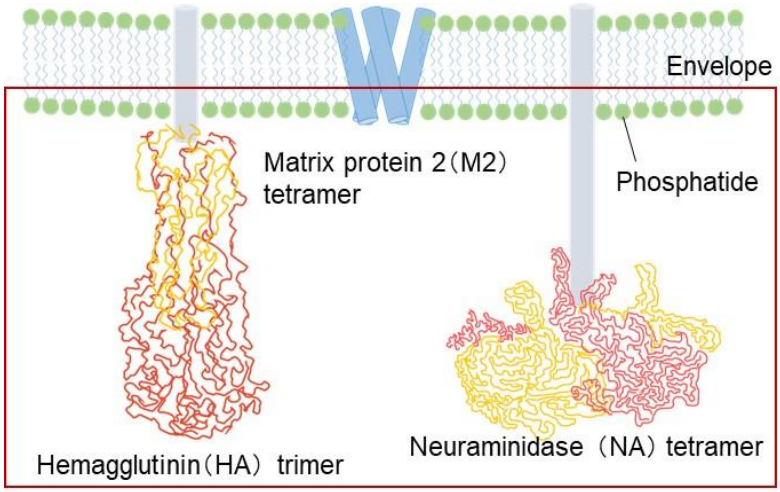

Figure 2.2.8 Schematic illustration of viral surfaces involved in FET responses.

Table 2.2.1 Number of units and charge numbers of viral membrane molecules

	HA trimer	NA tetramer	M2 tetramer	Phosphatide
Number of units	500	100	10	8.4×10^4
Charge per monomer	-13.0[*1]	-6.25[*2]	-2.71[*3]	-0.08[17]
Total charge	-2.0×10^4	-2.5×10^3	-1.1×10	-6.7×10^3

*1 UniProtKB - A7WRB7 (A7WRB7_9INFA), *2 UniProtKB - A7WRC1 (A7WRC1_9INFA), *3 UniProtKB - A7WRC4 (A7WRC4_9INFA)

2.2.3.3 Feasibility of glycan-immobilized FET toward surveillance of pandemic IFV outbreak

For the practical application of glycan-immobilized FET biosensors, it is necessary to detect IFV particles in biological samples. To evaluate the feasibility of glycan-immobilized FET biosensors, the detection of IFV particles spiked in human nasal mucus was attempted. First, the electrical responses of Siaα2,6'Lac-immobilized FET biosensor were obtained by directly adding the nasal samples with and without $10^{7.5}$ $TCID_{50}$/mL H1N1 human IFV. As a result, the FET responses, regardless of existence of IFVs, and wide error bars were confirmed (Figure 2.2.9). Furthermore, the glycan-immobilized surfaces after the addition of mucus samples were observed by using AFM. The AFM images show no granular materials derived from the IFV particle were observed, indicating that the viral particles did not adsorb to the glycan-immobilized surface (Figure 2.2.10a). Additionally, the glycan-immobilized surface after the addition of only nasal mucus was uneven (Figure 2.2.10b). These results suggested that high viscous nasal mucus induced the inhibition of the adsorption of IFV particles and the nonspecific adsorption of nasal mucus components, such as mucin, albumin, IgG, and lysozyme.[18] Hence, it was necessary to suppress the influence of nasal mucus to detect IFV particles.

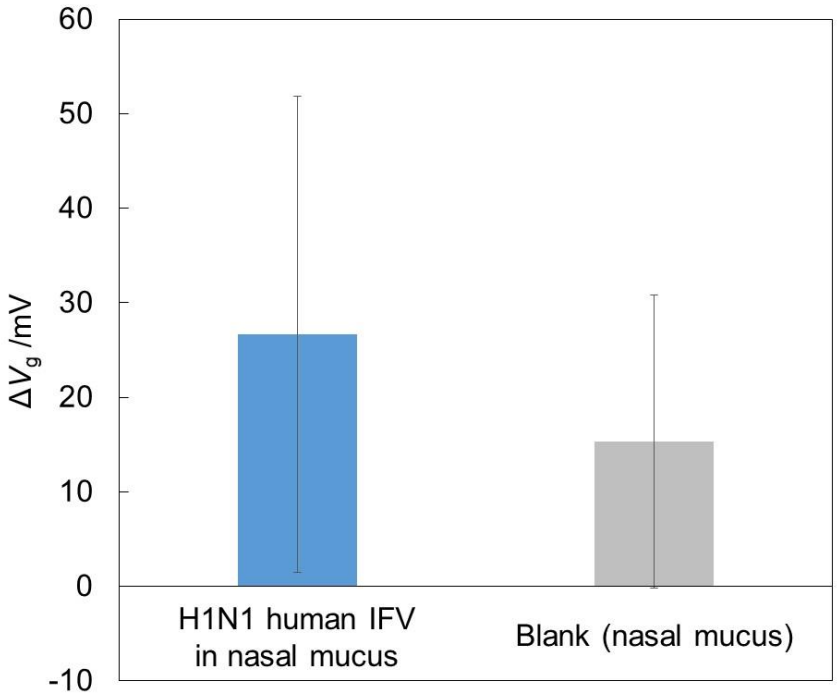

Figure 2.2.9 The magnitude of ΔV_g caused by the addition of human nasal mucus with or without $10^{7.5}$ $TCID_{50}$/mLH1N1 human IFVs. The nasal mucus was collected from a healthy adult. Error bars indicate the standard deviation (n = 3).

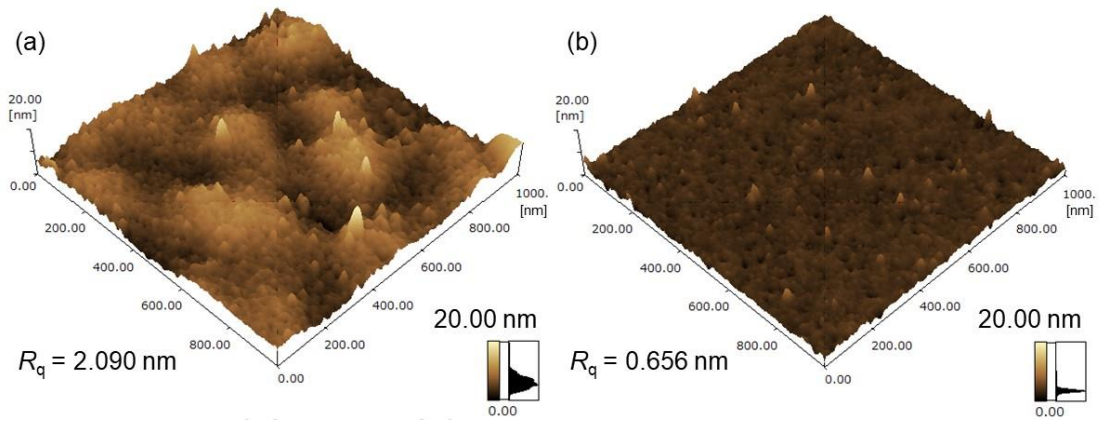

Figure 2.2.10 Atomic force microscopic images of the Siaα2,6'Lac-immobilized FET gate surface after the addition of untreated nasal mucus (a) with and (b) without H1N1 human IFV.

The above results suggest that the viscosity of nasal mucus affects the detection of IFV by FET biosensors. Nasal mucus is viscous due to the aggregation of mucin molecules, which are glycoproteins. To suppress the viscosity of nasal mucus, I proposed the viscosity reduction treatment using LCEE, a mucoactive agent. Thiol groups of LCEE cleave the disulfide bonds between mucin molecules, thus reducing the viscosity of nasal mucus. To optimize the condition of LCEE treatment for reducing the viscosity of nasal mucus, the relationship between the magnitude of ΔV_g caused by the addition of nasal mucus containing $10^{6.5}$ $TCID_{50}$/mL H1N1 human IFV and the concentration of LCEE was examined. As shown in Figure 2.2.11, when 10 mg/mL LCEE solution was added to the mucus sample, the electrical responses of the Siaα2,6'Lac-immobilized FET biosensor were higher than that of other conditions. In the case of 1 mg/mL LCEE, the responses derived from the adsorption of IFV particles to the glycan-immobilized surface was relatively small because the viscosity reduction was insufficient. Moreover, at the concentration of 10 mg/mL to 100 mg/mL, the magnitude of signal decreased with increasing LCEE concentration. This result was assumed that the higher-order structure of the H1N1 HA was denatured at pH 5.6[19], resulting in a decrease in the ability of HA to recognize glycan (pH 5.86 at 10 mg/mL LCEE, pH4.93 at 50 mg/mL, and pH 4.05 at 100 mg/mL LCEE). Additionally, as negative charges of mucin decreased at low pH values, the viscosity was increased due to a decrease in the electrostatic interaction between mucin molecules.[20] Subsequently, AFM was used to observe the glycan-immobilized surface after the addition of IFV-containing nasal mucus with viscosity reduction treatment. The granular materials derived from IFV particles were observed (Figure 2.2.12a). After dropping the treated nasal mucus, the roughness value of the glycan-immobilized surface was reduced compared with that of the untreated nasal mucus, suggesting inhibition of nonspecific adsorption of mucus components (Figure 2.2.12b). Therefore, 10 mg/mL LCEE solution was the optimal condition to reduce the viscosity of nasal mucus.

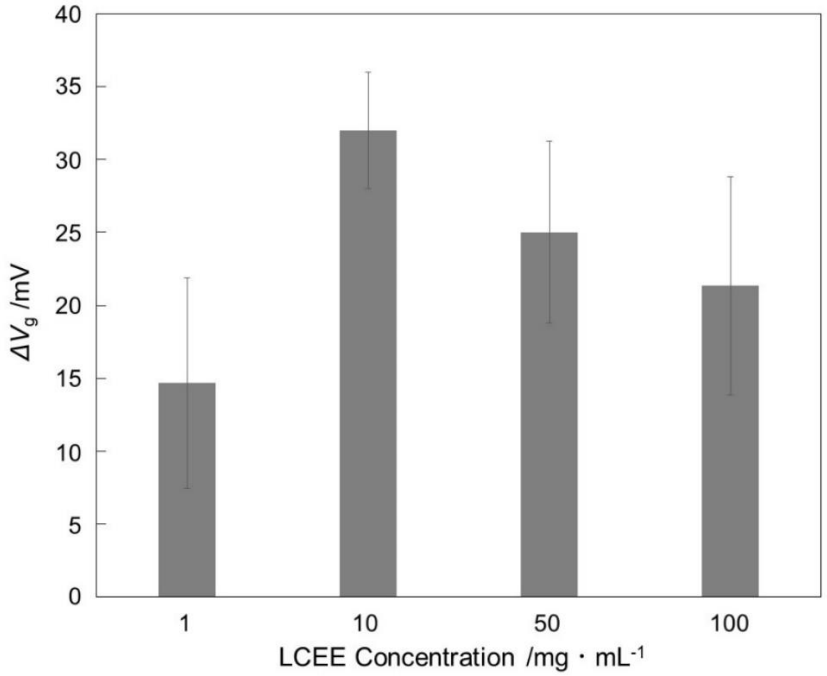

Figure 2.2.11 Relationship between ΔV_g caused by the addition of $10^{6.5}$ $TCID_{50}$/mL H1N1 human IFV in nasal mucus and the LCEE concentration to reduce the viscosity of nasal mucus (n = 3).

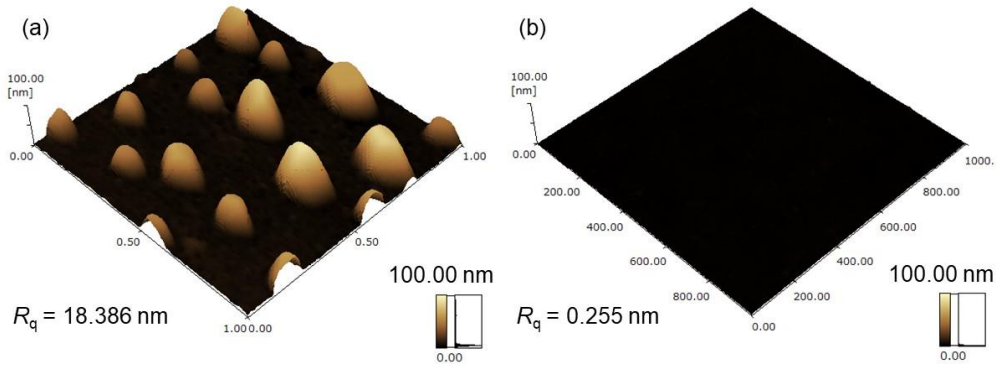

Figure 2.2.12 Atomic force microscopic images of the Siaα2,6'Lac-immobilized FET gate surface after the addition of nasal mucus sample treated by 10 mg/mL LCEE (a) with and (b) without H1N1 human IFV.

Subsequently, the detection of IFV in LCEE-treated nasal mucus using the glycan-immobilized FET biosensors was examined. As a result, Siaα2,6'Lac- and Siaα2,3'Lac-immobilized FET biosensors showed specific responses to H1N1 human IFV and H5N1 avian IFV, respectively. In contrast, little sensor response was observed when only nasal mucus was dropped as a blank measurement (Figure 2.2.13). Therefore, glycan-immobilized FET biosensors that strongly capture IFVs due to the cluster glycoside effect was suggested to discriminate IFV subtypes in nasal mucus. Furthermore, to evaluate the versatility of LCEE treatment, FET responses of $10^{6.5}$ $TCID_{50}$/mL H5N1 avian IFV suspended in nasal mucus collected from multiple individuals were measured (Figure 2.2.14). The glycan-immobilized FET biosensors showed almost identical responses to mucus samples from each individuals. Therefore, LCEE treatment could be useful for the treatment of nasal mucus and specific detection of IFV strains using the glycan-immobilized FET biosensors.

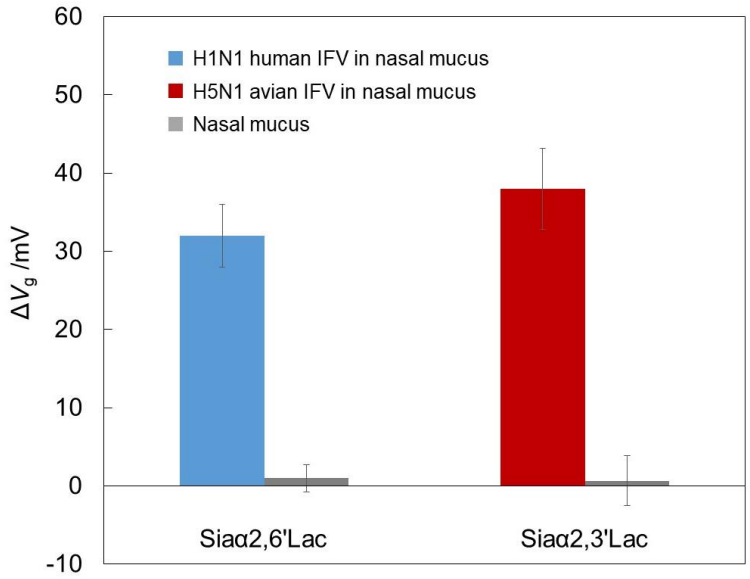

Figure 2.2.13 ΔV_g of Siaα2,6'Lac- and Siaα2,3'Lac-immobilized FET biosensors obtained by the addition of H1N1 human IFV and H5N1 human IFV suspended in nasal mucus, respectively (n = 3). The nasal mucus was treated by 10 mg/mL LCEE.

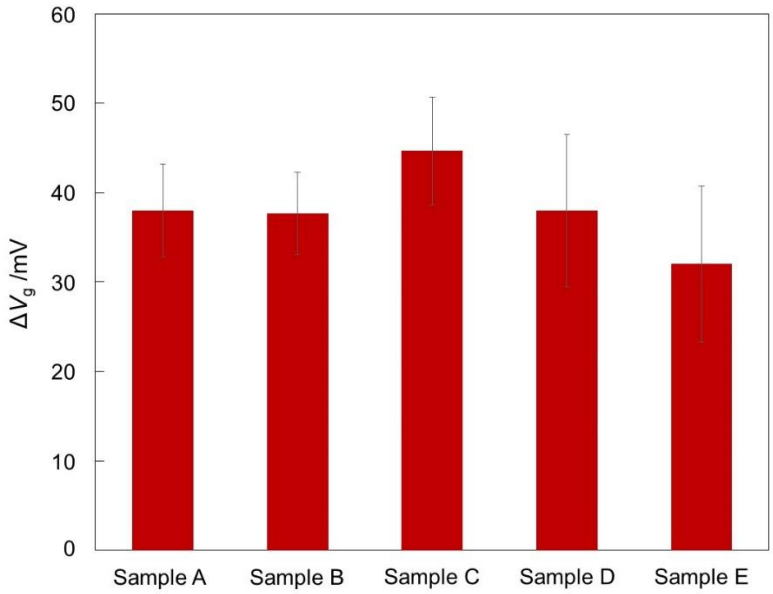

Figure 2.2.14 Reproducibility of viscosity reduction treatment using LCEE for the detection of $10^{6.5}$ $TCID_{50}$/mL H5N1 avian IFV suspended in nasal mucus. Error bars represent standard deviation (n = 3).

Finally, the discrimination capability of the glycan-immobilized FET biosensor was assessed toward surveillance of pandemic IFV outbreak. Each subtype of the influenza virus is usually not infectious beyond the host. However, pandemic occurs when highly pathogenic influenza virus strains, such as H5N1 and H7N9 avian IFV, acquire the ability to infect humans through mutation. Thus, careful surveillance is required for the preparation for new pandemics.[21,22] Here, the glycan-immobilized dual-channel FET biosensors were developed to check the infectivity of IFV in one step. Siaα2,6'Lac and Siaα2,3'Lac were separately immobilized on each gate surface of the FET, which has two FET elements on the one chip. Then, the FET responses caused by the addition of H1N1 human IFV, H5N1 avian IFV, and Newcastle disease virus (NDV) spiked in nasal mucus were measured (Figure 2.2.15). It should be noted that the NDV was used as a model of a pandemic IFV because the NDV's surface protein, hemagglutinin-neuraminidase, has an affinity to both α2,6 and α2,3 sialic acid-linkages.[23,24] As a result, H1N1 human IFV and H5N1 avian IFV were detected by the Siaα2,6'Lac- and Siaα2,3'Lac-immobilized FET elements, respectively. On the other hand, both glycan-immobilized FET elements yielded the FET responses corresponding to the NDV particles. Therefore, dual-channel FET biosensors could be useful for the surveillance of pandemic IFV outbreak by a combination of glycan immobilization and viscosity reduction treatment.

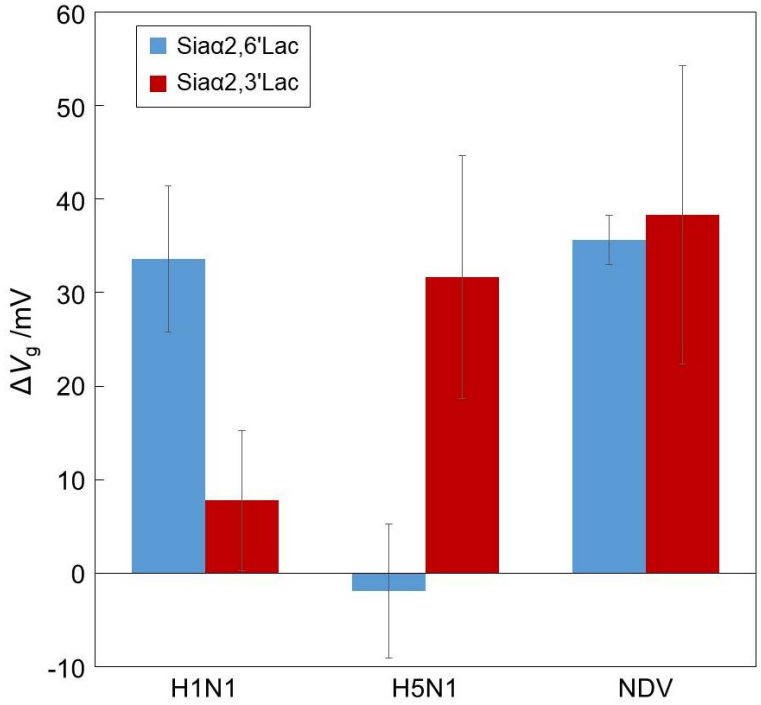

Figure 2.2.15 Identification of infectivity of three kinds of viruses, H1N1 human IFV, H5N1 avian IFV, and Newcastle disease virus (NDV), using glycan immobilized dual-channel FET biosensors. Siaα2,6'Lac and Siaα2,3'Lac were immobilized on each gate surface of the FET chip. Error bars represent standard deviation (n = 3).

2.2.4 Conclusion

In chapter 2.2, the detection of IFV particles using the glycan-immobilized FET biosensors was demonstrated. The multivalent binding between HA molecules on the viral membrane and glycans showed the robust interaction, and thus IFV particles were considered to be adhered to the glycan-immobilized surface. As a result, the FET biosensor specifically and sensitively detected a wide range of IFV concentrations under high ionic strength. It was suggested that the interface with densely immobilized glycans enables the detection of viral particles under a physiological environment by FET biosensors due to the expression of the cluster glycoside effect. Additionally, since the sialyllactose-immobilized FET biosensors determined the infectious ability of the IFV to hosts, they were expected to be a surveillance device for the next pandemic outbreak.

References

1. Lundquist, J. J. & Toone, E. J. The cluster glycoside effect. *Chem. Rev.* **102**, 555–578 (2002).
2. Xiong, X. *et al.* Receptor binding by a ferret-transmissible H5 avian influenza virus. *Nature* **497**, 392–396 (2013).
3. Lee, Y. C. & Lee, R. T. Carbohydrate-Protein Interactions: Basis of Glycobiology. *Acc. Chem. Res.* **28**, 321–327 (1995).
4. Varki, A. Biological roles of glycans. *Glycobiology* **27**, 3–49 (2017).
5. Xu, H. & Shaw, D. E. A Simple Model of Multivalent Adhesion and Its Application to Influenza Infection. *Biophys. J.* **110**, 218–233 (2016).
6. Nakamura, T., Sakurai, Y., Hideshima, S., Kuroiwa, S. & Osaka, T. Sialylglycan-modified field effect transistor for detection of charged lectin under physiological conditions. *Chem. Lett.* **39**, 1245–1247 (2010).
7. Gaymard, A., Le Briand, N., Frobert, E., Lina, B. & Escuret, V. Functional balance between neuraminidase and haemagglutinin in influenza viruses. *Clin. Microbiol. Infect.* **22**, 975–983 (2016).
8. Hideshima, S. *et al.* Attomolar detection of influenza A virus hemagglutinin human H1 and avian H5 using glycan-blotted field effect transistor biosensor. *Anal. Chem.* **85**, 5641–5644 (2013).
9. Imai, M. *et al.* Experimental adaptation of an influenza H5 HA confers respiratory droplet transmission to a reassortant H5 HA/H1N1 virus in ferrets. *Nature* **486**, 420–428 (2012).
10. Herfst, S. *et al.* Airborne Transmission of Influenza A/H5N1 Virus Between Ferrets. *Science* **336**, 1534–1541 (2012).
11. Michen, B. & Graule, T. Isoelectric points of viruses. *J. Appl. Microbiol.* **109**, 388–397 (2010).
12. Horiguchi, Y. *et al.* Direct and label-free influenza virus detection based on multisite binding to sialic acid receptors. *Biosens. Bioelectron.* **92**, 234–240 (2017).
13. Chan, K. H. *et al.* Analytical sensitivity of seven point-of-care influenza virus detection tests and two molecular tests for detection of avian origin H7N9 and swine origin H3N2 variant influenza a viruses. *J. Clin. Microbiol.* **51**, 3160–3161 (2013).
14. Murti, K. G. & Webster, R. G. Distribution of hemagglutinin and neuraminidase on influenza virions as revealed by immunoelectron microscopy. *Virology* **149**, 36–43 (1986).

15. Zebedee, S. L. & Lamb, R. A. Influenza A virus M2 protein: monoclonal antibody restriction of virus growth and detection of M2 in virions. *J. Virol.* **62**, 2762–2772 (1988).
16. Schaap, I. A. T., Eghiaia, F., Des George, A. & Veigel, C. Effect of envelope proteins on the mechanical properties of influenza virus. *J. Biol. Chem.* **287**, 41078–41088 (2012).
17. Tanford, C. *The Hydrophobic Effect: Formation of Micelles and Biological Membranes*. *John Wiley & Sons* **2nd edition**, (1980).
18. Majima, Y. *et al.* Effect of Biochemical Components on RheologicProperties of Nasal Mucus in Chronic Sinusitis. *Am J Respir Crit Care Med* **160**, 421–426 (1999).
19. Scholtissek, C. Stability of infectious influenza A viruses at low pH and at elevated temperature. *Vaccine* **3**, 215–218 (1985).
20. Bhaskar, K. R. *et al.* Profound increase in viscosity and aggregation of pig gastric mucin at low pH. *Am. J. Physiol. Liver Physiol.* **261**, G827–G832 (1991).
21. Kain, T. & Fowler, R. Preparing intensive care for the next pandemic influenza. *Crit. Care* **23**, 337 (2019).
22. Neumann, G. & Kawaoka, Y. Predicting the Next Influenza Pandemics. *J. Infect. Dis.* **219**, S14–S20 (2019).
23. Sánchez-Felipe, L., Villar, E. & Muñoz-Barroso, I. α2-3- and α2-6- N-linked sialic acids allow efficient interaction of Newcastle Disease Virus with target cells. *Glycoconj. J.* **29**, 539–549 (2012).
24. Yusoff, K. & Wen Siang Tan. Newcastle disease virus: Macromolecules and opportunities. *Avian Pathol.* **30**, 439–455 (2001).

Chapter 3:

Control of aptamer immobilization density on FET biosensor toward detection of charged and uncharged salivary stress markers

3.1 Introduction

For the practical application of FET biosensors, sensitive and stable biosensing element is desired. Recently, aptamers, which were single-stranded nucleic acid molecules, have been attracting attention as receptors instead of antibodies as described in Chapter 1. Aptamers have a wide range affinity to various molecules; metal ions,[1] organic compounds,[2] proteins,[3,4] viral particles,[5] and many more. Additionally, aptamers are more thermally stable and reversible than antibodies, which is expected to increase the shelf-lives and reusability of point-of-care devices functionalized with aptamers. Thus, aptamers are excellent candidates as receptors of FET biosensors to detect not only charged but also uncharged molecules, taking advantage of their small size (several nanometers) and the possibility of introducing conformational changeability.[6,7]

The binding efficiency of aptamers to target molecules was affected by the immobilization density on the sensing surface.[8] Hence, adjusting the immobilization density of aptamers is expected to be effective in increasing surface potential changes on the FET gate surface to improve the sensitivity of aptamer-immobilized FET biosensors. In general, the immobilization density is determined by varying the concentration of the aptamer solution or incubation time. Alternatively, I attempted to immobilize aptamer molecules by utilizing their properties, negative charges and conformational changeability. As the negative charges originated from the phosphate groups of the nucleotide are shielded by cation species, the magnitude of intermolecular electrostatic interactions of aptamers can vary with ionic strength.[9] Therefore, changing the electrostatic repulsion between aptamer molecules via the ionic strength of the buffer solution may allow to control the immobilized density of aptamers. Furthermore, when conformation-changeable aptamers are densely immobilized on an interface, conformational changes are inhibited by steric hindrance between adjacent aptamers.[10] A conformation-changeable aptamer often forms the higher-order structure (e.g., the G-quadruplex (G4) structure[11]) by binding target molecules. Additionally, it is known that the G4 structure is formed by coordination of K^+ ions.[12] The higher-order structure in the aptamer molecule is a bulky and relatively stable region. Thus, immobilization of conformational changed aptamers was expected to form a certain distance to involve a

conformational change during target molecule capture.

In this chapter, two strategies during immobilization of aptamer for controlling immobilization density were demonstrated based on its characteristics; (1) varying the ionic strength of buffer solution and (2) inducing the conformational change. To evaluate the above effects, the stress markers, chromogranin A (CgA), secretory immunoglobulin A (s-IgA), and cortisol, were selected as target molecules.[13] First, the relationship between the immobilization density of the aptamer and ionic strength was evaluated in order to fabricate aptamer-immobilized surfaces of FET biosensors that are able to efficiently capture charged CgA and s-IgA (Figure 3.1). Next, a strategy for overcoming the steric hindrance between cortisol aptamers to conformational change was investigated to induce the conformational change during immobilization. Applying the immobilization of conformational changed aptamers, which have a G4 structure in their structure, forms a space for conformational changes during target detection. Specifically, the induction of conformational change of aptamers was attempted by either binding to the target molecule or induction of G4 structure by K^+ ions coordination (Figure 3.2).

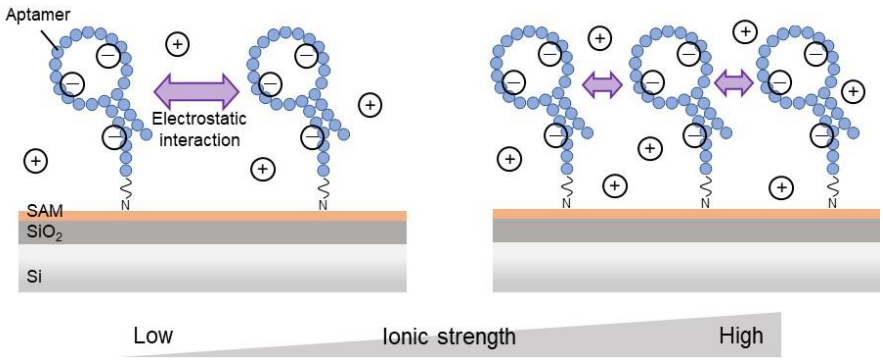

Figure 3.1 Schematic illustration of the effect of ionic strength on the aptamer immobilization density.

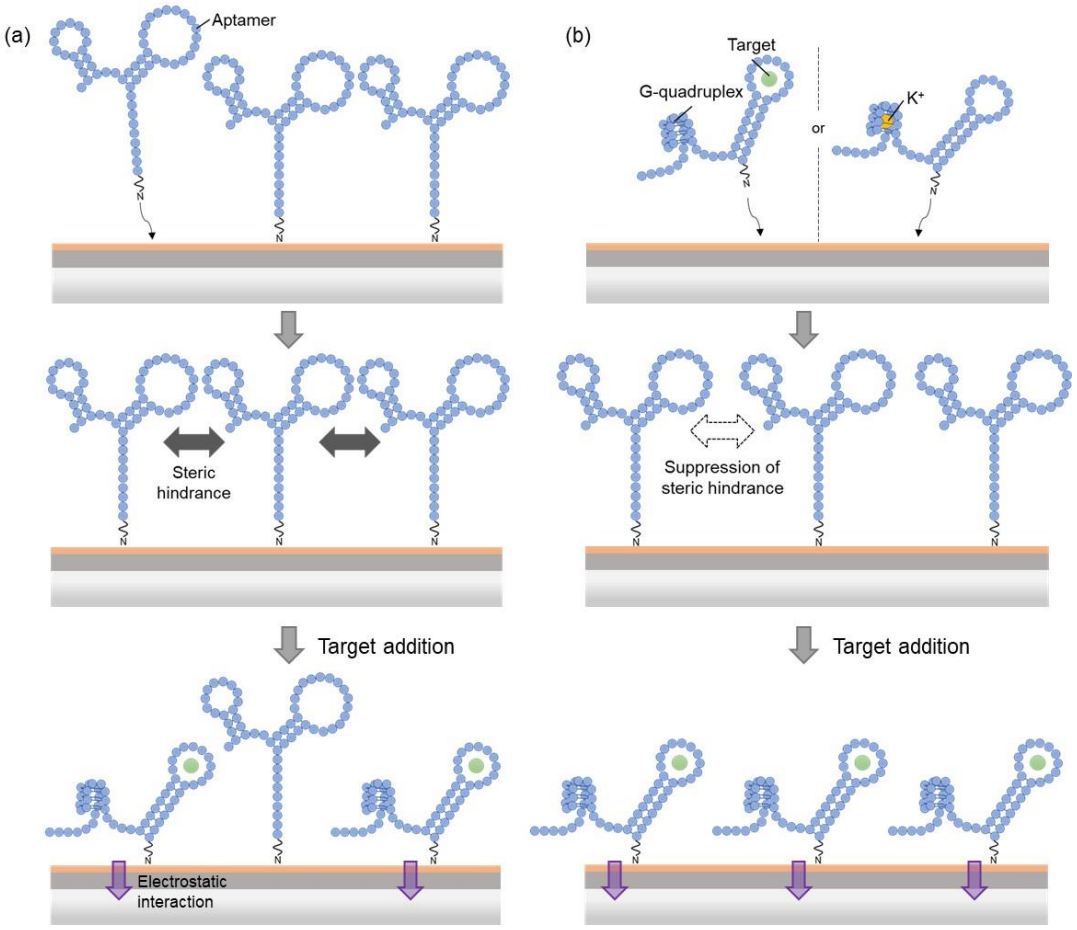

Figure 3.2 Schematic illustration of (a) conformationally unchanged aptamer and (b) conformationally changed aptamer immobilization.

3.2 Experimental

3.2.1 Nucleic acid sequence of aptamers

Each DNA aptamer was synthesized by NEC Solution Innovators, Ltd. (Tokyo, Japan). Table 3.1 shows the nucleotide sequences for each aptamer. CgA and s-IgA aptamers were purified using NG7 (represented by lowercase t in Table 3.1), a modified nucleic acid (Figure 3.3a). The 5'-terminus of the CgA and s-IgA aptamers and the 3'-terminus of the cortisol aptamers were modified with an amino group (Figure 3.3b and c).

Table 3.1 Nucleic acid sequence of each aptamer

	Nucleic acid sequence[*1]
CgA aptamer	5'- GTCAGCCTCC TAAAGAACGt GCtAAGttCC CCGttGtGCG CGCtGGtGAA GAACC -3'
s-IgA aptamer	5' - GCAATCTCCC TAATCtGCtG AtGtttGtAt ttCAAAttAG C – 3'
cortisol aptamer	5' - ACCTCTGTGG GTGGGAGGGT CGGGCCCTCA GAGGTCTCTT TGCCCGTGAA CTCTG-3'

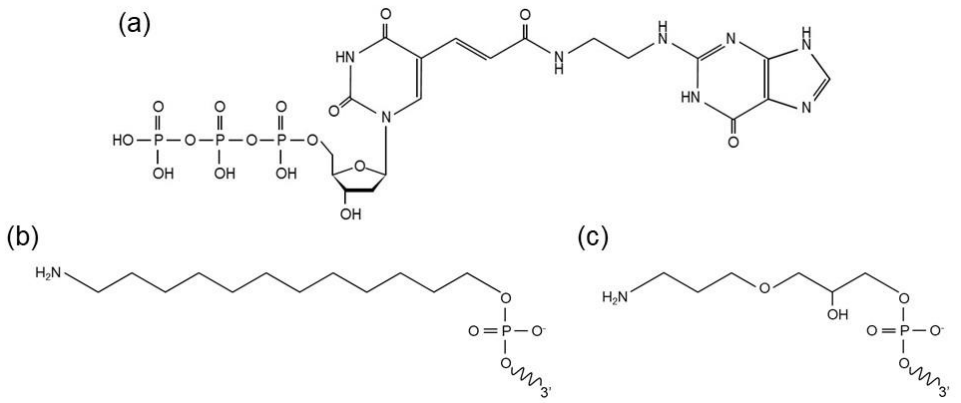

Figure 3.3 Structural formula of (a) NG7, (b) the 5'-terminus of the CgA and s-IgA aptamers, and (c) the 3'-terminus of the cortisol aptamers.

3.2.2 Fabrication of aptamer-immobilized FET biosensors

The n-type FET was exposed to O_2 plasma (200 W, 1 min) using a gas plasma reactor (PR301; Yamato Scientific Co., Ltd., Tokyo, Japan) to introduce hydroxyl groups onto the SiO_2 gate insulator surface. Then, a self-assembled monolayer (SAM) of APS was modified by immersing in 1% (v/w) APTES diluted in toluene solution under an argon atmosphere (60°C, 7 min). Following the modification of 2.5% glutaraldehyde (GA), the gate voltage swept to reduce Schiff bases. The hybridization of aptamer molecules was cleaved by heating (95°C, 5 min) and quenching with ice (5 min). After that, 100 nM of aptamers diluted in buffer solution was dropped onto the FET gate insulator surface and incubated for 60 min. Then, 10 mM ethanolamine was reacted with unreacted aldehyde groups. The immobilization density of the aptamers on the Si wafer, whose SiO_2 insulator was thermally oxidized, was evaluated based on fluorescence measurements using a variable mode imager (Typhoon 9410; Cytiva).

3.2.3 Preparation of conformational changed aptamer

First, to prepare the target-bound aptamers, 0 to 1,000 μM cortisol were added to 100 nM aptamers, which were heated and quenched for the cleavage of hybridization, in K^+-rich phosphate-buffered saline (PBS). Here, the K^+-rich PBS buffer, hereafter denoted as PBS_K, was prepared by replacing the sodium ions in PBS with potassium ions. After incubation (60 min) of the mixture, the cortisol-bound aptamer was dropped onto the GA-modified surface. It should be noted that the condition of 0 μM cortisol means that the aptamer molecules with no conformational change were immobilized to the FET gate surface. After immobilization, to remove cortisol molecules from the cortisol-bound aptamer, the FET chips were immersed in 8 M urea aqueous solution[14] (60 min). Second, aptamers with induced conformational change were prepared by varying the K^+ concentrations of PBS. As with the conformational changed aptamers were reacted with the GA-modified surface (60 min). Finally, each aptamer-immobilized FET biosensor was treated with 10 mM tris(hydroxymethyl)aminomethane (Tris) for capping the unreacted aldehyde groups of GA.

3.2.4 Electrical measurement

The gate voltage (V_g) – drain current (I_d) curves were made in buffer solution by scanning V_g from -3.0 V to +0.5 V with drain voltage (V_d) of +0.1 V using a System SourceMeter (2612A, Keithley Instruments Inc., USA). The reference electrode was Ag/AgCl (ALS Co., Ltd.). 0.01 × PBS for CgA and s-IgA detection and 0.04 × PBS_K for cortisol detection were used as measurement solution, respectively. The gate voltage shift (ΔV_g) was calculated from the $V_g - I_d$ curves before and after the addition of stress markers diluted in 1 × PBS. In this study, CgA, s-IgA, and cortisol were purchased from Creative BioMart Inc. (USA), MP Biomedicals (California, USA), and Sigma-Aldrich Inc. (USA).

3.2.5 Preparation of sweat samples

The human saliva was collected from two healthy adults using the Cryovial and the Saliva Collection Aid (Salimetrics LLC., USA). Saliva samples were centrifuged for removal of contaminating substances (1,500 × g, 15 min), and the supernatant liquid was used. The cortisol concentration in human saliva was determined by the salivary cortisol ELISA enzyme immunoassay kit (Salimetrics LLC., USA).

3.3 Results and discussion

3.3.1 Control of aptamer immobilization density by electrostatic interaction on FET biosensors for detection of charged CgA and s-IgA

The effect of ionic strength on the immobilization density of aptamers was evaluated to detect charged CgA and s-IgA using the FET biosensor. First, the electrical responses caused by the addition of 10 μg/mL (143 nM) CgA were measured using aptamer-immobilized FET biosensors, which were prepared by the immobilization of the CgA aptamer in different buffer solutions of 0.01 ×, 0.1 ×, and 1 × PBS. With the CgA-aptamer sensors, the shift of the FET characteristics toward the positive direction was attributed to the negative charges of CgA (pI = 4.6, 4.7[13]) captured by the CgA aptamer within the Debye length (7.5 nm) of 0.01 × PBS as the measurement solution. The increase in ΔV_g with the addition of 10 μg/mL CgA was confirmed to be dependent on ionic strength (Figure 3.4), with a maximal response at 1 × PBS. In addition, the dependence of the immobilization density of the CgA aptamers on ionic strength was confirmed from fluorescence measurements using fluorescent-labeled aptamers. The immobilization density of the CgA aptamers was found to increase under high ionic strength conditions (Table 3.2). These results indicate that ionic strength has a significant effect on the intermolecular electrostatic interaction between the CgA aptamer molecules. With the increase in ionic strength, it is presumed that the counterionic species shield the negative charges of the entire aptamer molecule, and the electrostatic repulsion is suppressed. Hence, CgA aptamers were densely immobilized under high ionic strength conditions, resulting in an increase in the amount of CgA molecules captured by the aptamers.

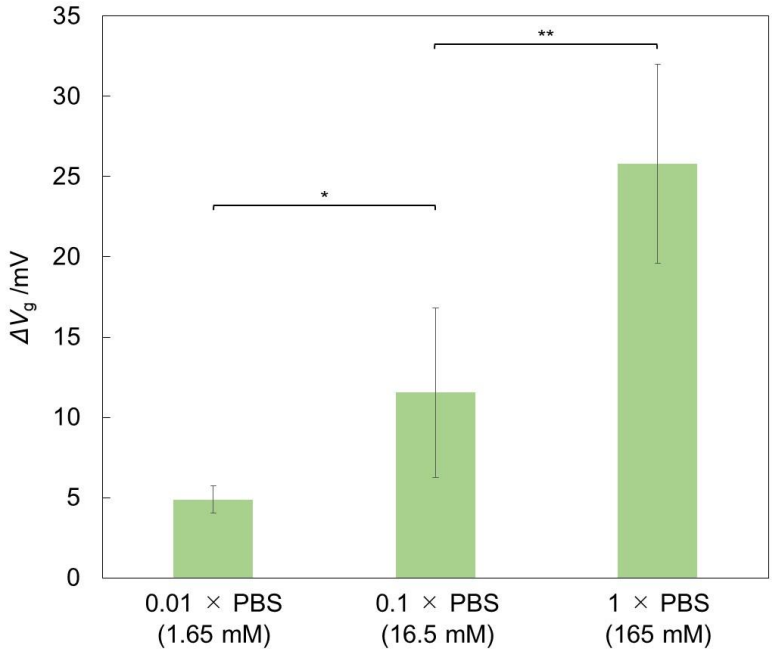

Figure 3.4 Effect of ionic strength of buffer solution on the magnitude of ΔV_g of CgA aptamer-immobilized FET biosensor. The FET responses were induced by the addition of 10 μg/mL CgA (n = 4–6). Error bars indicate the standard deviation. The asterisks (* and **) are $p < 0.05$ and $p < 0.01$, respectively.

Table 3.2 Immobilization density of CgA aptamer under various ionic strength

	0.01 × PBS	0.1 × PBS	1 × PBS
Immobilization density / cm^{-2}	0.3×10^{12}	0.5×10^{12}	1.1×10^{12}
Radius of the occupied space / nm	9.8	7.6	5.1

Next, the effect of ionic strength on immobilization density during aptamer immobilization in s-IgA-aptamer sensors was investigated from response to the addition of 100 μg/mL (294 nM) s-IgA. The results confirmed that the immobilization density of the s-IgA aptamer was controlled by the ionic strength as well as that of the CgA aptamer. The ΔV_g values obtained from the FET biosensor with aptamers immobilized in 0.1 × and 1 × PBS were higher than the values obtained from those immobilized in 0.01 × PBS (Figure 3.5). Consequently, each ΔV_g was caused by the field effect from a part of a negatively charged s-IgA molecule (pI = 5.4 - 6.2[15]), since the s-IgA molecules were captured by the aptamer within the Debye length of 0.01 × PBS. Additionally, the increase in the immobilization density of the s-IgA aptamer with the increase in ionic strength was confirmed by fluorescence measurements (Table 3.3). The change in the ionic strength affected the intermolecular electrostatic interaction between the aptamers, resulting in the suppression of electrostatic repulsion and an increase in the immobilization density of the s-IgA aptamer at high ionic strength. Furthermore, the immobilization density of the s-IgA aptamer was saturated at the ionic strength of 0.1 × PBS. In 0.1 × PBS, the electrostatic interactions between the other aptamers were weakened by the shielding effect of the counterions. This may be because the total negative charge of the s-IgA aptamer (41 mer) is less than that of the CgA aptamer (55 mer). These results indicate that the immobilization density of the s-IgA aptamers can be increased by suppressing the intermolecular electrostatic interactions between aptamer molecules at high ionic strength.

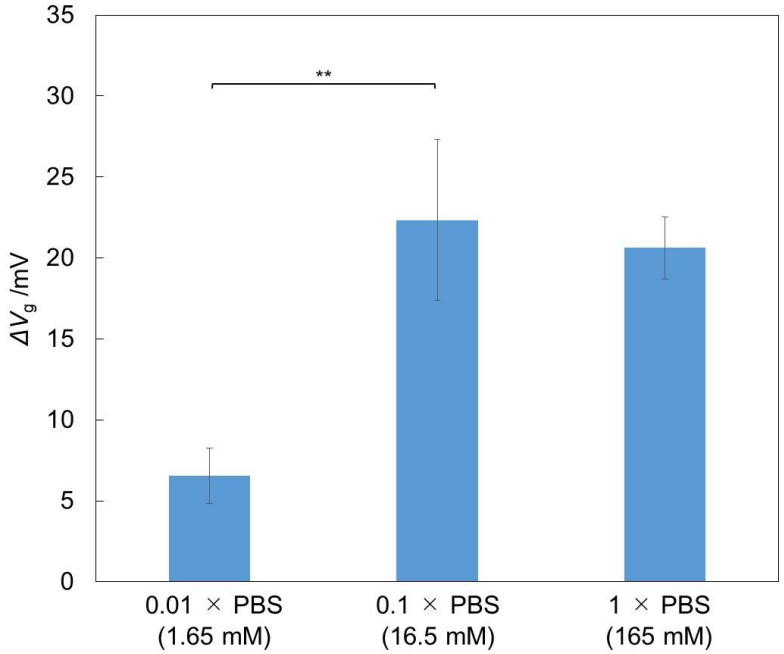

Figure 3.5 Effect of ionic strength of buffer solution on the magnitude of ΔV_g of s-IgA aptamer-immobilized FET biosensor. The FET responses were induced by the addition of 100 μg/mL s-IgA (n = 4–5). Error bars indicate the standard deviation. The asterisk (*) is $p < 0.05$.

Table 3.3 Immobilization density of s-IgA aptamer under various ionic strength

	0.01 × PBS	0.1 × PBS	1 × PBS
Immobilization density / cm^{-2}	1.5×10^{12}	4.1×10^{12}	3.2×10^{12}
Radius of the occupied space / nm	4.4	2.7	3.0

To evaluate the quantitative detectability of aptamer-immobilized FET biosensors, the dependences of ΔV_g on the CgA and s-IgA concentrations were measured. Based on the above results, the CgA and s-IgA aptamers were immobilized on the FET gate surface in 1 × PBS and 0.1 × PBS, respectively. As shown in Figure 3.6, the CgA aptamer-immobilized FET biosensor exhibited a quantitative relationship between the ΔV_g and CgA concentrations of 0.1 to 10 μg/mL (1.4 to 143 nM). In addition, the s-IgA aptamer-immobilized FET biosensor provided quantitative detection between 0.1 and 1 μg/mL (0.3 to 2.9 nM). The FET response was saturated at s-IgA concentrations above 1 μg/mL (2.9 nM). As s-IgA (420 kDa[16]) is larger than CgA (70 kDa[17]), the adsorption of s-IgA molecules on the aptamer-immobilized surfaces may be spatially inhibited by a steric hindrance from the neighboring adsorbed s-IgA molecules. Additionally, to evaluate the specificity of the CgA aptamer and s-IgA aptamer-immobilized FETs, the magnitudes of ΔV_g caused by addition of 1.8 μM α-amylase (pI = 6.0 - 6.9[18]) were +8.9 ± 0.6 mV (n = 3) and +5.0 ± 1.6 mV (n = 3), respectively. From the 3σ limit of detection, the CgA aptamer-immobilized FET biosensor and s-IgA aptamer-immobilized FET biosensor detected each target at 1.4 and 0.3 nM. Thus, both aptamer-immobilized FET biosensors were able to detect charged stress markers at the nM-level.

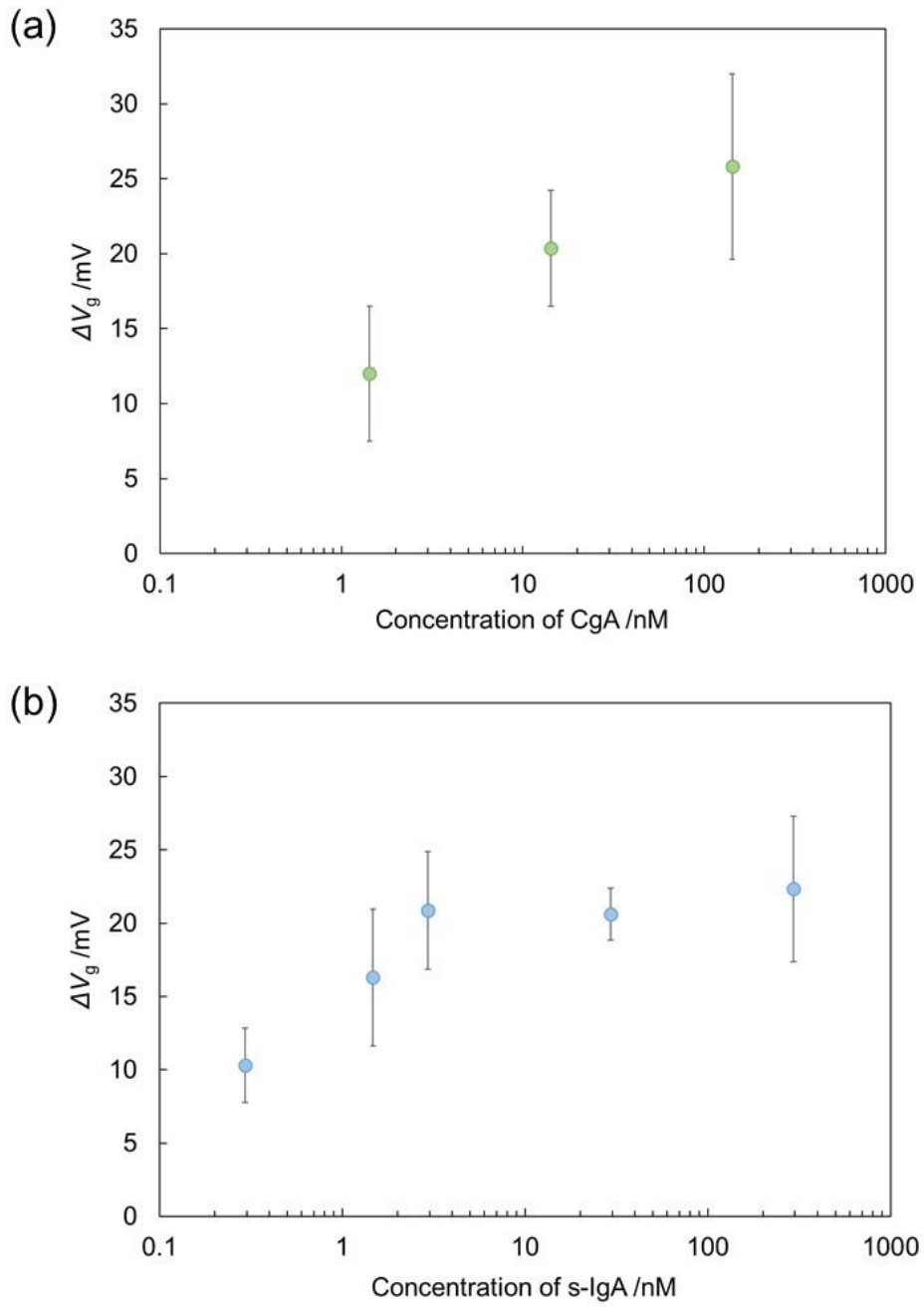

Figure 3.6 Quantitative detection of (a) CgA aptamer- and (b) s-IgA aptamer-immobilized FET biosensors with concentrations of CgA (n = 6) and s-IgA (n = 4–6) ranging from 0.1 to 10 μg/mL (1.4 to 143 nM) and 0.1 to 100 μg/mL (0.3 to 294 nM), respectively. Error bars indicate the standard deviation.

3.3.2 Control of aptamer immobilization density using conformational changeability on FET biosensors for detection of uncharged cortisol

Initially, the detectable ability of conformation-changeable aptamer to detect uncharged cortisol using FET biosensors was conformed. The cortisol aptamer used in this study forms the G-quadruplex (G4) structure by binding to cortisol. The charge density within the Debye length of 0.04 × PBS_K (λ_D = 3.7 nm) from the FET gate surface was considered to be increased due to the formation of the G4 structure attributed to cortisol binding (Figure 3.7). Here, PBS_K was used as a solvent to stabilize the G-quadruplex structure of the aptamers by potassium ions.[19] Besides, it should be noted that secondary structures are calculated using the Mfold algorithm.[20] Based on the results mentioned above, the immobilization of aptamers in 1× PBS was used to suppress electrostatic repulsion and increase immobilization density. The electrical response caused by the addition of 1 mM cortisol was measured. As shown in Figure 3.8, the gate voltage was shifted to a positive direction when cortisol was added. In contrast, hardly FET response was observed due to the addition of 1 × PBS as a blank measurement or 20 μM α-amylase as a negative control. These results indicated that FET biosensors specifically detected uncharged cortisol via conformational changes in aptamers. These results suggest that the FET biosensor detects uncharged cortisol by using a conformation-changeable aptamer.

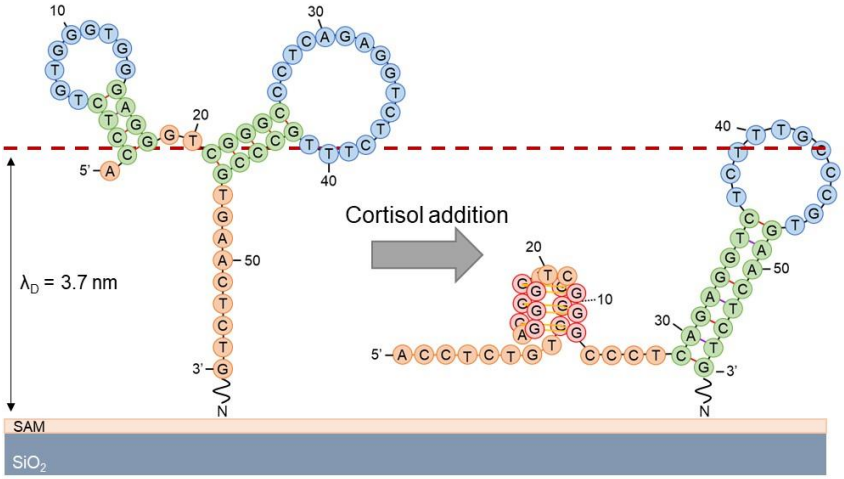

Figure 3.7 Schematic image of the secondary structure of cortisol aptamer. Conformational changes induced by binding cortisol molecules in 0.04 × PBS_K. Each color indicates a loop structure (blue), stem structure (green), single-stranded region (orange), and G-quadruplex (red).

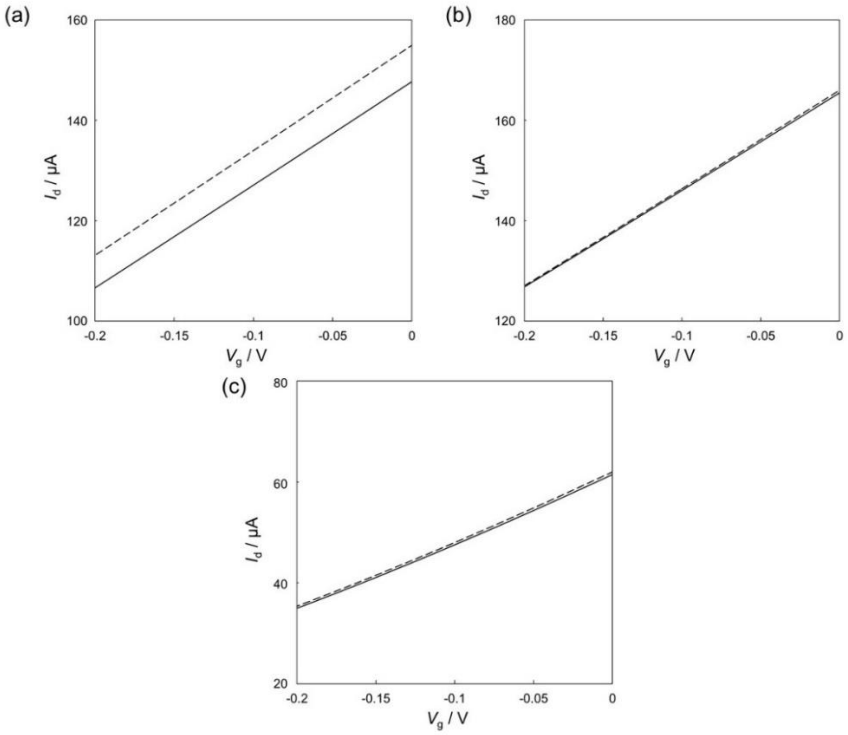

Figure 3.8 Gate voltage shifts (ΔV_g) of cortisol aptamer-immobilized FET biosensor caused by the addition of (a) 1 mM cortisol, (b) 1 × PBS, and (c) 20 μM α-amylase. All electrical measurements were performed using 0.04 × PBS_K as the buffer solution.

The above investigation indicated that the conformational changeability of aptamers enables the detection of uncharged cortisol molecules using FET biosensors. However, when aptamer molecules are densely immobilized on the FET gate insulator surface by suppressing intermolecular electrostatic repulsion, a decrease in the distance between adjacent aptamers may inhibit the conformational changes of aptamers owing to steric hindrance.[10] Here, inducing the conformational change of aptamer during the immobilization process was attempted to achieve a favorable density to capture cortisol molecules by reducing the steric hindrance of aptamers. First, I examined the conformational changes induced by binding to the target molecules. The amount of immobilized aptamer depending on mixed cortisol concentration was investigated to determine the cortisol concentration for the formation of the target-bound aptamers. Gate voltage changes before and after the immobilization of the aptamers, which reacted with different concentrations of cortisol molecules in 1 × PBS_K, were measured. As shown in Figure 3.9, the magnitude of the changes in V_g decreased with increasing cortisol concentration, indicating that the amount of immobilized aptamer was decreased. It should be noted that each FET characteristic was measured in 0.04 × PBS_K after removing the cortisol bound to the aptamer at the time of immobilization. It means that the structures of immobilized aptamers were the same in each FET measurement regardless of the immobilization conditions. Therefore, the FET biosensors would detect an equal number of negative charges from the single aptamer. At the 500 or 1,000 μM cortisol, the gate voltage shifts derived from the immobilization of aptamer molecules were significantly decreased compared with responses caused by the addition of target-unbound aptamers. There was concern that adding too much of the insoluble cortisol molecules would inhibit the immobilization of aptamers. Then, the immobilization density of the target-bound aptamers prepared by binding with 50 μM of cortisol was investigated using fluorescence measurements. As a result, the immobilization density of the cortisol-bound aptamers was 0.5 × 10^{12} cm^{-2} lower than that of the target-unbound aptamer immobilized in 1× PBS (Table 3.4). Therefore, mixing 50 μM cortisol with aptamers was found to be effective for decreasing the immobilization density towards forming a space for conformational changes.

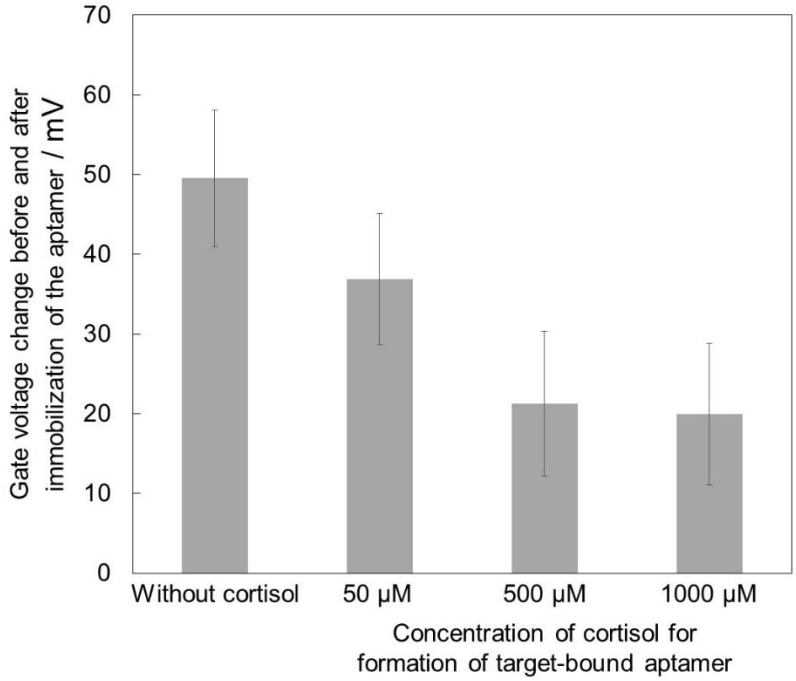

Figure 3.9 The change in V_g before and after immobilization of the aptamer, which reacted with the various cortisol concentrations for the formation of target-bound aptamer (n = 3–6). Error bars indicate the standard deviation.

Table 3.4 Immobilization density of cortisol aptamer with and without 50 μM cortisol

	Cortisol-unbound aptamer	Cortisol-bound aptamer
Immobilization density / cm^{-2}	1.4×10^{12}	0.9×10^{12}
Radius of the occupied space / nm	4.5	5.6

To evaluate the effect of the spacing the immobilized aptamer by using the target-bound aptamer immobilization, the quantitative detectability was compared with FET biosensors functionalized with aptamers without any target molecules in 1× PBS. As a result, FET biosensors fabricated with target-bound aptamers showed higher responses to each concentration of cortisol than FET biosensors immobilized the target-unbound aptamers (Figure 3.10). In Figure 3.7, the radius occupied by the aptamer after the conformational change was estimated to be 4.8-6.4 nm by assuming that the aptamer rotates on the 3'-terminus. Also, note that half of the Debye length of 1×PBS was added to the occupancy radius, assuming charges of aptamer affected electrostatically to other aptamers. The radius of the unbound aptamer was 4.5 nm from the fluorescence measurement (Table 3.4), suggesting that the steric hindrance occurred during cortisol capture. On the other hand, target-bound aptamer immobilization increased the radius occupied by the aptamer. These results indicated that an increase in the space of the immobilized aptamers reduced the steric hindrance between adjacent aptamer molecules. Additionally, no significant responses of target-bound aptamer-immobilized FET biosensors were observed due to the addition of 20 μM α-amylase as a negative control. Since the decrease in immobilization density by the target-bound aptamer immobilization could lead to an increase in unreacted glutaraldehyde, the sensing surface was treated by Tris molecules, which have three hydroxy groups, as a capping agent. As a result, the ability to suppress the non-specific adsorption of amylase was improved. Moreover, in the case of applying the target-bound aptamer immobilization, the aptamer-immobilized FET biosensors could quantitatively detect cortisol as low as 1 μM calculated by the 95% significant difference from the negative control. On the other hand, the FET biosensor with directly immobilized aptamers was found to detect 10 μM or more cortisol quantitatively. Therefore, target-bound aptamer immobilization could increase the spacing between each aptamer to bind to a cortisol molecule effectively.

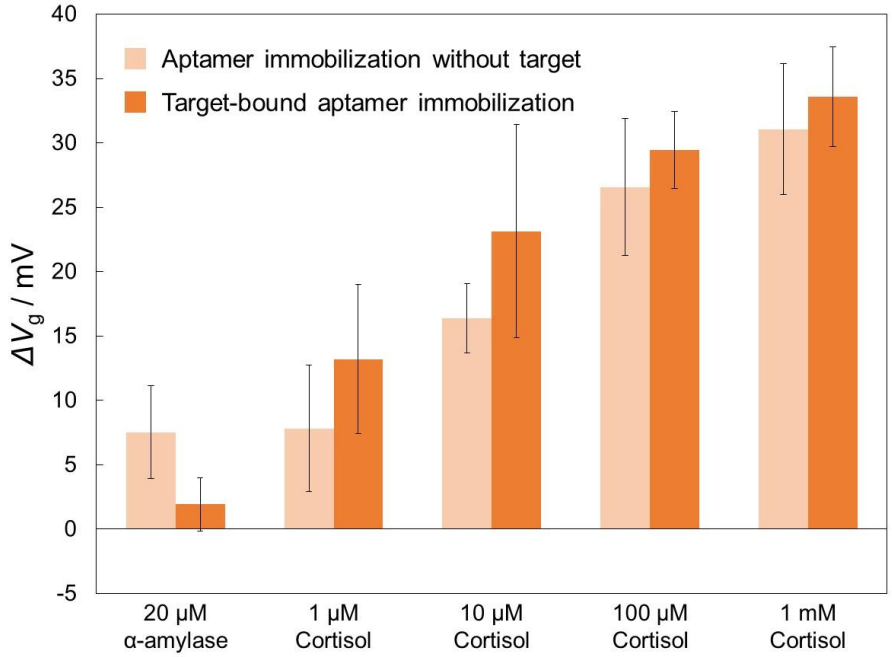

Figure 3.10 Comparison of ΔV_g of aptamer-immobilized FET biosensors prepared by aptamer immobilization without target and target-bound aptamer immobilization caused by the addition of cortisol ranging from 1 μM to 1 mM or 20 μM α-amylase (n = 3–5). Error bars indicate the standard deviation.

Immobilization of aptamers using the conformational change was found to be useful in forming the space to reduce the steric hindrance between aptamer molecules. The sensitivity of FET biosensors applying the above concept is affected by the residual of the target molecules used to form target-bound aptamers. The aptamer structure is dependent on ionic concentration, temperature, and pH.[21] In particular, it has been reported that K^+ ions induce the formation of G4 structures.[12] Thus, if it was possible to change the cortisol aptamer structure with only K^+ ions, it was expected to further improve the sensitivity of biosensors by eliminating the influence of residual target molecules, which were used for target-bound aptamer. To investigate the effect of K^+ ions for the conformational change of aptamer molecules, the formation of the G4 structure was confirmed by fluorescence analysis using N-methyl mesoporphyrin IX (NMM), which specifically binds to G4.[22] It should be noted that aptamer-immobilized surface was prepared by the addition of 100 nM aptamer molecules in 1 × PBS. It means that the immobilization density of aptamer molecules was considered being equivalent. As shown in Figure 3.11, the aptamer-immobilized surface, which was treated with 200 nM NMM diluted in 1 × PBS_K (C_{K+} = 157 mM) for 60 min, showed 1.8 times higher fluorescence intensity than that treated using 1 × PBS (C_{K+} = 4 mM). This result suggested that K^+ ions induced the formation of G4 structures.

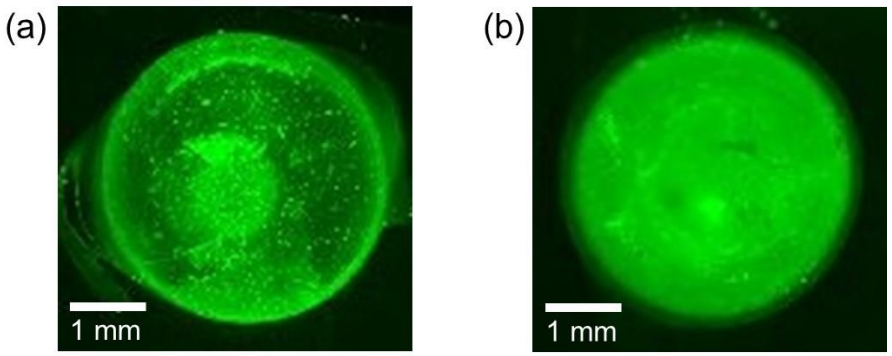

Figure 3.11 Fluorescence images of aptamer-immobilized Si substrates treated with 200 nM NMM diluted (a) 1 × PBS and (b) 1 × PBS_K.

Subsequently, to optimize the K^+ concentration for the favorable immobilization density of aptamer, electrical responses caused by the addition 1 mM cortisol was measured using the FET biosensors, which were functionalized with 100 nM aptamer in various ratios of 1 × PBS and 1 × PBS_K. As shown in Figure 3.12, the magnitude of the ΔV_g increased with K^+ concentration. These results suggested that conformationally changed aptamers due to K^+ ions were spaced on the FET gate surface, resulting in effective capture of cortisol by reducing steric hindrance between adjacent aptamers. Moreover, when 20 μM α-amylase as a negative control was dropped to the aptamer-immobilized FET biosensors, which were prepared in the ratio of PBS : PBS_K = 1:9 (C_{K+} = 142 mM) or 0:10 (C_{K+} = 157 mM), the magnitudes of ΔV_g were significantly different from the positive control (Figure 3.13). Thus, the aptamer-immobilized FET biosensors showed the specificity to cortisol molecules. The negative control response of the FET biosensor immobilized with the aptamers at the ratio of PBS : PBS_K of 1:9 was smaller than that of 0:10. Furthermore, the immobilization density of the conformational-changed aptamers prepared by PBS : PBS_K of 1:9 was 0.3×10^{12} cm^{-2} (the radius occupied by the aptamer was 10.4 nm) using fluorescence measurements, indicating that the number of immobilized aptamer molecules was decreased compared with that of target-bound aptamer immobilization. It was assumed that the aptamer structure of the cortisol-binding region was stable by cortisol binding. Hence, the K^+-induced conformational changed aptamers without cortisol binding might reduce immobilization density due to the flexible structure of cortisol-binding region compared to the target-bound aptamers. From these results, the ratio of PBS : PBS_K = 1:9 was selected as an immobilization condition for the formation of the conformational-changed aptamer by K^+ ions coordination.

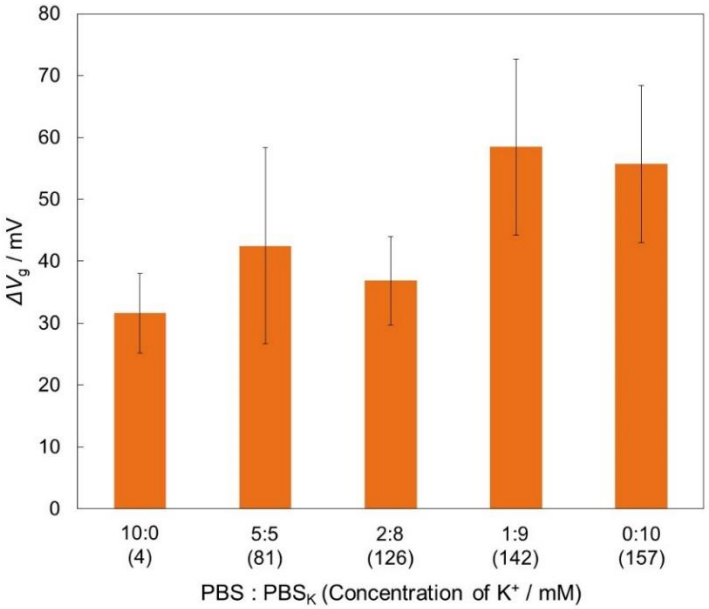

Figure 3.12 The effect of K^+ ions during aptamer immobilization to the ΔV_g caused by the addition of 1 mM cortisol. The K+ ion concentration was varied by the ratio of PBS to PBS_K (165 mM). Error bars indicate the standard deviation (n = 4).

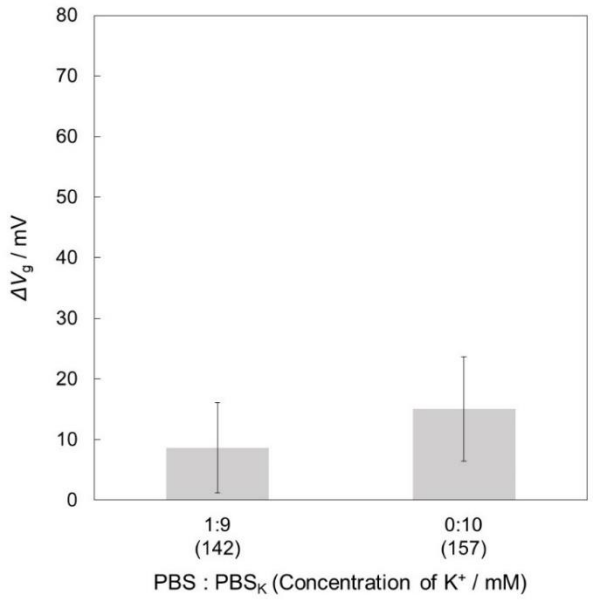

Figure 3.13 The ΔV_g caused by the addition of 20 μM α-amylase to the aptamer-immobilized FET biosensors, which were prepared with PBS and PBS_K in a ratio of 1:9 or 1:10. Error bars indicate the standard deviation (n = 4).

To evaluate the quantitative detectability of density-controlled aptamer-immobilized FET biosensor by K^+ ions coordination, ΔV_g caused by the addition of different concentrations of cortisol was measured. As a result, linearity between the FET responses and broad cortisol concentrations ranging from 1 nM to 1 mM, which correspond to salivary cortisol concentration,[23] was obtained (Figure 3.14). The limit of detection (LOD) of aptamer-immobilized FET biosensor, calculated by the 3σ method compared with blank measurement (+4.8 ± 4.4 mV, n =4), was 10 nM, indicating higher sensitivity than that of the conventional immobilization or the target-bound aptamer immobilization. The difference in sensitivity is due to the aptamer immobilization density discussed above. Moreover, in the target-bound aptamer immobilization method, the number of aptamers, which are able to bind to the target, could have decreased due to the residual cortisol utilized during immobilization. Thus, these results indicated that the immobilization technique utilizing the conformational changeability of aptamers by the formation of G4 structure could improve the sensitivity of FET biosensors.

Finally, detection of cortisol in human saliva was examined. Since cortisol concentrations are known to change with circadian rhythm,[24] saliva samples were collected from one person in the morning and night. As a result, the FET responses caused by the addition of two saliva samples were +19 ± 6 mV (n = 4) and +11 ± 8 mV (n = 4), respectively. Moreover, the ΔV_g of saliva samples collected from a different person in the morning was +19 ± 5 mV (n = 3). The cortisol concentrations in saliva samples determined by the aptamer-immobilized FET biosensors based on the calibration curve in Figure 3.14 were approximately matched with that obtained by a commercial ELISA kit (Table 3.5). Therefore, the aptamer immobilization using conformational change induced by K^+ ions was useful to improve the sensitivity of FET biosensors and enable the detection of salivary cortisol concentration.

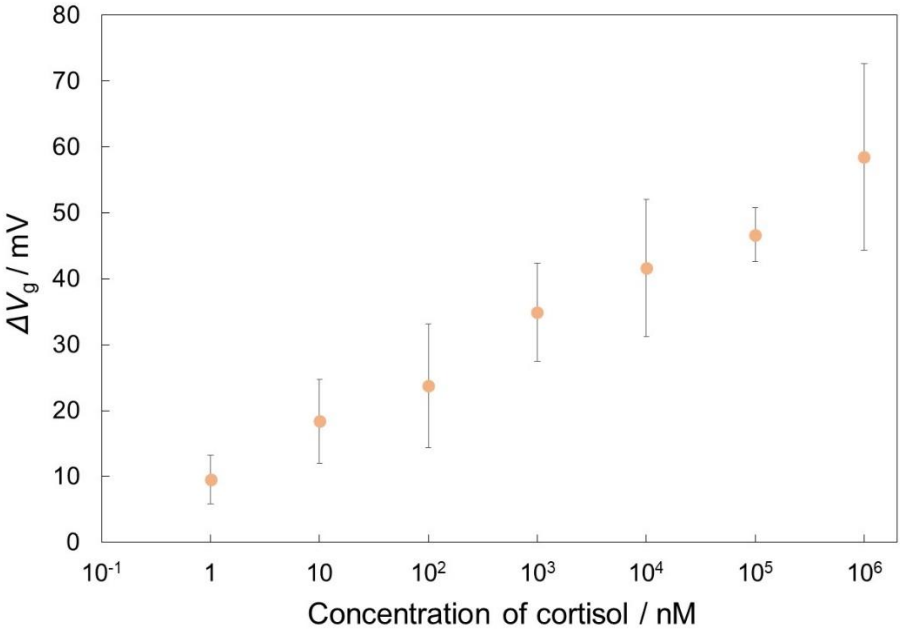

Figure 3.14 The relationship between ΔV_g and different concentrations of cortisol from 1 nM to 1 mM. Error bars indicate the standard deviation (n = 3–4).

Table 3.5 Comparison of cortisol concentration in human saliva by the aptamer-immobilized FET biosensor and ELISA

	Time	Concentration from ELISA / nM	Average of ΔVg / mV	Calculated concentration / nM
Saliva sample 1 – (1)	9:30	10.6	19 ± 5.8	14.9
Saliva sample 1 – (2)	21:39	1.5	11 ± 8.2	1.5
Saliva sample 2	9:38	10.5	19 ± 5.0	14.2

3.4 Conclusion

In chapter 3, techniques to control the immobilization density based on the characteristics of aptamers were demonstrated. First, by focusing on the negative charge originated from phosphate groups, the electrostatic interaction between aptamers was changed by varying the ionic strength during immobilization. As a result, the detectability of FET biosensors to charged CgA and s-IgA was increased by the formation of a high-density aptamer-immobilized interface. Subsequently, control of the aptamer immobilization density by using the conformational changeability introduced by the aptamer design was attempted. The formation of higher-order structures by conformational change increased the spacing between adjacent aptamers, resulting in effective binding to small cortisol. In particular, the immobilization density was reduced by the formation of G4 structures due to the coordination of K^+ ions. Therefore, the design of aptamer-immobilized interfaces based on the interaction between aptamer molecules was suggested to improve the sensitivity of FET biosensors.

References

1. Ciesiolka, J. & Yarus, M. Small RNA-divalent domains. *RNA* **2**, 785–793 (1996).
2. Kaneko, N. *et al.* An aptamer-based biosensor for direct, label-free detection of melamine in raw milk. *Sensors* **18**, 3227 (2018).
3. Minagawa, H. *et al.* Selection, Characterization and Application of Artificial DNA Aptamer Containing Appended Bases with Sub-nanomolar Affinity for a Salivary Biomarker. *Sci. Rep.* **7**, 42716 (2017).
4. Minagawa, H. *et al.* Fluorescence Polarization-Based Rapid Detection System for Salivary Biomarkers Using Modified DNA Aptamers Containing Base-Appended Bases. *Anal. Chem.* **92**, 1780–1787 (2020).
5. Pan, W. *et al.* Isolation of virus-neutralizing RNAs from a large pool of random sequences. *Proc. Natl. Acad. Sci. U. S. A.* **92**, 11509–11513 (1995).
6. Maehashi, K. *et al.* Label-free protein biosensor based on aptamer-modified carbon nanotube field-effect transistors. *Anal. Chem.* **79**, 782–787 (2007).
7. Nakatsuka, N. *et al.* Aptamer-field-effect transistors overcome Debye length limitations for small-molecule sensing. *Science* **362**, 319–324 (2018).
8. Simon, L., Bognár, Z. & Gyurcsányi, R. E. Finding the Optimal Surface Density of Aptamer Monolayers by SPR Imaging Detection-based Aptamer Microarrays. *Electroanalysis* **32**, 851–858 (2020).
9. Herne, T. M. & Tarlov, M. J. Characterization of DNA probes immobilized on gold surfaces. *J. Am. Chem. Soc.* **119**, 8916–8920 (1997).
10. Macdonald, H. *et al.* Influence of Aptamer Surface Coverage on Small Target Recognition: A SPR and QCM-D Comparative Study. *J. Phys. Chem. C* **123**, 13561–13568 (2019).
11. Davis, J. T. G-Quartets 40 Years Later: From 5′-GMP to Molecular Biology and Supramolecular Chemistry. *Angew. Chem. Ed.* **43**, 668–698 (2004).
12. Takenaka, S. & Juskowiak, B. Fluorescence detection of potassium ion using the G-quadruplex structure. *Anal. Sci.* **27**, 1167–1172 (2011).
13. Obayashi, K. Salivary mental stress proteins. *Clin. Chim. Acta* **425**, 196–201 (2013).
14. Xu, X. *et al.* Reconfigurable Carbon Nanotube Multiplexed Sensing Devices. *Nano Lett.* **18**, 4130–4135 (2018).
15. Elkon, K. B. Isoelectric focusing of human IgA and secretory proteins using thin layer agarose gels and nitrocellulose capillary blotting. *J. Immunol. Methods* **66**, 313–321 (1984).

16. Björk, I. & Lindh, E. Gross Conformation of Human Secretory Immunoglobulin A and Its Component Parts. *Eur. J. Biochem.* **45**, 135–145 (1974).
17. Small, D. H., Ismael, Z. & Chubb, I. W. Acetylcholinesterase hydrolyses chromogranin a to yield low molecular weight peptides. *Neuroscience* **19**, 289–295 (1986).
18. Takeuchi, T., Matsushima, T. & Sugimura, T. Separation of human α-amylase isozymes by electro-focusing and their immunological properties. *Clin. Chim. Acta* **60**, 207–213 (1975).
19. Verdian-Doghaei, A., Housaindokht, M. R., Bozorgmehr, M. R. & Abnous, K. Conformational switch of insulin-binding aptamer into G-quadruplex induced by K+ and Na+: An experimental and theoretical approach. *J. Biomol. Struct. Dyn.* **33**, 1153–1163 (2015).
20. Zuker, M. Mfold web server for nucleic acid folding and hybridization prediction. *Nucleic Acids Res.* **31**, 3406–3415 (2003).
21. Phan, A. T. & Mergny, J. L. Human telomeric DNA: G-quadruplex, i-motif and Watson-Crick double helix. *Nucleic Acids Res.* **30**, 4618–4625 (2002).
22. Nicoludis, J. M. *et al.* Optimized end-stacking provides specificity of N-methyl mesoporphyrin IX for human telomeric G-quadruplex DNA. *J. Am. Chem. Soc.* **134**, 20446–20456 (2012).
23. Manetti, L. *et al.* Usefulness of salivary cortisol in the diagnosis of hypercortisolism: Comparison with serum and urinary cortisol. *Eur. J. Endocrinol.* **168**, 315–321 (2013).
24. Keller, J. *et al.* Cortisol Circadian Rhythm Alterations in Psychotic Major Depression. *Biol. Psychiatry* **60**, 275–281 (2006).

Chapter 4:

General Conclusion

This thesis described the guidelines of the design of the FET biosensing interface suitable for binding to target molecules based on the characteristics of receptors and their biomolecular interaction. In particular, glycan, lectin, and aptamers were used as recognition elements in FET biosensors, as an alternative to antibodies.

In Chapter 2.1, utilizing multimeric lectin as a receptor was shown to be useful for the increase in the number of available binding sites on the FET biosensors. Generally, bioreceptors are immobilized to the sensing interface in a random orientation by covalent bonding via cross-linkers, resulting in a decrease in the available binding sites. The multimeric lectin, which has several glycan-binding sites in their structure symmetrically, suppressed the influence of the random orientation on the FET biosensor, because any of the binding sites were capable of binding to target molecules. Thus, it was suggested that the strategy of using multimeric biomolecules as a receptor was effective for the increase in the sensitivity of FET biosensors. From the findings, the use of symmetric lectins (e.g., jacalin, concanavalin A, PA-IL, PA-IIL) will enable the development of FET platforms for the detection of various glycans and glycoproteins, and thus novel glycan arrays using FET biosensors are expected to become tools for the analysis of glycan-lectin interactions.

In Chapter 2.2, a dense and oriented glycan-immobilized surface enabled the detection of viral molecules under the high ionic strength using the FET biosensors by expression of the cluster glycoside effect. This was due to the multivalent binding between glycans and viral membrane proteins, and thus reduction of the Debye screening effect. For the practical application of FET biosensors, it is necessary to detect biomolecules in a physiological environment. Therefore, the formation of a highly dense and oriented glycan-immobilized surface is effective for the detection of many biomolecules; virus, microbe, and cell. In particular, since various infectious viruses bind the glycans of cells for the infection, glycans were shown to be promising receptors for the development of FET biosensors to survey the next pandemics.

In Chapter 3, the strategies for immobilization of aptamer molecules on the FET gate surface were proposed. Since aptamers are immobilized in a fixed orientation by a modifying group at the terminus, it is important to adjust the immobilization density to increase the number of aptamers that are able to capture the target molecule. An increase in the available binding sites of the aptamer-immobilized surface was attempted by focusing on the control of immobilization density based on the properties of aptamers. First, varying the ionic strength of the buffer solution during immobilization changed the Debye screening effect. A decrease in the electrostatic repulsion between negatively-charged aptamers in high ionic strength formed a dense aptamer-immobilized surface, increasing the detectable ability to charged molecules. Next, utilizing conformational changeability was exploited to aptamer immobilization in high ionic strength. In this chapter, techniques on forming the higher-order structure of aptamer were shown to be useful for achieving a sensing surface functionalized with aptamers at favorable high-density corresponding to the conformational change during binding small target molecules. These methods provide guidelines for the design of aptamer-immobilized interfaces, as they allow for effective interaction with the target molecule.

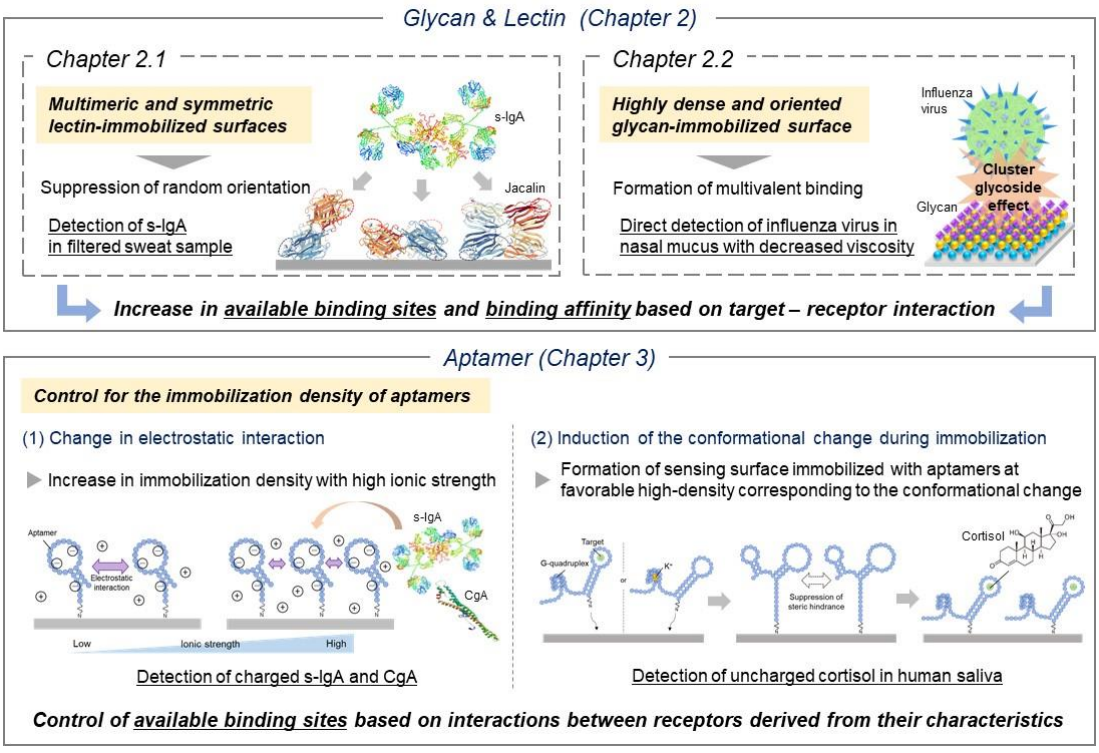

Schematic illustration of thesis findings

This thesis indicated the usefulness of glycan-lectin and aptamer as receptors for FET biosensors instead of antibodies. In particular, the functionalization method for receptor-immobilized surfaces that effectively bind target molecules was demonstrated by designing interfaces based on biomolecular interactions. Furthermore, the sensing interface enabled the detection of target molecules in non-invasive biological samples by FET biosensors. Thus, these results showed the feasibility of using FET biosensors to measure non-invasive samples for daily health monitoring instead of invasive samples. For the further development of FET biosensors in the future, it will be necessary to improve the reproducibility of the sensor response. The reproducibility of the sensor response is affected by variations in fundamental processes (e.g., SAM modification and receptor immobilization) on the sensing surface, as well as external factors (e.g., temperature and pH) and internal factors (e.g., semiconductor-derived noise) in electrical measurements. Hence, it is considered to be effective to apply automation of the formation process of sensing surface and multivariate analysis using multiple FET elements. In summary, the findings of this study are expected to contribute to the expansion of functionalization methods for biosensing surfaces and accelerate the practical application of FET biosensors for simple daily measurements.

List of Achievements

1. Pubications

Original Papers

H. Hayashi, R. Toyama, R. Takibuchi, S. Hideshima, S. Kuroiwa, N. Kaneko, K. Horii, K. Ohashi, T. Momma, T. Osaka, “Immobilization of Target-Bound Aptamer on FET Biosensor to Improve Sensitivity for Detection of Uncharged Cortisol”, *Electrochemistry*, in press.

S. Kuroiwa, H. Hayashi, R. Toyama, N. Kaneko, K. Horii, K. Ohashi, T. Momma, T. Osaka, "Potassium-Regulated Immobilization of Cortisol Aptamer for Field-Effect Transistor Biosensor to Detect Changes in Charge Distribution with Aptamer Transformation", *Chemistry Letters*, in press.

H. Hayashi, N. Sakamoto, S. Hideshima, Y. Harada, M. Tsuna, S. Kuroiwa, K. Ohashi, T. Momma, T. Osaka, “Tetrameric jacalin as a receptor for field effect transistor biosensor to detect secretory IgA in human sweat”, *Journal of Electroanalytical Chemistry*, **873**, 114371, (2020).

S. Hideshima, H. Hayashi, H. Hinou, S. Nambuya, S. Kuroiwa, T. Nakanishi, T. Momma, S.-I. Nishimura, Y. Sakoda, T. Osaka, “Glycan-immobilized dual-channel field effect transistor biosensor for the rapid identification of pandemic influenza viral particles”, *Scientific Reports*, **9**, 11616, (2019).

Proceedings

R. Toyama, S. Kuroiwa, H. Hayashi, K. Ohashi, T. Momma, T. Osaka, “Fabrication of Aptamer-immobilized FET Biosensor for Sensitive Detection of Uncharged Molecules Using Target-Aptamer Complex”, Proceedings of the 66th Chemical Sensor Symposium, Supplement B, 35, 97-99 (2019)

S. Sakamoto, H. Hayashi, S. Sato, S. Hideshima, Y. Harada, M. Tsuna, S. Kuroiwa, K. Ohashi, T. Momma, T. Osaka, “Detection of Secretory IgA by Field Effect Transistor Biosensor Using Jacalin as a Small Receptor”, Proceedings of the 65th Chemical Sensor Symposium, Supplement A, **35**, 28-30, (2019).

2. Presentations

International

H. Hayashi, N. Sakamoto, S. Hideshima, Y. Harada, M. Tsuna, S. Kuroiwa, K. Ohashi, T. Momma, T. Osaka, "Detection of Stress-Related Secretory IgA in Human Sweat Using Lectin-Immobilized Field Effect Transistor Biosensor", PRiME 2020, Online, (October 2020).

K. Ohashi, S. Kuroiwa, R. Toyama, H. Hayashi, T. Momma, T. Osaka, "Saliva Stress Marker Monitor Using Aptamer Immobilized FET Biosensor", PRiME 2020, Online, (October 2020).

H. Hayashi, T. Momma, T. Osaka, "Discrimination of Influenza virus subtypes in mucus samples using glycan-immobilized semiconductor-based biosensor", 6th DGIST-Waseda Workshop on Electrochemistry 2018, Daegu, Korea, (November 2018).

S. Hideshima, H. Hayashi, S. Kuroiwa, T. Osaka, "Detection of Whole Influenza Viral Particle in High Ionic Strength Solution by using Glycan-Immobilized Field Effect Transistor Biosensor", The 12th International Symposium on Electrochemical Micro & Nano System Technologies (EMNT2018), Milano, Italy, (September 2018).

H. Hayashi, S. Hideshima, S. Kuroiwa, T. Momma, T. Osaka, "Discrimination of influenza virus subtypes in nasal mucus using glycan-immobilized field effect transistor biosensor", International Symposium on Biological Material Science for Agriculture and Engineering- Aiming at Future Interdisciplinary Collaborations, Tokyo, Japan, (June 2018).

H. Hayashi, S. Hideshima, H. Hinou, SI. Nishimura, Y. Sakoda, S. Kuroiwa, T. Nakanishi, T. Momma, T. Osaka, "Detection of Influenza virus in nasal mucus by viscosity reduction using glycan-immoobilized FET biosensor", 28th Anniversary World Congress on Biosensors 2018, Florida, USA, (June 2018).

H. Hayashi, S. Hideshima, S. Kuroiwa, T. Nakanishi, T. Momma, T. Osaka, "Development of glycan-immobilized FET biosensor toward the detection of Influenza virus from biological sample", 5th DGIST-Waseda Workshop on Electrochemistry 2017, Tokyo, Japan, (December 2017).

Domestic

黒岩繁樹，林宏樹，坂本尚輝，原田義孝，綱美香，大橋啓之，門間聰之，逢坂哲彌，「非侵襲なストレスセンサに向けた半導体バイオセンサの作製」，第 3 回 COI 学術交流会，オンライン，2020 年 7 月

林宏樹，「簡便なストレスマーカー検出のための半導体センサ界面の構築とバイオセンシングシステム」，第 2 回 COI 学会，東京，2019 年 9 月

遠山良，黒岩繁樹，林宏樹，大橋 啓之，門間聰之，逢坂哲彌，「FET バイオセンサによる非荷電分子検出の感度向上を目的としたターゲット-アプタマー複合体を用いた認識界面の構築」，2019 年電気化学秋季大会，山梨，2019 年 9 月

遠山良，林宏樹，黒岩繁樹，秀島翔，大橋啓之，門間聰之，逢坂哲彌，「ストレスマーカーの低侵襲測定に向けたアプタマー固定化電界効果トランジスタセンサの作製」，TOBIRA 第 8 回研究交流フォーラム，東京，2019 年 5 月

坂本尚輝，林宏樹，佐藤慎，秀島翔，原田義孝，綱美香，黒岩繁樹，門間聰之，逢坂哲彌，「小型受容体ジャカリンを用いた電界効果トランジスタバイオセンサによる分泌型 IgA の検出」，電気化学会第 86 回大会，京都，2019 年 3 月

林宏樹，秀島翔，比能洋，西村紳一郎，迫田義博，黒岩繁樹，門間聰之，逢坂哲彌，「インフルエンザウイルスの宿主域識別に向けた糖鎖固定化半導体センサの評価」，第 18 回 Conference for BioSignal and Medicine (CBSM)，神奈川，2018 年 10 月

林宏樹，秀島翔，比能洋，西村紳一郎，迫田義博，黒岩繁樹，中西卓也，門間聰之，逢坂哲彌，「糖鎖固定化電界効果トランジスタバイオセンサによるインフルエンザウイルス粒子の高感度検出」，Conference for BioSignal and Medicine (CBSM) 第 16 回大会，大分，2016 年 9 月

3. Awards

International

Best Presentation Award, International Symposium on Biological Material Science for Agriculture and Engineering, June 2018.

Domestic

優秀賞・異分野賞，第 2 回 COI 学会，2019 年 9 月

優秀ポスター賞，第 18 回 Conference for BioSignal and Medicine (CBSM)，2018 年 10 月

4. Others

Original Papers

S. Hideshima, S. Wustoni, M. Kobayashi, H. Hayashi, S. Kuroiwa, T. Nakanishi, T. Osaka, "Effect of human serum on the electrical detection of amyloid-β fibrils in biological environments using azo-dye immobilized field effect transistor (FET) biosensor", *Sensing and Bio-Sensing Research*, **17**, 25-29, (2018).

Proceedings

S. Kuroiwa, H. Hayashi, S. Hideshima, T. Momma, T. Osaka, "Detection of Amyloid-β Fibrils in Human Serum Using Congo-red immobilized FET Biosensor", Proceedings of the 64th Chemical Sensor Symposium, Supplement B, **34**, 22-24, (2018).

International Presentations

M. Fujita, H. Hayashi, S. Kuroiwa, K. Ohashi, T. Momma, T. Osaka, M. Okada, and F. Shibasaki, "Detection of Uncharged 5-Fluorouracil Exploiting Sequential Adsorption of 5-Fluorouracil-Modified Bovine Serum Albumin Using Field Effect Transistor Biosensor", PRiME 2020, Online, (October 2020).

S. Hideshima, S. Kuroiwa, H. Hayashi, Y. Harada, M. Tsuna, T. Momma, T. Osaka, "Semiconductor-Based Portable Biosensor for Food Allergen Detection", The IEEE International Symposium on Circuits and Systems 2019 (ISCAS2019), Hokkaido, Japan, (June 2019).

Domestic Presentations

黒岩繁樹，林宏樹，秀島翔，門間聰之，逢坂哲彌，「コンゴーレッド固定化 FET バイオセンサを用いたヒト血清中アミロイドβ凝集体の検出」，2018 年電気化学秋季大会，石川，2018 年 9 月

林宏樹，秀島翔，黒岩繁樹，大橋啓之，門間聰之，逢坂哲彌，「電界効果トランジスタバイオセンサを用いたアミロイドβ凝集体の検出」，東京バイオマーカー・イノベーション技術研究組合(TOBIRA) 第 7 回研究交流フォーラム，東京，2018 年 5 月

Patents

逢坂哲彌，大橋啓之，黒岩繁樹，林宏樹，「アプタマー固定化半導体センシングデバイス及び非荷電分子の検出方法」特願 2019-204856 号，2019 年 11 月 12 日出願

逢坂哲彌，大橋啓之，黒岩繁樹，林宏樹，「アプタマー固定化半導体センシングデバイス及び非荷電分子の検出方法」，特願 2019-150267 号，2019 年 8 月 20 日出願

逢坂哲彌，門間聰之，秀島翔，林宏樹，綱美香，原田義孝，「レクチン固定化半導体センシングデバイス及び糖化合物の検出方法」，特願 2019-043864 号，2019 年 3 月 11 日出願

Funding

COI 若手連携研究ファンド 若手デジタル FS，国立研究開発法人 科学技術振興機構（JST），2018 年 12 月

国際交流助成，一般社団法人 丸文財団，2018 年 6 月

Acknowledgments

Firstly, I am deeply grateful to Professor Dr. Toshiyuki Momma for giving me an environment for research on the FET biosensor. He has been given guidance about the scientific knowledge and logical thinking perspective. I would also like to express my gratitude to Professor Dr. Tetsuya Osaka for his kind suggestion and encouragement. I appreciate Professor Dr. Yoshiyuki Sugahara and Professor Dr. Takayuki Homma for their valuable advice to improve my thesis.

I want to express my appreciation to Professor Dr. Keishi Ohashi for teaching the research design methods and data analysis. I would like to acknowledge associate professor Dr. Shigeki Kuroiwa for a lot of discussions and for providing the experimental environment. I would like to show my greatest appreciation to associate professor Dr. Sho Hidesima. His suggestions helped me not only with the research process of my doctoral thesis but also my attitude towards various things. Professor Dr. Takuya Nakanishi gave me multifaceted and logical advice during undergraduate and master theses research.

I wish to thank Dr. Mika Tsuna and Mr. Yoshitaka Harada in Nippon Flour Mills Co. Ltd. for collaboration of research on Chapter 2.1. Professor Dr. Yoshihiro Sakoda, Professor Dr. Shin-Ichiro Nishimura, and Professor Dr. Hiroshi Hinou in Hokkaido University gave me constructive comments and warm encouragement for research on Chapter 2.2. I would also like to offer my special thanks to Dr. Katsunori Horii and Mr. Naoto Kaneko for valuable comments and the provision of experimental reagents for research in Chapter 3.

I would like to thank all the colleagues of the Sensor group; Dr. Shofarul Wustoni, Mr. Shunsuke Nambuya, Mr. Keisuke Fujita, Ms. Akane Matsuzaka, Mr. Ryota Takibuchi, Ms. Mai Saito, Mr. Shin Sato, Mr. Ryo Takeuchi, Mr. Guo Jun, Mr. Ryo Toyama, Ms. Fumika Matsuzawa, Mr. Naoki Sakamoto, Ms. Shiori Inomata, Ms. Emi Miyagawa, Mr. Tomoya Inagaki, Ms. Mayuri Fujita, Mr. Akihiro Enami, Ms. Ayaka Osakada, and Mr. Yuya Sato. They gave me invaluable discussions, assistance, and thoughtfulness. I would

also thank Dr. Shofu Matsuda for his advice and encouragement to doctoral student life.

Special thanks to all members of the Applied Physical Chemistry Laboratory for their kind assistance and friendship.

Finally, I would like to express the deepest appreciation to my father Akihiro Hayashi and my mother Keiko Hayashi for their warm-hearted encouragement and support during my all student life.

February, 2021
Hiroki Hayashi